Analysis Report Review

Report Title: **REPORT DRAFT 4**

Report Number: **Final Report EP-C-12-014 WA 3-01**

This Analysis Report has been reviewed and complies with the quality assurance procedures of FEV, Inc.

☐ The Analysis Report is adequate for delivery to the customer.

(Signature)	(Signature)
Print Name:	Print Name:
Title: **Manager of Technology Center**	Title: **Project Engineer**
Date:	Date:

Battery Durability in Electrified Vehicle Applications:

A Review of Degradation Mechanisms and Durability Testing

Prepared for Environmental Protection Agency:

Jeff Cherry
Assessment and Standards Division
2000 Traverwood Drive
Ann Arbor, Michigan, 48105

Submitted by Thomas Merichko:

FEV North America, Inc.
4554 Glenmeade Lane
Auburn Hills, MI 48326

January 6, 2016

ABSTRACT

FEV North America, Inc. has been tasked with conducting an extensive literature review on the subject of EV battery durability. The literature review is intended to inform the participants of the United Nations Economic Commission for Europe (UNECE) Electric Vehicles and the Environment Informal Working Group (EVE IWG) and their colleagues in developing and/or improving EV programs and policy, including the consideration of any GTRs needed to fill gaps related to EV regulation. All classes of Electrified Vehicles (xEVs) are considered, with these being BEVs, HEVs, and PHEVs. The review examines the electrochemical basis for the deterioration of batteries used in xEV applications along with testing activities performed on xEVs and automotive grade cells, battery packs, etc.

TABLE OF CONTENTS

LIST OF FIGURES

LIST OF TABLES

Definitions & Terminology

Unless otherwise indicated, the definitions given here are derived from those given by the USABC Battery Test Procedures

cycle	The period commencing from the start of one charge/discharge to the start of the next charge/discharge where said period includes discharge time, open-circuit time, and charge time. The depth of discharge (or percentage of capacity) associated with each cycle must be specified.
cycle life	The number of cycles, each to specified discharge and charge termination criteria, such as depth-of-discharge, under a specified charge and discharge regime, that a battery can undergo before failing to meet its specified end-of-life criteria.
LMO	Lithium Manganese Spinel, $LiMn_2O_4$
NiMH	Nickel metal hydride
NCA	Lithium Nickel Cobalt Aluminum Oxide $LiNiCoAlO_2$
LFP	Lithium iron phosphate, $LiFePO_4$
LCO	Lithium cobalite, $LiCoO_2$
LTO	Lithium titanate, $Li4Ti_5O_{12}$
xEV	Electrified Vehicle, i.e. BEV, PHEV, HEV

Introduction

We present here a review of existing literature pertaining to the durability of xEV (BEV, HEV, and PHEV) battery systems. At present, no firm definition of "battery durability" exists in the literature. We will therefore seek to develop a definition for battery durability based on available literature, such as from other products and of course from the defined End-of-Life (EOL) criteria which exist for various xEV batteries.

In order to come to an understanding of the factors which impact the durability of such systems, we explore factors at the electrochemical level which influence battery performance at the cell and consequently module, pack, system, and vehicle levels. As we are ultimately interested in aiding in the development of the UNECE's **W**orldwide harmonized **L**ight vehicles **T**est **P**rocedures (WLTP), we will look at xEV testing activities so as to determine which factors affect the durability of an xEV battery system and ways in which existing testing standards, manuals, and procedures fail to account for these factors which can influence xEV durability.

Overview of xEV Architectures and Battery Technologies

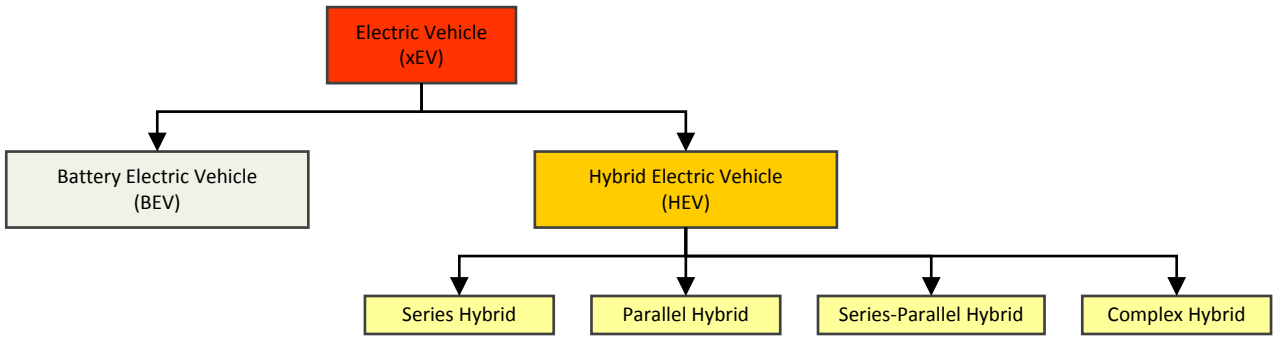

Figure 1 Classification of EVs according to the type(s) and combination of energy converters used (electric motor & ICE) **[1]**

Broadly speaking, electrified vehicles may be divided in to two subclasses: Battery Electric Vehicles (BEVs) or Hybrid Electric Vehicles (HEVs), with Plug-in Hybrid Electric Vehicles (PHEVs) distinguishing themselves in the sense that they are, like BEVs, capable of charging themselves from the grid. In this section we shall offer a brief overview of the architectures and operation modes used in xEVs.

Battery Electric Vehicles (BEVs)

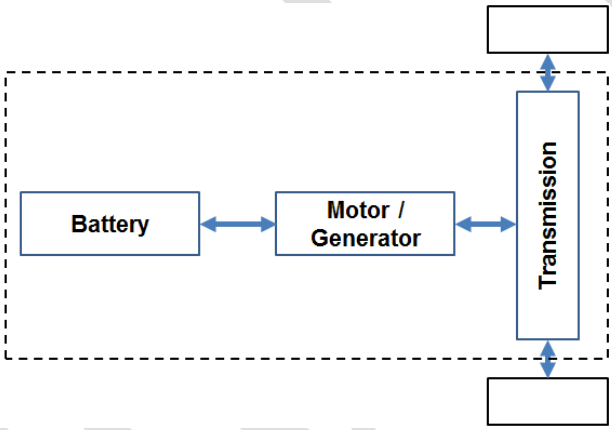

Figure 2 Basic Architecture of a BEV

A battery electric vehicle (BEV) is a vehicle that is powered entirely on electric energy, typically a large electric motor and a large battery pack [2]. Based on the type of transmission; the use of a clutch, gearbox, differential, and fixed gearing; and the number of battery packs and motors there are many variations on the BEV design. However, a basic BEV system is shown in Figure 2. Because the vehicle is powered only by batteries or other electrical energy sources, zero emission can be achieved. However, the high initial cost of BEVs, as well as its short driving range and long refueling time, has limited its use. Still, new BEV architectures have been proposed that use several energy sources (e.g., batteries, supercapacitors, and even reduced power fuel cells) connected to the same DC bus, which should eventually reduce the refueling time, expand the driving range, and drive down the price [3]

Hybrid Electric Vehicles (HEVs)

While BEVs are propelled by electric motors only, HEVs employ both ICE and electric motor in their powertrains. The way these two energy converters are combined to propel the vehicle determines to the three basic powertrain architectures: series hybrid, parallel hybrid, and series-parallel hybrid. Complex hybrid refers to architectures that cannot be classified as one of these three basic types.

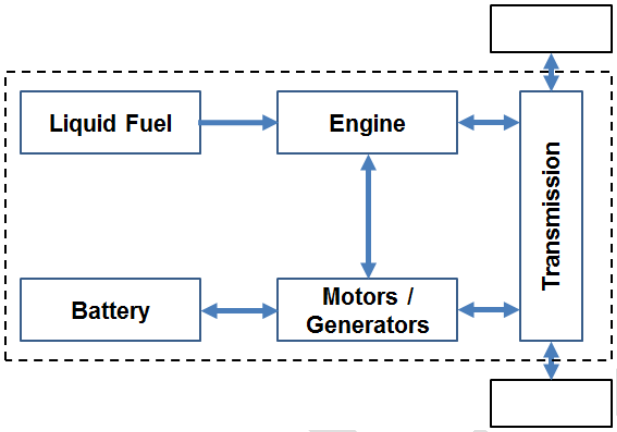

Figure 3 Basic Architecture of a Series-Parallel HEV

Series–Parallel HEVs: A Series-Parallel HEV has both Series and Parallel energy paths. As shown in figure 5, a system of motors and/or generators that sometimes includes a gearing or power split device couples allows the engine to recharge the battery. Variations on this configuration can be very complex or simple, depending on the number of motors/generators and how they are used. These configurations can be classified as Complex hybrids,Split-Parallel hybrids, or Power-Split hybrids [2].

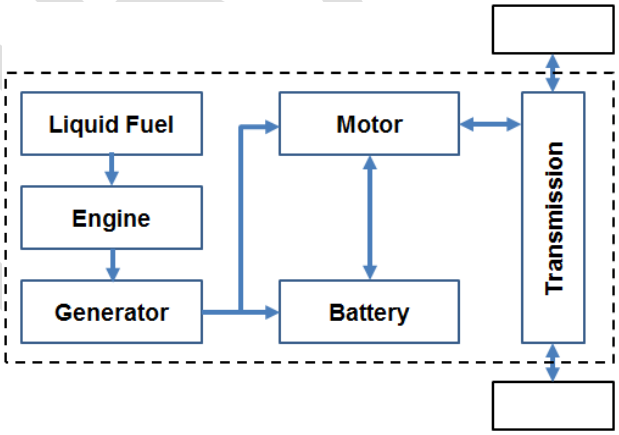

Figure 4 Basic Architecture of a Series HEV

Series HEVs: In series HEVs, all the traction power is converted from electricity, and the sum of energy from the two power sources is made in an electric node that is commonly in a dc bus. The ICE has no mechanical connection with the traction load, which means it never directly powers the vehicle. In series HEVs, the ICE mechanical output is first converted into electricity by a generator [3]. The ICE's role is charging (or recharging) the battery and supplying energy to the electric motor, always being operated at maximum efficiency [1]. The converted electricity can either charge the battery or directly go to propel the wheels via the electric motor and the transmission, thus bypassing the battery. [3]

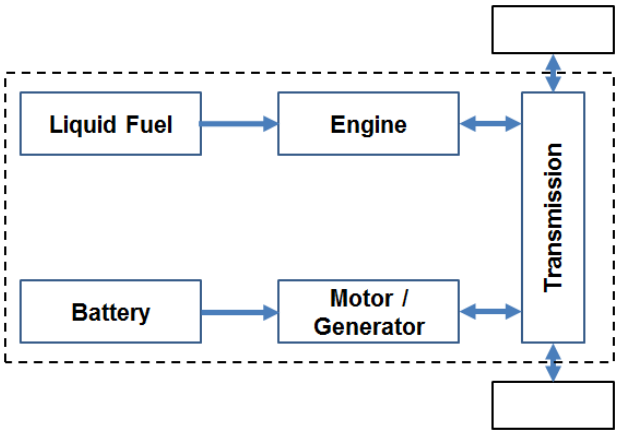

Figure 5 Basic Architecture of a Parallel HEV

Parallel HEVs: In a Parallel Hybrid, there are two parallel paths to power the wheels of the vehicle: an engine path and an electrical path, as shown in figure 4. The transmission couples the motor/generator and the engine, allowing either, or both, to power the wheels. Control of a Parallel Hybrid is much more complex that for a Series Hybrid because of the need to efficiently couple the motor/generator and engine in a way that maintains drivability and performance [2]. A Parallel Hybrid can also be referred to as a "Power-Assist Hybrid Vehicle" as the battery assists the engine in supplying power to the transmission.

The previous HEV architectures provide different levels of functionality. These levels can be classified by the power ratio between the ICE and EMs.

Table 1 Different Functions of the Various HEV Architectures

	Micro HEV	Mild HEV	Full HEV	Plug-in HEV
Series-parallel			x	x
Series			x	x
Parallel	x	x	x	

1. **Micro Hybrid**: Micro hybrid vehicles use a limited-power EM as a starter alternator [30], and the ICE insures the propulsion of the vehicle. The EM helps the ICE to achieve better operations at startup. Because of the fast dynamics of EMs, micro hybrid HEVs employ a stop-and-go function, which means that the ICE can be stopped when the vehicle is at a standstill (e.g., at a traffic light). Fuel economy improvements are estimated to be in the range of 2%–10% for urban drive cycles.
2. **Mild Hybrid**: In addition to the stop-and-go function, mild hybrid vehicles have a boost function, which means that they use the EM to boost the ICE during acceleration or braking by applying a supplementary torque. The battery can also be recharged through regenerative braking. However, the electrical machine alone cannot propel the vehicle. Fuel economy improvements are estimated to be in the range of 10%–20%.
3. **Full Hybrid**: Full hybrid vehicles have a fully electric traction system, which means that the electric motor can insure the vehicle's propulsion. When such a vehicle uses this fully electric system, it becomes a "zero-emission vehicle" (ZEV). The ZEV mode can be used, for example, in urban centers. However, the propulsion of the vehicle can also be insured by the ICE or by the ICE and the EM together. Fuel economy improvements are estimated to be in the range of 20%–50%.
4. **Plug-in Hybrid**: Described in its own section

Plug-in Hybrid Electric Vehicles (PHEVs):

A plug-in hybrid-electric vehicle (PHEV) is a hybrid-vehicle with the ability to recharge from the grid. It is endowed with a modest electric driving range (on the order of tens of miles), and a small gasoline-powered ICE. The PHEV offers a compromise between the drivability and affordability of the hybrid-electric vehicle (HEV), and the potential environmental and energy security benefits of the battery electric vehicle (BEV). Like the BEV, the PHEV possesses the capability to displace petroleum sourced energy with grid-sourced energy; and, like the HEV, the PHEV is not range limited in any meaningful sense [4].

Above a threshold minimum battery state-of-charge, the PHEV operates in "charge depleting" mode, in which it freely draws down the onboard battery to meet vehicle power demands. Once it reaches this minimum SOC threshold, the vehicle switches to "charge sustaining" mode (Figure 21). Charge-sustaining mode is functionally equivalent to vehicle operation in a conventional HEV. During this mode of operation, the vehicle maintains the SOC within a limited operating envelope (the overall SOC excursion during this mode of operation might be on the order of +/- 200 Wh), using stored battery energy to optimize ICE operation, and recharging via either regenerative braking or an accessory-like loading on the engine. [4]

Battery Technologies for xEVs

Currently, xEVs are primarily using six battery technologies: lithium-nickel cobalt aluminum (NCA), lithium oxide cobalt (LCO), lithium-nickel-manganese-cobalt (NMC), lithium-manganese spinel (LMO), lithium titanate (LTO), or lithium iron phosphate (LFP). [5]

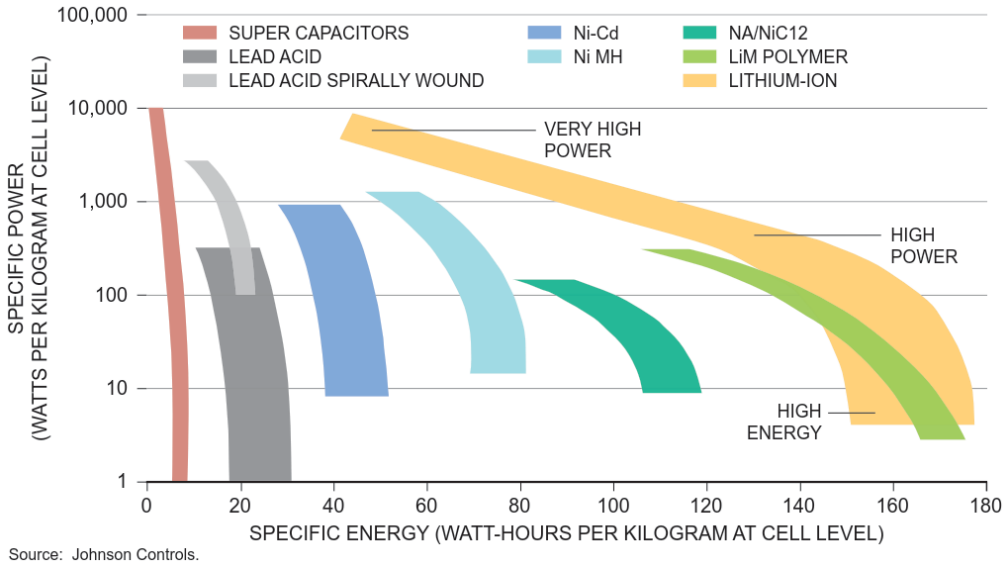

Figure 6 Ragone plot for various batteries / energy storage devices **[6]**

Cathode	Anode	Abbrev.	Energy Density	Power Density	Cycle Life	Safety*	Cost
Lithium Cobalt Oxide	Graphite	LCO	High	Fair	Fair	Fair	High
Nickel Cobalt Aluminum Oxide	Graphite	NCA	High	High	Fair	Fair	High
Lithium Iron Phosphate	Graphite	LFP	Low	High	High	Very good	Fair
Lithium Manganese Oxide	Graphite	LMO	High	High	Fair	Very good	Fair
Lithium Manganese Oxide Spinel	Graphite	LMO	High	High	Fair	Good	Low
Lithium Manganese Oxide Spinel Polymer	Graphite	LMO	High	High	Fair	Good	Low
Manganese Nickel Cobalt Oxide	Graphite	MNC	High	Fair	Low	Fair	High
Lithium Manganese Oxide Spinel	Lithium Titanate Oxide	LMO-LTO	Low	Low	High	Good	High
Lithium Nickel Oxide	Graphite	LNO	High	Fair	Fair	Fair	Fair
Lithium Manganese Nickel Oxide Spinel	Graphite	LMNS	High	High	Fair	Fair	Low
Lithium Manganese Nickel Oxide Spinel	Lithium Titanate Oxide	LMNS-LTO	Fair	High	High	Good	Low

* "Safety" refers to the thermochemical reactivity of the specific cathode/anode couples. Beyond this, (1) the reactivity with the electrolyte must be considered and (2) system-level safety is primarily determined by the battery management system, which includes thermal management.

Source: Shmuel De-Leon, "High Power Rechargeable Lithium Battery Market," presented at IFCBC Meeting, February 4, 2010.

Table 2 Comparison of Lithium-Ion Battery Chemistries Showing a Sampling of Key Performance Attributes **[6]**

Table 2 shows the types of cathode and anode combinations which can occur in xEV batteries, along with some of their characteristics. Figure 7 shows a graphical representation of LCO, NCA, MNC, LFP, NCA, and LTO-type batteries. Commercial xEVs, and their selected battery chemical compositions, can be found in the Appendix, Table 20.

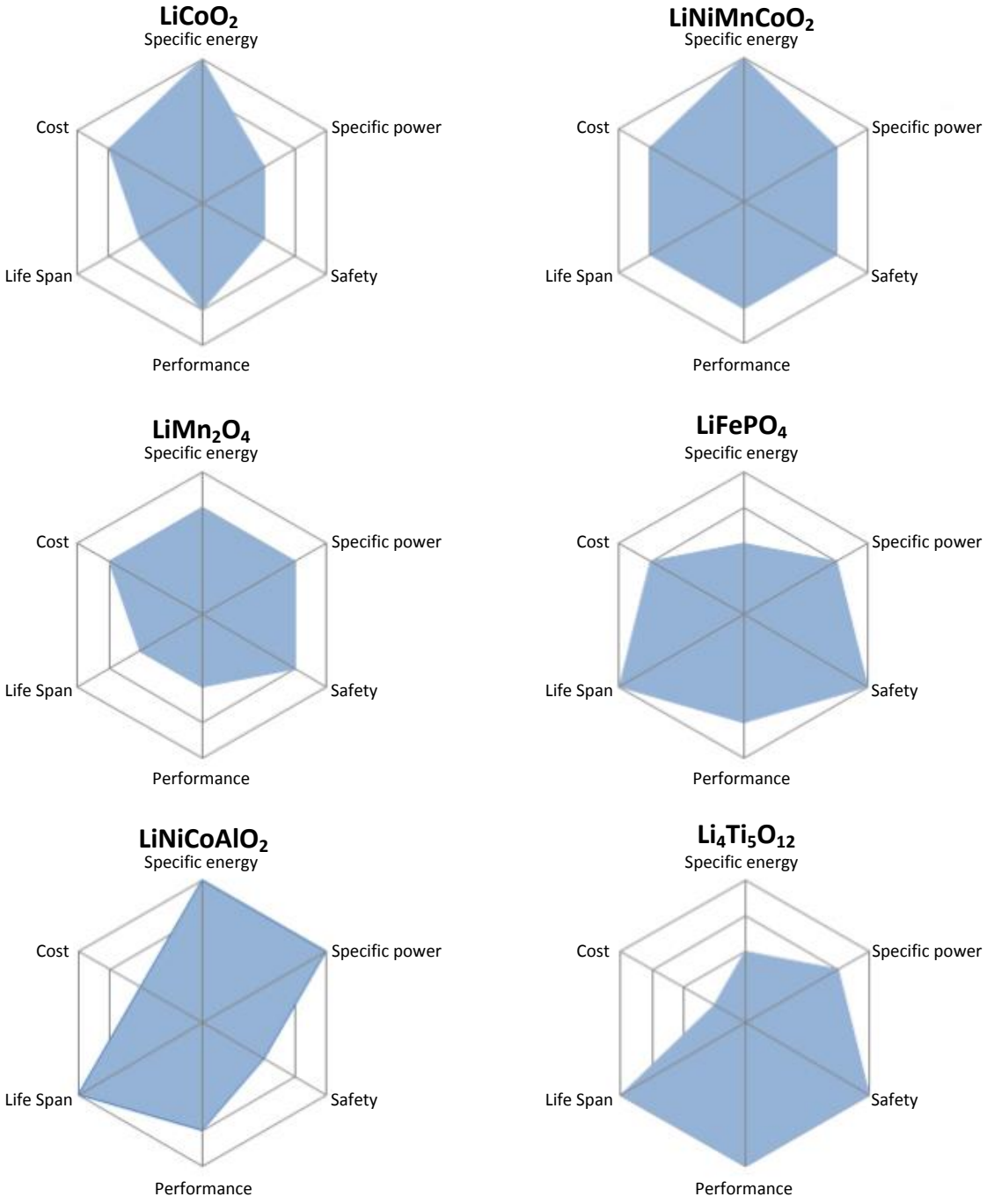

Figure 7 Properties of different Li-ion cell chemistries **[7]**

Existing Definitions of Battery Durability and End-of-Life Criteria

In 2010, the German National Platform for Electromobility [8] published a study regarding the future of standards for electrified vehicles. At the time, studies on battery durability were given as a potential research area but no pressing need for standards on the topic was identified [8]. Even today, the European Commission does not have any battery durability requirements in place [9]. We therefore turn to available literature in order to find other definitions used for durability which we may use to synthesize into a definition of durability which is applicable toward xEVs.

Boulos et al. [10] from Ricardo-AEA conducted a study into the definition of durability for products as part of an initiative from the European Commission – DG Environment. Specifically, the purpose of the study was to identify two priority products and develop a methodology for measuring their durability. To this end, the authors of [10] have compiled together a number of durability definitions from other works. It should be noted, however, that these definitions relate to a variety of products which are neither related to batteries nor to automotive applications. Nevertheless, these definitions shall assist us in formulating our own definition of durability as it specifically relates to xEV battery durability. These definitions are shown in Table 3.

From these definitions, the authors of [10] conclude: it becomes clear that the terms ‘product lifetime’ and ‘product durability’ are inextricably linked and that the terms are frequently used interchangeably.

The key practical aspect that must be considered when exploring the implication of durability for products, if product durability is to be taken forward as a single element to be improved in its own right through the application of European Product Policy measures, is testing:

- Any definition of durability needs to be able to be tested – i.e. a test method must exist or be developed that enables repeatable and replicable testing to be performed.
- Testing under normal conditions is the usual method to give the anticipated lifespan, for example, testing under typical ambient conditions (temperature and humidity) and typical frequency of use.
- Further testing can be done under ‘challenging’ conditions, which use foreseeable conditions that are more challenging than typical use patterns, such as higher temperatures, increased humidity, increased frequency of use. Other examples of testing under more challenging conditions could include cyclic corrosion testing, salt spray testing, thermal aging, thermal cycling or thermal shock, vibration – random or shock. The specific testing carried out will depend on the type of product and the range of potential conditions it may be subjected to during its lifetime.
- The lifetime of a product needs to be defined, as does the point at which a first lifetime ceases and a potential second lifetime begins, for example if the product is remanufactured.

Report/Paper Title	Definitions relating to product durability	Reference
Further steps towards a quantitative approach to durability design	Definition: The durability design objective is to keep the probability of failure within a specified time interval (or service life) below a certain threshold value that depends on the consequences of failure of the component or system.	Lounis et al., 1998
Design for environment: a method for formulating product end-of life strategies	Definition: Wear-out life: the length of time until the product no longer meets the original function(s). Product is obsolete when it is no longer able to perform its intended function; e.g. because of failure of key components or it is outmoded.	Rose, 2000
Timber – Design for Durability	Definition: The capacity of a timber product, component, system, building or structure to perform for a specified period of time, the function for which it was intended – be it aesthetic, structural or amenity.	National Association of Forest Industries, 2003
Durability and the Construction Products Directive (now repealed) together with the Guidance Paper issued in 2004	Definition: Durability of a product is the ability of a product to maintain its required performance over a given or long time, under the influence of foreseeable actions.	EC, 2004
The durable use of consumer products	Definition: Product life (or durability) is the product's actual life in use. It should be differentiated among the product's economic life (determined by the opportunity cost) and product's technical life (determined by the duration of the product's ability to fulfill its technical function).	Kostecki, 1998
Design for Durability	Definition: The concept of durability in design embraces longer lasting products that focus on a better use of finite resources through, for example, combining functionality, opportunities for secondary lives, and increasing overall lifespan and product information.	Monteiro de Barros et Dewberry, 2006
Life cycle, sustainability and the transcendent quality of building materials	Definition: Durability is the characteristic of those objects or materials that maintain their properties over time.	Mora, 2007
Longer Product Lifetimes	"the expected lifetime of a product under a typical consumer use profile"; "the number of years that the product is designed to last, or number of product uses"; "Increasing product design life is defined here as measures which seek to replace shorter life products with products with different specifications which are purposely designed to last longer."	ERM for Defra, UK, 2011
MEErP, Material efficiency module	Lifetime considerations form part of the non-energy related product considerations, and will be given as per year of use, as well as whole lifespan. The product lifetime can refer to: • The technical lifetime is the time that a product is designed to last to fulfill its primary function (technical lifetime). • The actual time in service is the time the product is used by the consumer (service lifetime). The actual time in service is not a typical parameter in industry and depends more on the user than on the manufacturers of the product design.	European Commission

Table 3 Definitions of durability in the literature [10]

The definition arrived at by Boulos et al. was: *Durability is the ability of a product to perform its function at the anticipated performance level over a given period (number of cycles – uses – hours in use), under the expected conditions of use and under foreseeable actions. Performing the recommended regular servicing, maintenance, and replacement activities as specified by the manufacturer will help to ensure that a product achieves its intended lifetime* [10].

For determining definitions of durability with respect to xEVs, we may turn our attention toward the requirements which are set for vehicle End-of-Life (EOL). A number of parameters which are to be met upon reaching EOL conditions are defined by the USABC (United States Advanced Battery Consortium). The requirements for HEVs, PHEVs, and BEVs are given for year 2018 and 2020 commercialization. These requirements are shown in Table 21 - Table 23 in the Appendix. If we treat battery durability as being intrinsically linked to battery life, then the values shown in these tables may be taken as a guideline for durability with respect to cycle and calendar life parameters.

These USABC standards established battery EOL for BEVs as: (1) "the net delivered capacity of a cell, module, or battery is less than 80% of its rated capacity when measured on the DST (Reference Performance Test); or (2) the peak power capability (determined using the Peak Power Test) is less than 80% of the rated power at 80% DOD." EOL conditions are therefore based upon performance metrics. But, returning to the EOL goals, we are left with limiting factors such as a calendar life of 15 years for all xEVs [11] [12] [13] and cycle life goals of 75000 cycles for HEVs, 5000 cycles for PHEVs, and 1000 cycles for BEVs. Therefore, a component of our definition of durability needs to ensure that the rated capacity and rated power are greater than or equal to the associated values specified in the EOL criteria.

Strictly speaking, durability is defined as "The ability to withstand wear, pressure, or damage" [14]. However, we shall make distinctions with the formal English definition of durability when considering existing types of tests of xEV batteries. Durability, insofar as we should be concerned, should not be confused with Abuse, or that is to say, damage inflicted upon the battery which is liable to cause outright, if not catastrophic, failure. ISO-12405 has provisions for Performance, Reliability, and Abuse testing. SAE J2464, for example, consists entirely of Abuse tests [15].

We therefore set a working definition of xEV Battery Durability as such:

"The ability of an electrified vehicle battery to withstand degradation of functionality such that power & energy performance targets are met during typical drive cycles, consumer usage, and storage conditions without exceeding its end-of-life cycle and calendar life specifications."

FEV does not intend for this definition to be applied outside of this document. However, in order for us to be able to discuss this topic for which there exists no clear formal definition, we shall make use of the above. In testing for battery durability using the above definition, xEVs and their battery systems will be subjected to drive cycles featuring various charge and discharge scenarios along with storage such that a vehicle will be able to (using USABC BEV goals [13] as an example) achieve either $\geq$ 15 years of calendar (storage) life or continue operating beyond 1000 cycles while maintaining $\geq$ 80% of its rated capacity and power.

Physical and Chemical Degradation Mechanisms of xEV Batteries

Introduction

Before we examine batteries in vehicles directly, we shall look at the mechanisms of degradation in batteries which occur at the physical and chemical level in cells. This type of investigation is valuable as well will be able to extrapolate effects which occur at the cell level to the module, pack, system, and thus vehicle level. We will primarily focus on lithium-ion battery technology in this section due to its proliferation in current and upcoming xEVs. We shall nevertheless also dedicate a section to NiMH batteries at the end.

As part of the review on physical degradation mechanisms, FEV would like to stress that the topics discussed herein pertain to degradation methods which are found in Li-Ion and NiMH battery chemistries. We present here mechanisms from reviewed literature which demonstrate many of the means by which degradation of various battery chemistries may occur, even though these may not necessarily occur in xEV batteries on account of, among other things, manufacturing process control or battery management systems.The active materials in Li-ion cells operate by reversibly incorporating lithium in an intercalation process, a reaction wherein lithium ions are reversibly removed or inserted into a host without a significant structural change to the host. The positive material in a Li-ion cell is a metal oxide, with either a layered or tunneled structure. The graphitic carbon materials have a layered structure similar to graphite. Thus the metal oxide, graphite, and other materials act as hosts, incorporating lithium ions, guests, reversibly to form sandwich-like structures [16].

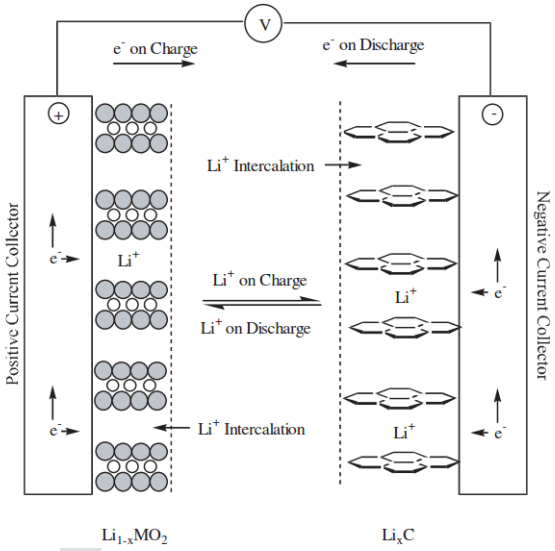

Figure 8 Schematic of the electrochemical process in a Li-ion cell. [16]

When a Li-ion cell is charged, the positive material is oxidized and the negative material is reduced. In this process, lithium ions are de-intercalated from the positive material and intercalated into the negative material. In this scheme, $LiMO_2$ represents the metal oxide positive material, such as $LiCoO_2$, and C the carbonaceous negative material, such as graphite. The reverse happens on discharge. As metallic lithium is not present in the cell, Li-ion batteries are chemically less reactive, safer, and offer longer cycle life than possible with rechargeable lithium batteries that employ lithium metal as the negative electrode material. The charge-discharge process in a Li-ion cell is further illustrated graphically in Figure 8. In the figure, the layered active materials are shown on metallic current collectors [16].

Physical and Chemical Degradation Mechanisms of Lithium-Ion Batteries

Degradation of the Anode

Formation of a Passivated Surface Layer

Graphite is one of the common anode materials for lithium ion batteries operating in organic electrolytes, such as $LiPF_6$, with cosolvents like ethylene carbonate (EC), dimethyl carbonate (DMC), diethyl carbonate (DEC), and methyl ethyl carbonate (EMC)). The reaction of the anode with the electrolyte solution in the formation stage results in the formation of the *solid electrolyte interphase (SEI).* The SEI forms with the first cycling of the battery [17] [18]. Anion contaminates, such as F^- from HF and PF_5, readily react with lithium to form insoluble reaction products which are non-uniform, electronically insulating, and unstable on the surface of the graphite particles [19]. In addition, the dissolution of the cathode electrode metal from the lattice into the electrolyte due to the disproportionation of Mn^{3+} (into Mn^{2+} and Mn^{4+}) by traces of hydrofluoric acid (HF) in the electrolyte, resulting in the deposition of contaminates on the anode electrode surface [19] [20].

At higher battery potentials, during the intercalation of lithium ions into the anode lattice structure, the graphite anode oxidizes. At this potential, electrolyte cosolvents, such as EC, which is highly reactive, react with the lithium ions which leads to growth on the anode surface [19]. The presence of these reaction products on the surface retards the intercalation kinetics of the carbon anode [19]. The surface layer grows in thickness as the decomposition reaction continues [19] [21] The layer thickness is established to be a function of operating cycles, regardless of the charging protocol (i.e., pulse charging or DC charging) [19] [22]. The layers become unstable and crack due to expansion and contraction of the graphite lattice during the insertion and de-insertion of the lithium ions [19]. This allows further surface reaction at these sites that may eventually isolate the graphite particles from the current collector. The crack formed on the surface does not typically travel to the carbon electrode. The formation of this surface film layer is the primary source of lithium ion loss in lithium ion battery during storage conditions [22]. It also leads to an increase in the charge transfer resistance, impedance, and clogs pores on the carbon anode electrode [19], which limits accessibility of lithium ions to the anode surface leading to an increase in irreversible capacity loss.

Anode Impedance

The growth of the passive surface layer on the anode creates resistance to lithium ion flow, which results in a rise in the charge transfer resistance and the impedance of the anode [19]. This increase in anode impedance is said to increase with charge rate, cycle number, temperature, and anode material particle size [19]. However, at temperatures in the range of 10–30°C and with a low charge rate (C/20), the anode electrode contribution to the overall battery impedance is low. This is attributed to the small amount of the surface film formed on the electrode surface [19]. The low charge rate limits the amount of excess Li^+ that is not intercalated into the electrode to react with the electrolyte [19]. Common surface reaction products formed on the anode surface include Li-alkyl carbonates, lithium carbonate species and fluorinated products. These products affect the intercalation and de-intercalation kinetics of the anode, and thus result in an increase in anode electrode impedance relative to the cathode [19].

Degradation Due to the Loss of Recyclable Lithium Ions

The irreversible lithium ion loss is generally attributed to two phenomena, namely: (i) solid electrolyte interface (SEI) layer formation via electrolyte decomposition at the formation stage; (ii) side reaction of lithium ion with decomposed electrolyte compounds and water (e.g., 10–1500 ppm) in the electrolyte at the later stage of the battery operation. The loss and/or consumption of recyclable lithium ions at the anode by the passive layer is a major cause of the reduction in the reversible capacity of the lithium ion battery [19] [18] [23]. As the layer grows, lithium is consumed in the reaction and the increased thickness inhibits Li^+ transfer, thus the lithium ions

must tunnel through the layer. This phenomenon is the main degradation mechanism in fully charged batteries at storage conditions [19] [24] [25], where the electronic insulating surface layer formed clog the pores and isolate graphite particles. The irreversible lithium ion loss is also a function of the specific area of the graphite particles, since an increase in area increases the volume of reaction products [19]. For a graphite anode with low specific area, the charge loss is low. The electrolyte additive, vinylene carbonate (VC) is one that increases the lithium ion loss rate at the anode for the Li/coke electrode during storage (ambient temperature conditions). Because it increases the rate of SEI formation reaction at ambient temperature conditions to increase the SEI thickness. However, its beneficial effect is seen at higher temperature (35–50 °C) and higher voltages >0.4 V for Li/coke, electrode as it slows down the side reaction rate and undergoes reduction and polymerization to form poly alkyl Li-carbonate species that suppress both solvent and salt anion reduction on the anode electrode. Similarly, in batteries stored at voltages greater than 3.6V, electrolyte oxidation at the cathode can also induce surface reaction deposits that cover the active cathode electrode area. These covered areas are insulating, which could result in a non-homogeneous local current distribution in the cathode electrode [19].

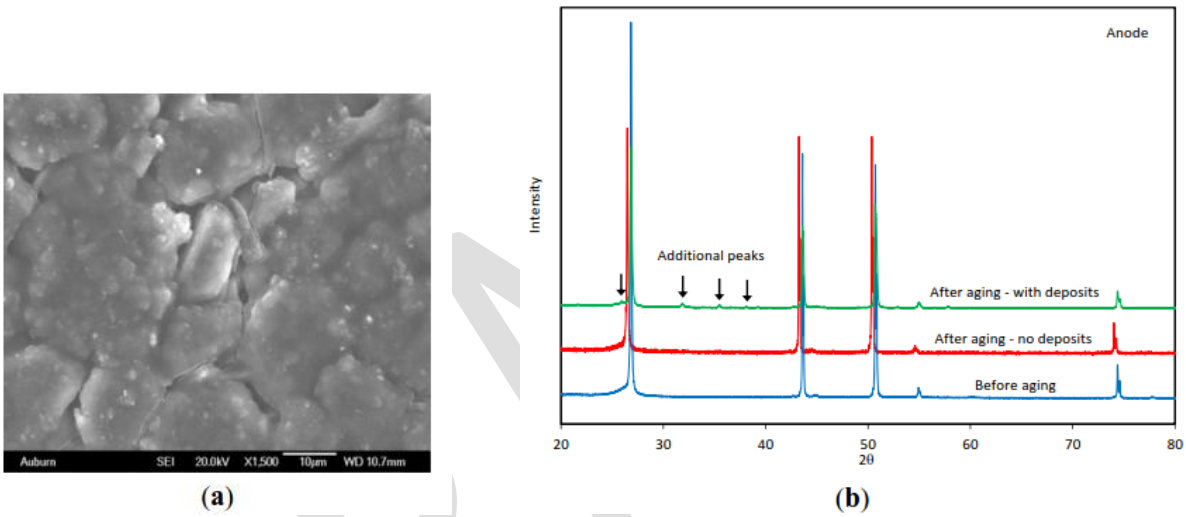

Figure 9 Structural changes on the anode electrode from degradation. (a) Surface cracks on the surface of aged anode electrode; (b) XRD spectra of aged anode electrode showing change in crystal structure (new phases). **[19]**

Metallic Lithium Plating on the Anode

The usage of well-ordered carbon and non-graphitizable carbon have gradually replaced lithium metal as the preferred anode material for the lithium ion battery due to benefits in capacity, cyclability, low electrode potential relative to Li^+/Li, and a lower susceptibility to lithium plating [19]. Nevertheless, metallic lithium deposits remain a factor in anodes.

There are several factors that initiate the formation of metallic lithium on the surface of the anode electrode, some of these include: (1) the nature of the electrolyte (i.e., electrolyte formulations with high EC content exhibit lithium plating); (2) the ratio between anode and cathode capacities (i.e., low anode/capacity ratio will polarize the anode and promote lithium plating); (3) the operating temperature and the charge rate [i.e., low temperature (−20 °C) coupled with a high charge rate] all influence plating on the anode. These factors affect the anode kinetics and the lithium ion diffusion rate, such that lithium plates on the surface of the electrode rather than intercalating into the lattice of the carbon.

The formed metallic lithium deposits on the graphite anode are affected by the degree of random orientation of the particles in the crystal structure in the anode material and the non-uniformity of the current distribution which is a function of diffusion and current density. This subsequently results in the formation of moss-like

deposits and dendrites [19]. These moss-like deposits and dendrites grow as a function of the temperature and current density between the polymer separator and the anode. As the temperature and charge rate increases, the reaction rate also increases and metallic lithium is deposited on the graphite at overcharge. Dendrites can cause the separator to disconnect and become isolated from the electrolyte and in some instances pierce through the separator. These dendrites can cause a short circuits and consequently to thermal runaway situations. Lithium plating can typically be identified by a voltage plateau on the discharge voltage profile and a low columbic efficiency [19].

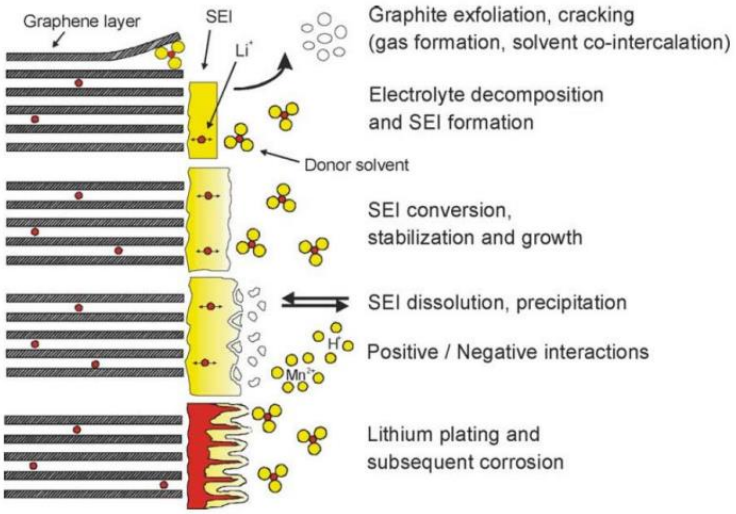

Figure 10 Degradation Methods for the Negative Electrode **[18]**

Regarding the anode, Vetter et al. [18] concluded that SEI formation and growth leads to an impedance rise at the anode. Usually, SEI formation takes place mainly at the beginning of cycling. SEI growth proceeds during cycling and storage and is favored by elevated temperatures. The rise in impedance which comes as a result of this growth can be directly linked to power fade. Furthermore, in parallel to SEI growth, corrosion of lithium in the active carbon takes place, leading to self-discharge and capacity fade due to loss of mobile lithium. The formation and growth of the SEI leads to gradual contact loss within the composite anode, and thus, increases the impedance in the cell. Lithium metal plating might occur at low temperatures, at high rates and for inhomogeneous current and potential distributions. The Li metal reacts with the electrolyte, which may contribute to accelerated aging. A strong influence of the specific cell components on the aging mechanism can be observed. Although the general mechanisms presented here hold true for most of the lithium-ion systems they may be pronounced differently for each particular system [18].

Cause	Effect	Leads to	Reduced by	Enhanced by
Electrolyte decomposition (→SEI)(Continuous side reaction at low rate)	Loss of lithium Impedance rise	Capacity fade Power fade	Stable SEI (additives) Rate decreases with time	High Temperatures High SOC (low potential)
Solvent co-intercalation, gas evolution and subsequent cracking formation in particles	Loss of active material (graphite exfoliation) Loss of lithium	Capacity fade	Stable SEI (additives) Carbon pre-treatment	Overcharge
Decrease of accessible surface area due to continuous SEI growth	Impedance rise	Power fade	Stable SEI (additives)	High temperatures High SOC
Changes in porosity due to volume changes, SEI formation and growth	Impedance rise Overpotentials	Power fade	External pressure Stable SEI (additives)	High cycling rate High SOC
Contact loss of active material particles due to volume changes during cycling	Loss of active material	Capacity fade	External pressure	High cycling rate High DOD
Decomposition of binder	Loss of lithium Loss of mechanical stability	Capacity fade	Proper binder choice	High SOC High temperatures
Current collector corrosion	Overpotentials Impedance rise Inhomogenous distribution of current and potential	Power fade Enhances other aging mechanisms	Current collector pre-treatment (?)	Overdischarge Low SOC
Metallic lithium plating and subsequent electrolyte decomposition by metallic Li	Loss of lithium (loss of electrolyte)	Capacity fade, power fade	Narrow potential window	Low temperature High cycling rates Poor cell balancing Geometric misfits

Table 4 Lithium-ion aging – causes, effects, and influences. Reproduced from Vetter et al. **[18]**

Lithium Titanate (LTO) anodes

Although much of the focus has been on graphite and carbon anodes, Morales et al. [26] investigated $Li_4Ti_5O_{12}$ (LTO) as an anode material coupled with a lithium-iron phosphate cathode. It was shown that LTO permitted allowed for high rate capabilities but is a particularly poor conductor. This sentiment was echoed by Etacheri et al. [27], who observed that LTO is inferior to graphite due to its low capacity and high voltage which in turn leads to poor energy density. One thing to note is that LTO features no passivation phenomena on account of its high reduction voltage. This gives LTO excellent low temperature performance [27].

Degradation of the Cathode

While a significant portion of negative electrode degradation is associated with SEI formation at the electrode/electrolyte interface, positive electrode degradation is often attributed to physical degradation of its components. However, several mechanisms are similar between the two electrodes (Figure 11). The aging mechanisms surrounding the cathode differ depending on its chemistry since the physical nature of the cathode will differ according to its composition and structure. We shall therefore investigate the applicable cathode chemistries and offer insight in to the degradation mechanisms and the susceptibility of each to aging.

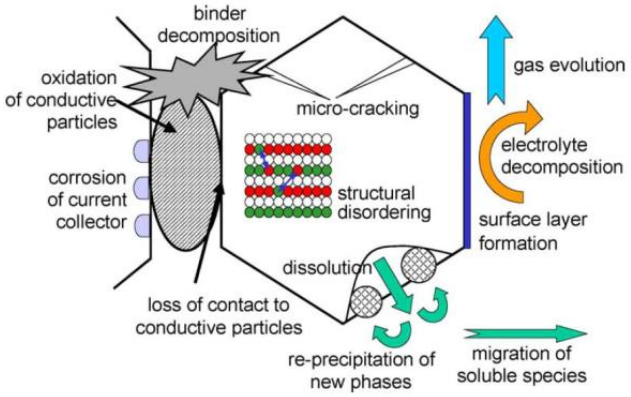

Figure 11 Degradation mechanisms for the positive electrode **[28]**

In much of the existing literature surrounding lithium ion battery degradation and aging, the authors of the various studies offer suggestions or solutions pertaining to ways which the cathode may be doped or coated so as to reduce effects/mechanisms which contribute to aging. For the scope of this review, however, such topics will not be considered and FEV will instead seek to focus on the mechanisms themselves.

$LiFePO_4$ (LFP)

Lithium Iron Phosphate

$LiFePO_4$ has recently attracted a significant interest as a cathode material for Li-ion batteries because it's a low cost material with excellent safety characteristics and also it has the potential of providing a long cycle and calendar life [5] [29] [25] [26]. Although $LiFePO_4$ shows good stability, traces of moisture in the $LiFePO_4$ material could be detrimental to its long-term storage since $LiFePO_4$ dissolution in the electrolyte was observed at high temperature [91] from [20].

In 2005, Amine et al. studied the high-temperature storage and cycling characteristics of prismatic Li- ion cells with carbon-coated $LiFePO_4$ cathodes, MCMB graphite anodes and a $LiFP_6$/EC-DEC electrolyte [30]. The cells showed a significant capacity fade when cycled at 37°C and 55°C with interfacial impedance of the graphite electrode showing significant increases during high-temperature cycling. Carbon-coated $LiFePO_4$ electrodes were found to release iron ions into the electrolyte when aged at these temperatures. The observed impedance rise of the graphite electrodes and the consequent capacity fade of the cells were attributed to the formation of interfacial films that were produced on the graphite electrodes as a result of possible catalytic effects of the metallic iron particles.

In order to evaluate the origins of the iron dissolution, $LiFePO_4$ was investigated in various electrolyte solutions, such as $LiClO_4$ and $LiPF_6$ 1–1.5M in mixtures of EC-DMC or EC-EMC [25] [31]. $LiFePO_4$ electrodes demonstrated higher stability at elevated temperatures, in solutions that contain no acidic or protic contaminants. The capacity loss due to iron dissolution does not result from bulk changes but rather to surface reactions, such as the parasitic reaction above 4.1V for Li^+/Li [32]. A systematic study of a series of $LiFePO_4$

samples containing different amount of Fe^{3+} impurities showed that the most contaminated sample exhibited the highest level of iron dissolution and consequently the lowest electrochemical performance [33].

A proposed mechanism for the dissolution of iron and the subsequent capacity fading is the reaction between acidic species in the electrolyte and Fe^{3+} impurities in the positive electrode. These dissolved iron ions migrate to the negative electrode and are then reduced into metallic iron, thereby causing an increase of the thickness of the existing SEI layer on the graphite electrode and consequently to an impedance rise, which in turn leads to capacity fading and a loss of power. In a failure case, the deposition of metallic iron can lead to the growth of iron dendrites which may penetrate through the separators and cause short-circuit [33] [34].

In addition to the iron dissolution, one has to consider the lithium insertion/extraction mechanism in $LiFePO_4/FePO_4$. It is highly anisotropic and involves the coexistence of a Li-rich and a Li-poor phases [20] [35]. Phase transitions along one of the lattice planes of the crystal surface can induce crack formation on another plane. These cracks may be caused by high internal strain upon lithium extraction/insertion. As a result of these cracks, increased polarization of the electrode may occur along with poor electric contact between active particles or the aluminum current collector. Altogether, these factors contribute to capacity fade in $LiFePO_4$.

$LiMn_2O_4$ (LMO)
Lithium Manganese Oxide

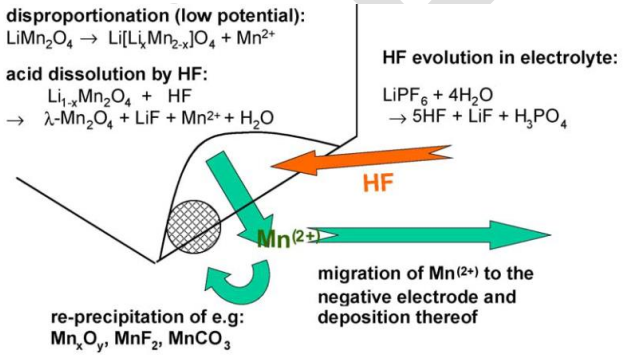

Figure 12 Dissolution of lithium manganese spinel **[18]**

$LiMn_2O_4$ is noted to have features at high (4.5V) and low voltages (3.3V) which are detrimental to its cyclability. These features are associated to phase transitions, which occur during cycling. A result of these transitions is a loss of electrical contacts. Although a composition of $Li_{1.05}Mn_{1.95}O_4$ can improve performance with respect to capacity retention, the usage of this particular composition demonstrates poor performance at high temperature and after storage at a low SOC [18].

The dissolution of Mn has been identified as the main cause of the capacity loss seen in LMO electrodes, and is also at the origin of the increase in the polarization through the contamination of the electrolyte and deposition on to the negative electrode. Furthermore, the limited high temperature performance of $LiMn_2O_4$ is attributed to failure mechanisms which vary depending on whether or not the cell is in a charged or discharged state [20].

When in a charged (high potential) state, electrolyte degradation occurs such that reactions with the SEI layer of the Li_xC_6 electrodes occur. The product of this reaction is LiF, which accumulates over time or upon cycling and contributes to irreversible capacity loss as the lithium used to form LiF is no longer available for subsequent cycles. [20]

In the discharged state (low potential), capacity fading is also associated with an irreversible loss of lithium which is linked to reactions on the positive electrode. In this case, the reasons for capacity loss are the

dissolution of Mn into the electrolyte following a disproportionate distribution of Mn^{3+}. This results in soluble Mn^{2+} species + Li^+ + H_2O which react with PF_6 salts thereby creating hydrofluoric acids, starting the destructive process again. [20]

$LiNiCoAlO_2$ (NCA)
Lithium Nickel Cobalt Aluminum Oxide

In NCA batteries, the increase of interfacial resistance at the positive electrode has been reported to be the primary factor affecting the capacity decay and the power fade of the battery [20] [36] [37]. Many studies on positive electrodes have been conducted to explain the structural changes that result from cycling or aging. Among these structural changes is the formation of a layer of NiO-like material, the loss of connectivity between particles, the development of SEI at the surface of the positive electrode, corrosion of the aluminum current collector, or an increase in the contact resistance between the components within the positive electrode.

The quantitative relationship between the deterioration of electrochemical properties and structural/chemical changes of the positive electrode is still unclear. Although no structural changes have been observed in the bulk structure of the NCA positive electrode, a lower valence of Ni was observed after cycling or aging at high temperature. By combining electrochemical, spectroscopic and electron microscopy methods, new insights on the capacity fading and impedance rise of batteries based on NCA positive electrode material were provided [20]. Inactive Ni ions with lower valence than expected are present in the NCA active material. Estimated proportion of inactive Ni ions provides a suitable quantitative explanation for the measured capacity fade of NCA electrodes. The formation of Ni-O phases during Li extraction leads to subsequent oxygen loss.

In addition to its structural instability, the use of NCA cathode material can lead to thermal runaway. The contributions of delithiated NCA sample and electrolyte on the overall thermal runaway mechanism were evaluated by different methods and a mechanism has been proposed. Exothermic reactions of the delithiated cathode occur at temperatures which are close to those at which structural changes in the delithiated cathode occur.

Jungst et al. studied the decrease in the capacity of a lithium-ion battery with a positive electrode of $LiNi_{0.8}Co_{0.15}Al_{0.05}O_2$ and the negative electrode of graphite, which were intended for powering an electric vehicle. The batteries with the SOC of 60, 80, and 100% were stored at 25–55°C and their impedance was periodically measured. The Li-ion battery's impedance steadily increased as a function of storage duration [24].

Wright et al. [42] from [24] analyzed the decrease in the capacity and power of LIB the size 18650 with positive electrodes based on multicomponent lithiated oxides $LiNi_{0.8}Co_{0.15}Al_{0.05}O_2$ and $LiNi_{0.8}Co_{0.10}Al_{0.10}O_2$ and negative electrodes of graphite when cycled at 25 and 45°C. At 25°C, the decrease in the power decreased with time linearly, whereas at 45°C, proportionally to the root square of the cycling duration. Wright et al. postulated that the drop of the power and the capacity of all the tested batteries (proportionally to the root square of the cycling duration) was caused by the thickening and modification of a layer of solid electrolyte (solid electrolyte interface) at the surface of electrodes and by modification of properties of the separator.

$LiNiCoMnO_2$ (NMC)
Lithium Nickel Manganese Cobalt Oxide

The electrochemical stability of NMC depends on the upper cut-off voltage during charging, and the material shows rapid capacity decay when charged at high voltage. A plateau in the high voltage region (>4.5 V vs. Li/Li^+) is observed during the first charge. It leads to an irreversible capacity loss proportional to the degree of over-lithiation but the capacity can be recovered by a deep discharge. The high-voltage plateau is explained by

structural changes due to oxygen loss from the NMC during lithium extraction. It can also be shown that over-lithiation stabilizes the structure during delithiation, thereby improving the cycling stability [20].

Structural rearrangements of delithiated NMC have been observed after aging at 70°C for 60 days. They were attributed to oxygen release and cation rearrangement. Moreover, changes in the stoichiometry of the transition metals have been reported in aged NMC materials. Thus, the ratio of Ni to Mn and Ni to Co became much greater than 1 near the surface of the NMC particles. It appeared that NMC particles present a strong reactivity towards the electrolyte solution [20].

$LiCoO_2$ (LCO)
Lithium Cobaltite

Aurbach et al. [38] performed a study on the electrochemical behavior and surface chemistry of $LiCoO_2$ cathodes as a function of cycling and storage at 25, 45, and 60°C and showed that, during prolonged storage and/or cycling at elevated temperatures in an electrolyte containing $LiPF_6$, positive electrodes based on lithium cobaltite undergo noticeable degradation. The major reason for the degradation of a battery as determined by the authors of [38] is not so much the change in the composition of the active mass of the positive electrode so much as the processes occurring on its surface. These processes are caused by the formation on a cobaltite electrode of a film of LiF, which forms as a result of interaction of lithium cobaltite with traces of hydrofluoric acid. This film leads to an increase in the impedance of the positive electrode, thereby impeding lithium ion migration through the SEI.

Lithium cobaltite may find itself subjected to chemical dissolution, which leads in particular to the formation of Co^{2+}. The Co^{2+} ions can then undergo discharge at the surface of the negative electrode. The authors of [104] in [24] reported on a direct link between the amount of metallic cobalt at the surface of the negative carbon electrode and the decrease in the capacity of LIB that had been charged to a voltage in excess of 4.2 V (considered here to be an overvoltage). The value of the decrease in the capacity of LIB with a positive electrode based on lithium cobaltite depends on the technology of the preparation of the latter, in the first place, on the character of thermal treatment during the synthesis of the active material [24].

The authors of [61, 62] in [24] showed that the decrease in the capacity of LIB during their cycling could have been caused by the disordering of the layered crystalline structure of $LiCoO_2$, resulting in deactivation of a fraction of lithium ions in the cathode, and by the emergence, in the $LiCoO_2$ particles, of a large number of cracks and pores that hindered the free solid-phase diffusion of lithium ions in the electrode material. The increase in the thickness of the passive film at the surface of the negative carbon electrode as a result of the electrolyte electroreduction also plays a substantial role in the capacity decrease.

Effects of Temperature on Degradation Mechanisms

Broussely et al. [22] performed a comprehensive analysis of the degradation of the capacity of LIB with different depths of discharge (monitored from the LIB voltage), which had been stored for a long time at 15–60°C. A year's storage at 60 and 30°C led to a capacity loss of 15–20 and 7–8%, respectively, as shown in Figure 13. No unambiguous dependence of the degradation on the depth of discharge was discovered.

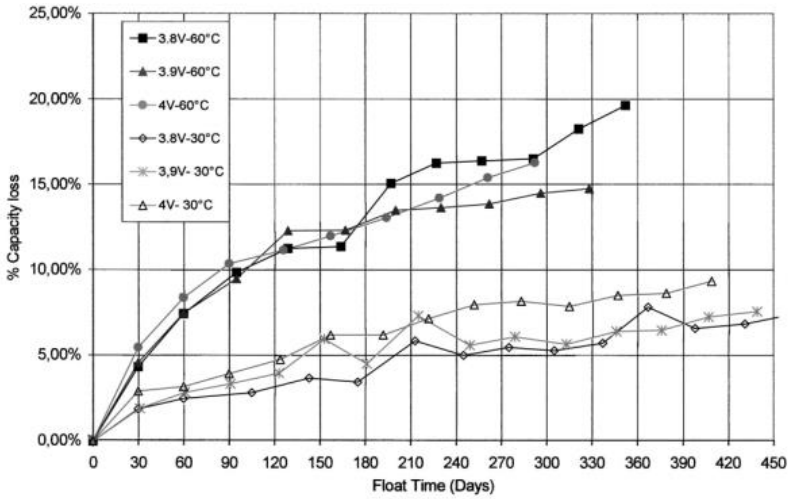

Figure 13 Capacity loss on cells measured at 30°C – C/3, during storage at 60 and 30°C under various voltages **[22]**

Operation of lithium-ion batteries at low temperatures (down to −40°C) can lead to an irreversible decrease in the capacity of the lithium-ion battery. The decrease in the capacity of LIB at low temperatures is usually attributed in the first place to the deposition of metallic lithium on the surface of negative electrodes during a charging process and to complications that a rise with the transport of lithium ions in the bulk of the electrode due to the decrease in the rate of their solid-phase diffusion in the carbon material [24].

In a presentation dealing with Electric Vehicle Battery Thermal Issues [39], Rugh et al. show how at low temperatures the relative resistance and relative capacity of Li-Ion batteries show worsening characteristics as temperature decreases, with resistance sharply spiking around -40°C and capacity also demonstrating a steep dropoff after freezing.

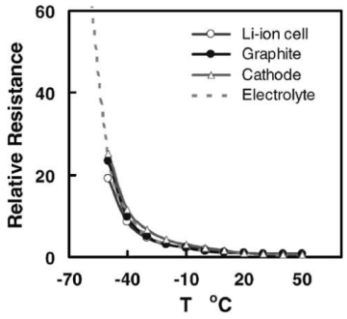

Figure 14 Li-Ion Battery Resistance Increases with Decreasing Temperature **[39]**

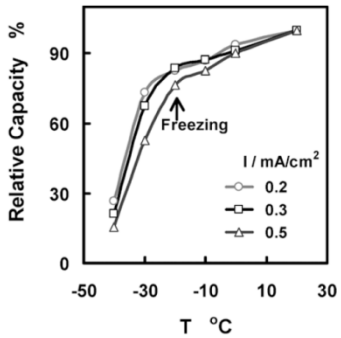

Figure 15 Li-Ion Battery Capacity Decreases with Decreasing Temperature **[39]**

An increase in the activation resistance of the process of discharge of lithium ions and the concentration polarization by lithium ions at low temperatures makes the electrode potential noticeably more negative, which eventually leads to electrodeposition of metallic lithium (lithium plating, as discussed in Degradation of the Anode) on the carbon surface. The electrolyte reduction on the freshly formed surface of metallic lithium is

responsible for the change in the structure (an increase in the density and thickness) of the solid-electrolyte film on the negative electrode, which is accompanied by an increase in its ohmic resistance, which in turn gives rise to an additional increase in the polarization. Such changes in the surface films lead to a gradual irreversible decrease in the capacity ([166] from [24]). While the discharge capacity changed during cycling to the 15th cycle following a relatively small decrease in the temperature (to –10°C) by no more than 5%, the capacity drop at −20°C amounted to 35%. Returning to room temperature did not lead to restoration of the initial state of the battery: the discharge capacity amounted to a mere 85% of the initial value.

The stability of negative electrodes is also negatively affected by the LIB storage at temperatures in excess of 40°C. The capacity decrease of fully charged carbon electrodes during storage is always smaller than that of fully discharged electrodes ([105] from [24]). The reason for this phenomenon is thought to be the destruction of the surface film of a solid electrolyte, which leads to continuous delithiation of the bulk of the electrode with a subsequent interaction of lithium atoms with the electrolyte, i.e. to irreversible self-discharge of LIB.

To evaluate the contribution made by the negative electrode to the self-discharge of LIB in a three-electrode cell with a lithium counter electrode and a lithium reference electrode, Yazami et al. [169] investigated the decrease in the capacity of a carbon electrode subjected to a tenfold cycling and then stored at 70°C. For the electrolyte they employed 1 M $LiPF_6$ in an EC–DMC mixture. Based on the impedance investigations (the electrode impedance perceptibly increased after storage) and charge–discharge characteristics (the electrode capacity dropped by 1.5–2.5 times as a function of the storage duration), the authors of [169] make the conclusion that, during storage at an elevated temperature, lithium that was intercalated into carbon diffuses out of the space between graphene planes towards their external surfaces, thus making it easier for the chemical reactions between lithium and electrolyte and its impurities to occur. The deposition of the products of these reactions at the electrode surface is responsible for the impedance increase, which in turn compromises the discharge characteristics [24].

The effect of elevated temperatures during storage on the negative carbon electrode was investigated in [170]. In new condition, the prepared electrode contained no noticeably pronounced film, whereas after storage at 50°C to 75°C, the surface was covered by a solid-electrolyte film of varying, non-uniform thickness (40 to 200nm). After 40 days in storage, the measured impedance of the negative carbon electrode increased by 8, 28, and 35% respectively, whereas reversible capacity decreased by 5, 12, and 18% respectively for storage temperatures of 50°C, 65°C, and 75°C ([170] from [24]).

The degradation of LIB and the decrease in the their capacity after storage at elevated temperatures (up to70°C) may be caused not only by destructive processes on negative electrodes but also by quite a number of processes occurring on positive electrodes.

Amine et al. ([16] from [24]) were studying the conservation of the capacity and stability of LIB the size 18650 with the chemical composition of graphite–$LiNi_{0.8}Co_{0.2}O_2$ along with an electrolyte of $LiPF_6$ in an equimolar mixture of EC and DEC, which was then stored at temperatures ranging from 40 to 70°C. The observed degradation of the LIB (in the first place, the decrease in the discharge capacity) was accompanied by a considerable increase in the impedance of the positive electrode, which was connected, in opinion of the authors of [16], with an excessive increase in the thickness of the solid-electrolyte film on the electrode. The correctness of this assertion is confirmed by the results obtained in [172, 173], whose authors used a variety of methods to investigate the properties and composition of surface films on the positive electrode based on LiNi0.8Co0.2O2 after a sufficiently long storage at elevated temperatures in an electrolyte based on $LiPF_6$. It was established that after storage the solid-electrolyte film contained a large amount of LiF; in so doing, the weight of the film after storing LIB at 70°C was greater than that after storage at 50°C by 10%.

During storage at elevated temperatures and when discharged by high currents, when the temperature inside LIB may exceed 80°C, there can occur a phase transformation of cobaltate and a disproportionation of $Li_{0.5}CoO_2$ to $LiCoO_2$ and Co_3O_4 [24].

When stored in conditions of an elevated temperature, $LiMn_2O_4$ may also be subjected to disproportionation ($2Mn^{3+} \leftrightarrow Mn^{4+} + Mn^{2+}$). In the presence of hydrofluoric acid, which forms as a result of hydrolysis of $LiPF_6$ at an elevated temperature, the spinel undergoes dissolution. [18]. Water generated in this reaction accelerates the electrode degradation and the capacity sharply decreases [24].

Jungst et al. [40] performed a study wherein Li-ion cells were stored at 40, 50, 60, or 70°C for times of 2-8 weeks for the calendar and cycle life aging studies. Some cells were maintained at a single SOC (60 or 80%) for the calendar life tests, while others were cycled at a defined ΔSOC of 3, 6, or 9%. The chemistry used in the high-power cells was a mixed metal (Ni/Co) oxide cathode material, a graphite carbon anode, and an ethylene carbonate / diethyl carbonate (DEC) electrolyte containing 1M $LiPF_6$ salt. Here, it was shown that the total impedance is significantly increased after aging and that most of the change occurs in the cathode interfacial impedance.

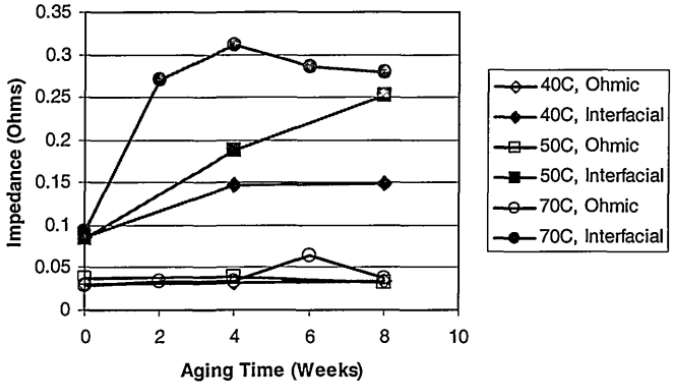

Figure 16 Changes in Interfacial Impedance and Ohmic Resistance after Aging at Different Times and Temperatures. **[40]**

Interfacial impedance and ohmic resistance values were compared at high SOC. Figure 16shows these results for three different aging temperatures. The largest step increase in the interfacial impedance occurs after the first aging interval at 40 or 70°C and thereafter it nearly levels off. At 50°C, the interfacial impedance continues to increase for at least 8 weeks. The total increase is largest at the highest temperature [40].

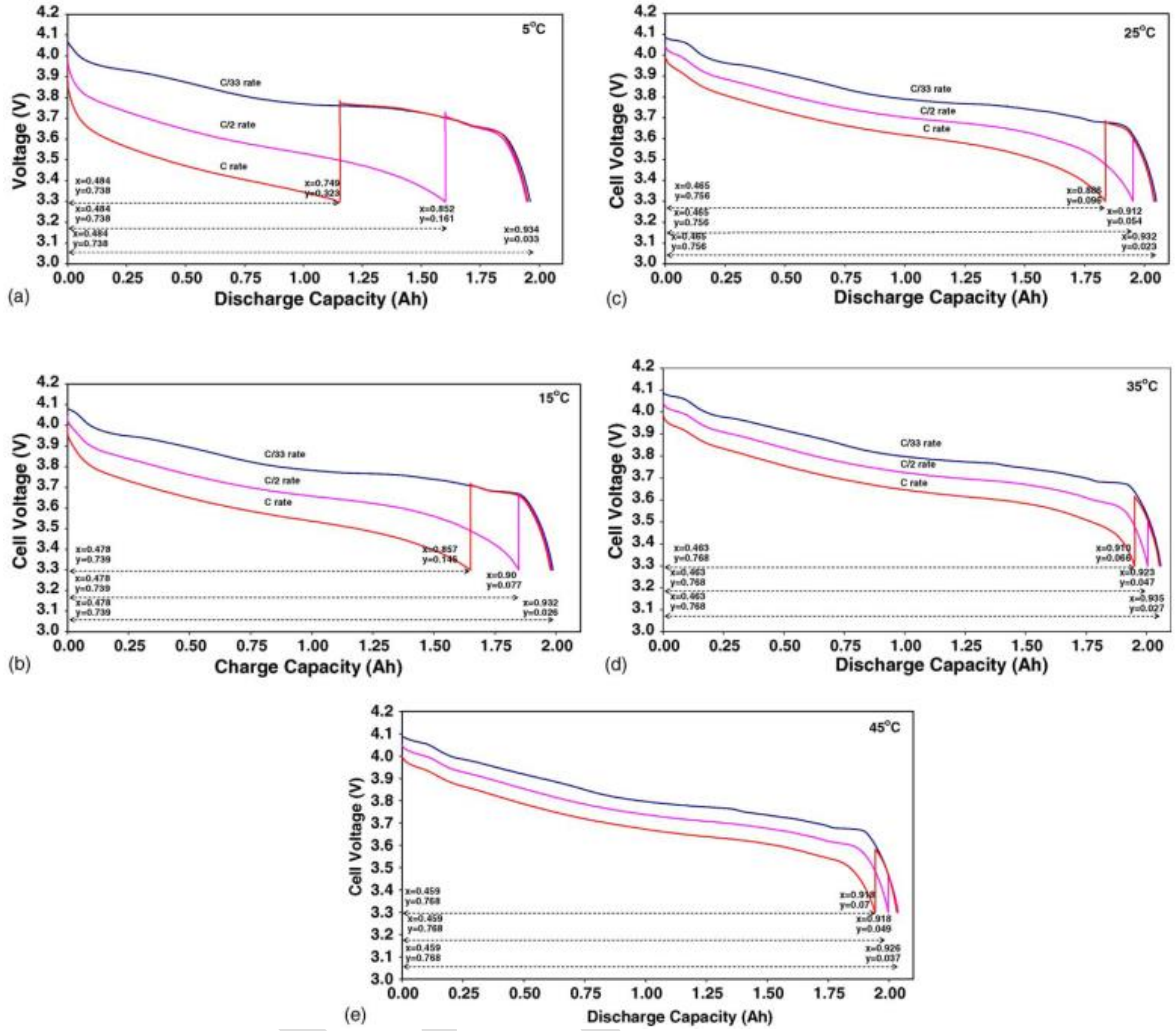

Figure 17. Rate capability at various temperatures. The vertical lines of curves at the end of C/2 and C rates correspond to the 30 min relaxation period. The states of charge of anode (y in Li_yC_6) and cathode (x in Li_xCoO_2) are given at the beginning and end of discharge at each rate. (a) 5 °C, (b) 15°C, (c) 25°C, (d) 35°C and (e) 45°C. **[21]**

Effects of Cycling on Degradation Mechanisms

The majority of the SEI forms during the first cycle of the battery, and this continues to grow slowly over the remainder of the battery's lifetime. During this first cycle, reduction reactions of the electrolyte additives occur on the surface of the active material. The chemical reduction reactions for ethylene carbonate (EC), propylene carbonate (PC), dimethyl carbonate (DMC), and diethyl carbonate (DEC) are described in Eqs. (4.1) – (4.12) in [41].

Effect of Fast Cycling

A study at Sandia National Laboratories was conducted in order to observe the effect of cycling on $LiCoO_2$ [42]. In addition to the cathode for this study being $LiCoO_2$, the anode material selected was mesocarbon microbeads (MCMB).

Cycling at two different rates, C/2 ("fast") and C/5 ("slow"), was performed, and the entropy profiles of the cycled electrodes in half-cells were subsequently measured. Cycling results (capacity vs. cycle number) for half-cells cycled at C/2 (the "fast" rate) are shown in Figure 18. The first five cycles are formation cycles, in which the charging rate was C/5 and the discharge rate was C/2. Only a small number of cycles were studied at this fast rate, so the cycling was performed in half-cells without concern for lithium dendrite formation at the

anode. As shown in Figure 18, cycling capacity after 20 cycles was 20% lower than the initial discharge capacity. This represents a significant amount of cycling-induced degradation. The loss in capacity is wholly attributable to the $LiCoO_2$ electrode because the molar amount of lithium at the lithium metal electrode was in great excess of that at the $LiCoO_2$ electrode**.** Any lithium lost to side reactions at the cathode (electrolyte decomposition and electrochemical formation of passivating surface layers) would be readily replenished upon discharge with lithium from the anode. Thus, the loss in capacity at the $LiCoO_2$ cathode was due to changes in the composite electrode or the $LiCoO_2$ itself and not simply to a depletion of electroactive lithium in the cell. The OCP and entropy (as dE/dT in mV K-1) of $LiCoO_2$ electrodes after cycling at C/2 rate are shown in Figure 19. The full ~140 mAh g^{-1} capacity was recovered during the performed thermodynamics measurements on account of the cells being charged at such a slow rate (one-hour charging steps at C/20 with open-circuit rest periods of 20-24 hours between steps, for an effective rate of ~C/500). In that case, there were only minor changes in full cell OCP after 1000 cycles at C/2 despite ~30% losses in cycling capacity. In the view of the authors of [42], the loss in cycling capacity at the C/2 rate is purely due to kinetic effects and not to a fundamental change in the thermodynamics or structure of $LiCoO_2$. Examples of kinetic degradation effects are the continued growth of the passivating layer on the cathode (which would cause increasing ohmic and transport barriers) and particle breaking or cracking (which would increase ohmic resistance and create electrochemically inaccessible regions of $LiCoO_2$).

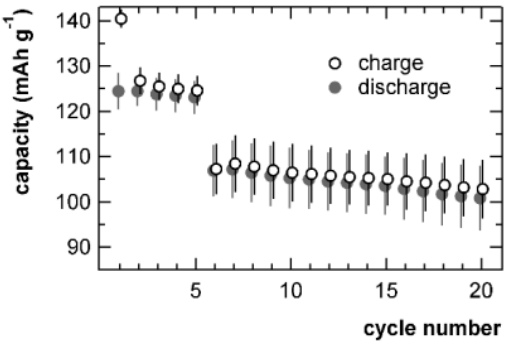

Figure 18. Specific (gravimetric) capacity of galvanostatically cycled half-cells containing $LiCoO_2$ cathodes and lithium anodes. Cycling rate was C/5 (charge) and C/2 (discharge) for the first five cycles and C/2 (charge and discharge) thereafter. [42]

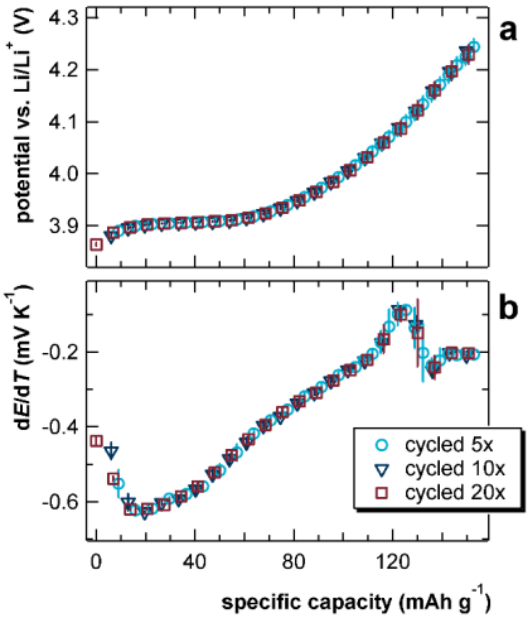

Figure 19. (a) Open-circuit potential and (b) dE/dT of half-cells containing $LiCoO_2$ cathodes and lithium anodes after cycling according to the conditions in Figure 18 (C/2 rate). **[42]**

Furthermore, Aurbach et al. [38] concluded that capacity loss in $LiCoO_2$ electrodes resulting from cycling or storage was due to surface phenomena and not structural changes. The effect of particle cracking or breaking was previously observed using transmission electron microscopy (TEM) on $LiCoO_2$ particles that had been cycled 50 times at C/5 rate or 286 times at 1C rate. Thus, the previous reports and the results reported here are all in agreement that kinetic degradation effects are a significant contributor to cycling-induced performance losses in cells with $LiCoO_2$ cathodes. [42]

Effect of Slow Cycling

For longer-term cycling experiments, a slower rate of C/5 (relative to $LiCoO_2$) was used. Capacity data for full cells ($LiCoO_2$ vs. MCMB) cycled at C/5 (the "slow" rate) are shown in Figure 20. The first five cycles are formation cycles (for SEI growth), in which the charging rate was C/10 and the discharge rate was C/5. The use of full cells is a closer representation of commercial, rechargeable, lithium-ion batteries and allows high amounts of cycling without concern for dendrite formation. As shown in Figure 5.5, cycling capacity after 500 cycles was 46% lower than the initial discharge capacity. The loss in capacity in these full cells is not readily attributable to either the $LiCoO_2$ electrode or the MCMB electrode because the capacities of both electrodes were roughly matched. Any lithium consumed in side reactions (electrolyte decomposition and electrochemical formation of passivating surface layers) would be irreversibly lost and at least partially responsible for the loss in cycling capacity.

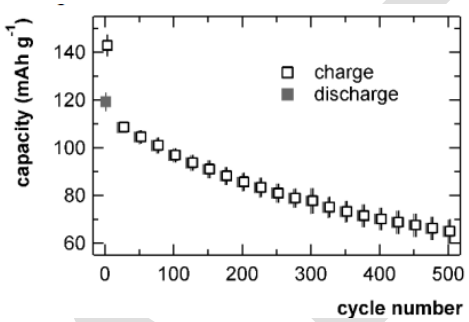

Figure 20 Specific (gravimetric) capacity of galvanostatically cycled cells containing $LiCoO_2$ cathodes and MCMB anodes. Cycling rate was C/10 (charge) and C/5 (discharge) for the first five cycles and C/5 (charge and discharge) thereafter. Markers and error bars are the average and standard deviation, respectively, of measurements from three identically prepared cells.

Studies of commercial lithium-ion cells previously demonstrated that the $LiCoO_2$ cathode was largely responsible for voltage fade, and the graphitic anode was largely responsible for capacity fade. However, it was shown by experimentation that both electrodes experienced both types of performance degradation to some extent. After cycling at C/5 to the designated number of cycles (5, 200, or 500), the full cells were disassembled and examined. The OCP and entropy (as dE/dT) of these $LiCoO_2$ electrodes after cycling are shown in Figure 21. The OCP and entropy profiles of electrodes that were cycled five times (Figure 5.6) match those of uncycled electrodes (Figure 5.2) very closely. As shown in Figure 21, electrodes that were cycled 200 and 500 times lost a significant amount of capacity. They did not reach the 140 mAh g^{-1} full capacity even at this low effective rate of ~C/500. This suggests that a significant amount of the loss in cycling capacity of the full cells was due to degradation of the $LiCoO_2$ cathode. Some of the capacity loss could also be due to a slight loss of material in transferring the electrode from a spent, full cell to a new half-cell. Regardless of the latter possibility, $LiCoO_2$ electrodes that were cycled 500 times at C/5 and re-assembled into new half-cells had severe rate limitations. This suggests that the kinetic effects discussed above (surface resistance and particle cracking) were also a significant contributor to the performance losses of $LiCoO_2$ electrodes cycled at the slower rate of C/5. [42]

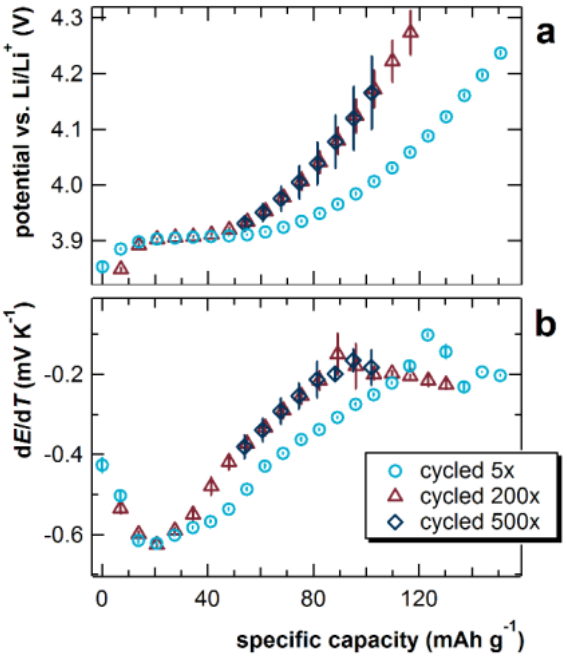

Figure 21 (a) Open-circuit potential and (b) dE/dT of half-cells containing $LiCoO_2$ cathodes and lithium anodes. The $LiCoO_2$ electrodes were cycled in full cells (vs. MCMB) according to the conditions in Figure 20 (C/5 rate), removed from the full cells, and then placed in new half-cells for the measurements in a and b. Markers and error bars are the average and standard deviation, respectively, of measurements from three identically prepared cells **[42]**.

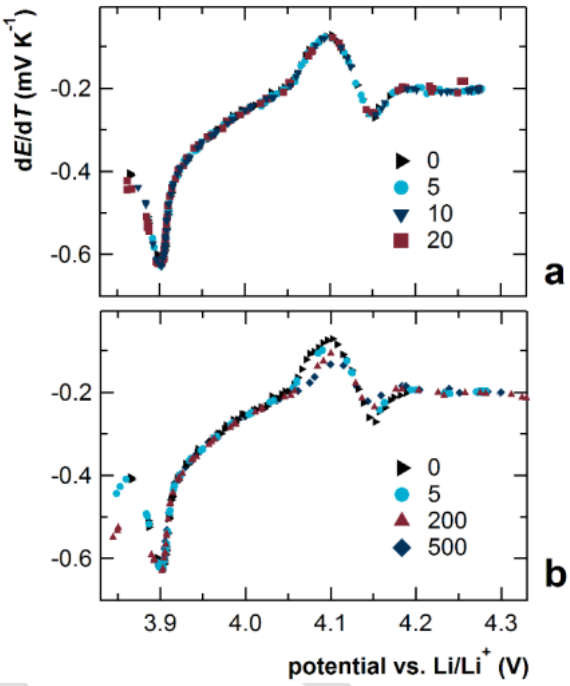

Figure 22. Thermodynamic data for LiCoO2 from Figure 19 and Figure 21 expressed as dE/dT vs. OCP (entropy vs. Gibbs free energy). The $LiCoO_2$ electrodes were cycled at (a) the "fast" rate of C/2 and (b) the "slow" rate of C/5, and the number of cycles is shown in the legends. All of the data points from three identically prepared cells for each condition (cycling rate and number of cycles) are shown individually **[42]**.

The profiles of $LiCoO_2$ electrodes that were cycled 200 and 500 times appear to have retained the same general shape as those of uncycled electrodes. However, the loss in capacity with cycling resulted in a loss of resolution in the OCP curves and entropy profiles, as shown in Figure 5.6. Furthermore, the samples that experienced high amounts of cycling exhibited larger amounts of error. These factors make it difficult to determine whether there were any real changes in the thermodynamic quantities of $LiCoO_2$ after cycling or whether the observed changes were primarily due to a loss in capacity. The two dependent variables have a unique relationship because OCP changes monotonically with the independent variable, gravimetric capacity. Thus, any changes in the thermodynamics can be observed clearly and independently of changes in total capacity. Furthermore, each replicate data point can be plotted separately (as entropy vs. OCP for an individual sample cell) rather than plotting averages of replicate samples. This results in higher-resolution data as the slight OCP variations among repeat samples result in a more continuous entropy curve. Both fast-rate and slow-rate data are presented in this manner in the following section. [42]

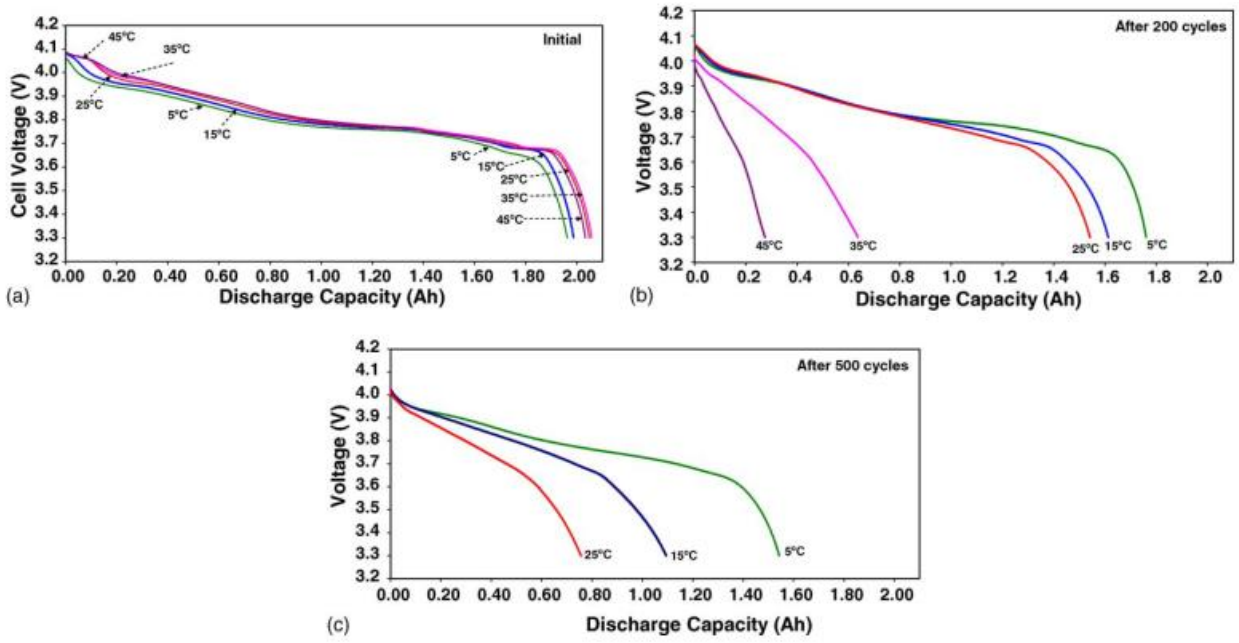

Figure 23 (a) Comparison of slow rate (C/33) discharge profiles before cycling. (b) Comparison of slow rate discharge profiles at the end of 200 cycles. (c) Comparison of slow rate discharge profiles at the end of 500 cycles. **[21]**

Effects of Depth-of-Discharge on Degradation Mechanisms

Shim et al [43] performed tests using $LiNi_{0.8}Co_{0.15}Al_{0.05}O_2$/graphite lithium-ion pouch cells which were cycled over 100% DOD at both room temperature and 60°C so as to investigate the effect of high temperature degradation mechanisms. For the cells used in their experiments, they were subjected to a formation cycle by charging and discharging at a rate of C/25, which allowed for the initial SEI layer to form smoothly. Following this procedure, the cells were charged to 4.1V and held at this voltage until current dropped below C/20 or for two hours, whichever came first. Discharging was performed with a constant current until 3.0V was reached, considered to be 100% DOD.

Cycling of the cells was conducted as follows: 10 cycles at C/5, C/2, C, and 2C. Following cycling at these rates, the cells were subjected to 100 cycles at a rate of C/2. Each cell underwent a total of 140 cycles. The capacity losses are shown in Figure 24.

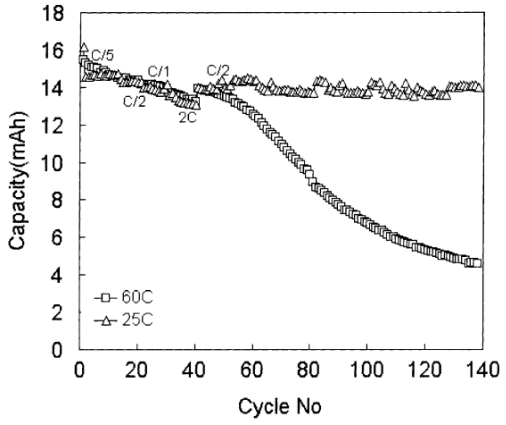

Figure 24 Cycling performance for pouch cells at 25 and 60°C. Cut-off voltage 3.0-4.1V [43]

As much as 65% of the initial capacity was lost after 140 cycles at 60°C. The authors of [43] concluded that the loss of cycling capacity and the rise in impedance in the cathode of the cell which was cycled at 60°C was due to a low-conductivity SEI layer forming on the cathode.

Effects of Overcharging and Overdischarging

Under overcharge conditions resulting from forced charging, the negative electrode of a lithium-ion battery is subject to overpolarization. When this occurs, lithium is liable to deposit on the negative carbon electrode. The lithium that was deposited on the negative carbon electrode rapidly reacts with the solvent to form a film which consists of a salt (Li_2CO_3 and LiF [68] from [24]) and other products. This film blocks the pores in the carbon electrode and diminishes the magnitude of its working surface area, which leads to a decrease in the activity of the negative electrode and to the capacity degradation [24].

The number of electrochemical and chemical reactions which occur on an overcharged positive electrode is quite large. The reactions depend on particular conditions: the electrode material, the electrolyte composition, the temperature, and so on. An overcharge may lead to the capacity loss because of the formation of an inert material, for example, Co_3O_4 in the case of a cathode of lithium cobaltite [69] from [24]; $LiNi_2O_4$, in the case of a cathode of $LiNiO_2$ [69] from [24]; and a compound of di-or tetravalent Mn in the case of a cathode of $LiMn_2O_4$ [70] from [24].

The high potentials (sometimes in excess of 4.5 V),which are realized in conditions of overcharge on positive electrodes, may lead to exothermic reactions of oxidation of organic solvents with the formation of gaseous and insoluble solid products (in particular, Li_2CO_3) which block the electrode pores [71] from [24]. The combination most stable against the oxidation happens to be a mixture of EC with dimethyl carbonate (DMC) [72] from [24].

Leising et al. ([15] from [24]) performed a study into the effect of overcharge conditions by analyzing the behavior of model cells of three types: graphite/$LiCoO_2$, Li/$LiCoO_2$, and Li/graphite. Comparing the heat evolution in the said cells, the authors established that the main source of the heat evolution in lithium-ion batteries is the reactions that occur on the positive electrode (in this particular case, based on lithium cobaltite).

Overcharge and overdischarge of rechargeable cells and batteries can occur due to charger failure or cell imbalance within a series/parallel connected battery. During charge, if several cells are connected in series and one has a higher SOC than the others do, it will reach full charge before the others. If the charger is designed to charge series strings (rather than individual cells), as the string reaches full charge, the cell will be overcharged. Modern sophisticated BMS instrumentation can be programmed to detect and avoid this condition. Likewise, during discharge of a battery pack, if one cell has a slightly lower beginning voltage or lower capacity than the others do, it will reach full discharge before the others. If the string is then forced to continue discharging—a situation that can occur if system electronics are not sufficiently smart to identify the condition—it will discharge below 0.0 V into a state of “overdischarge” or “voltage reversal” [44]. This will usually highly degrade the battery’s ability to be recharged. Prolonged exposure to this condition (depth of reversal) can lead to safety problems, such as evolution of hydrogen and oxygen gases in large amounts sufficient to cause cell venting or metal plating on the cathode. In systems where multiple cells are used, a common quality-control standard condition is to use cells that have been matched to within ±5% cell capacity [45].

The ability to withstand overcharge depends strongly on the current level (low charging current is more likely to result in benign failure) as well as the chemistry of the battery. Aqueous electrolyte systems (e.g., lead-acid, nickel/cadmium, and NiMH) are relatively insensitive to overcharge because after 100% SOC is reached, additional current drives the electrolysis of water (which produces hydrogen and oxygen) and limits the maximum voltage that the cell experiences. Cells with an aqueous electrolyte may contain catalysts to recombine the H_2 and O_2 evolved during overcharge to reform water, which will minimize the accumulation of potentially explosive gas mixtures. However, this feature is not widely used in commercial lead-acid batteries and the prevalence of lead-acid battery explosions during charging is the major contributor to more serious injuries attributable to batteries.

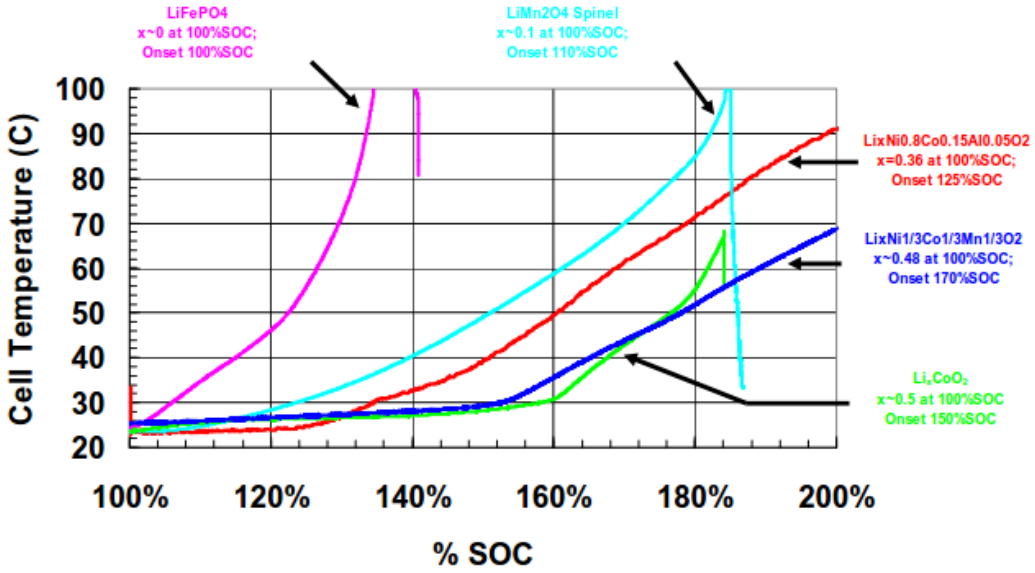

Figure 25. Heat output during overcharge for different cathode oxide chemistries, showing an increase in heat output when final lithium is removed from the cathode. **[46]**

Li-ion and Li-polymer cells have poor response to overcharge abuse when compared with aqueous electrolyte cells because they do not have the protection of water electrolysis as an energy sink. In part, this poor response results from the higher energy content, more reactive electrode materials, and flammable electrolytes that create the potential for thermal runaway during the overcharge event.

The response of cells and battery packs during overcharge depends on overcharge parameters (current, maximum voltage), thermal environment, and cell materials and is a complex function of several failure mechanisms.65 Extended overcharge can result in cell heating that initiates internal decomposition reactions of the electrodes and electrolyte that lead to thermal runaway.

In addition, increased cell temperatures can result in melting of the separator material and subsequent internal shorting of the cell. This behavior is particularly problematic for shutdown separators that result in high-cell impedance at shutdown. For a single cell or a series configuration of cells, the charging power supply will apply the full compliance voltage across the single cell after separator shutdown occurs. Many separator materials have been observed to fail immediately or within a short time after shutdown in this condition, as shown in Figure 10. [45]

The thermal response of Li-ion cells during overcharge is largely determined by the cathode chemistry. During the charge cycle, lithium is removed from the cathode oxide material. Different cathode oxide chemistries have different levels of lithium when fully charged, varying from $Li_{0.5}CoO_2$ to $Li_{0.0}FePO_4$ at 100% SOC. Overcharging continues to remove lithium from the structure, resulting in permanent crystallographic changes and increased oxidation potentials. Measurements of heat flow from the cells and cell skin temperature during overcharging has shown that there is a rapid increase in heat generation when all of the lithium has been removed from the cathode.

If the stability of the cathode becomes sufficiently good, other problems can become the determining factor in cell stability. For example, cells made with lithium iron phosphate cathode materials have the best thermal stability and overcharge stability. $LiFePO_4$ is thermally stable up to 250°C and does not evolve oxygen. The lithiated anode is still a significant source of energy. At high temperature, the SEI protective layer decomposes, exposing the lithiated carbon to the electrolyte. Reduction of the electrolyte can generate sufficient heat to cause a thermal runaway reaction with associated gas generation, venting, and possible fire. The electrolyte itself breaks down above 160°C, generating sufficient gas volume to cause cell venting.

Yamaki et al. demonstrated that overcharge response of a lithiated graphite (LiC_6)/$LiMn_2O_4$ cell depended on charge current; at low current, overcharge test results were benign, but at high current levels, the cells entered thermal runaway. Lithium plating on the anode is a possible failure mode during fast charge at low temperature. Lithium plating has the potential to create a finely divided lithium powder within the cell that may become electronically isolated from the anode. In addition, dendrites of lithium may grow from the anode through the separator, possibly resulting in an internal short circuit. This situation, if it arises, creates a safety vulnerability that could persist after the overcharge event terminated. [45]

Considerations for NiMH Batteries

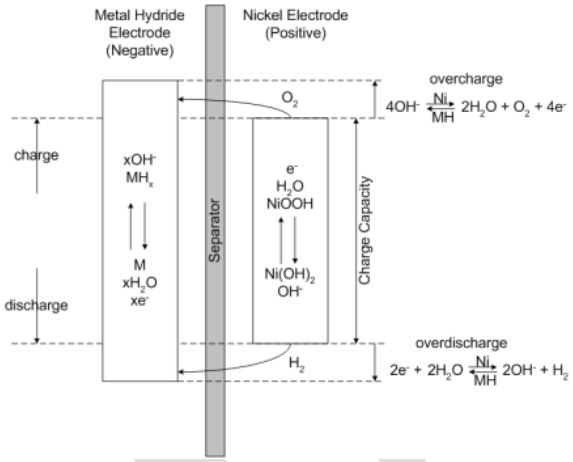

Figure 26 Schematic Representation of NiMH Cell

The active materials in the NiMH battery are composed of metal compounds or metallic oxides [47]. The nickel oxide – hydroxide electrode only exchanges a proton in the charge-discharge reaction and the electron transfer is very rapid, contributing to the power capacity. The small change in size of the electrode between charge and discharge also results in mechanical stability and thereby longer cycle life [47]. We present here the factors which affect the aging characteristics of NiMH batteries.

Overcharge and Overdischarge: it was noted that overcharging causes irreversible chemical reactions which can damage the battery. The reason behind this is that after all the active chemicals have been transformed, forcing more electrical energy will cause some chemical components to break down into forms that cannot be recombined [48]. Overcharging also causes a significant increase in temperature and pressure, which may in turn lead to mechanical failures such as swelling of the battery, short circuits between parts, and interruptions in the current path. Should the overcharging process not be terminated, it will cause the battery to explode and release dangerous chemicals and gases that may cause fire. Excessive discharge also causes permanent damage to the battery and speeds up the aging process Tests have shown that a small amount of overcharging or over-discharging will not cause premature failure of the batteries but will significantly shorten its life. For example, some tests showed that over-charging NiMH batteries by 0.2 V will result in a 40% loss of cycle life just as a 0.3 V over-discharge of lithium-ion batteries can result in 66% loss of capacity [48].

Surface Corrosion of the negative electrode is generally the main cause of NiMH aging. The battery can be operated under ideal conditions through ‘small’ cycles (with a periodic full discharge to reduce memory effects) and still not be able to avoid corrosion of the negative electrode. This failure mode does not cause catastrophic failure, but it does cause capacity loss. The active material of the metal hydride is very conductive, so corrosion at the surface results in a reduction of capacity, as well as, reduction of ability to supply power. The corrosion also has a side effect of reducing the content of water in the electrolyte, which is described later in this section [47].

Decrepitation of Alloy Particles often occurs along with surface corrosion. Normal aging of the battery will cause decrepitation of the negative electrode. This is not technically a failure mode by itself. It only increases the surface area of the electrode, which at first can increase conductivity by increasing the area available for the chemical reactions. However, it also increases the area available for surface corrosion. Some literature suggests that alloy decrepitation and surface corrosion of the negative electrode is the main cause of normal battery aging and can be quantified as a function of DOD with EIS [49].

Loss of Water in the Electrolyte can be caused by a number of conditions, such as surface corrosion, but is mostly encountered during abusive operation. Operating in abusive conditions whether it is overcharge, overdischarge, or improper temperature ranges can cause the pressure inside the battery to build and the gas to vent. Venting the gasses reduces the battery's ability for electrolysis, and thus reduces its power. Another contribution to loss of water in the electrolyte is diffusion through the case only if the case is plastic. This is not a problem with steel constructed casing [47].

Crystalline Formation is the cause of battery memory. If the NiMH battery is not periodically discharged to 0% SOC, then crystals will form around the electrodes of the battery. A full discharge usually restores the electrode surface. However, if not properly maintained, the crystalline surface will grow and can damage the separator. If the growth reaches through the separator, the battery will simply short circuit and be rendered useless [50].

Cell Reversal only occurs through abusive operation, most notably, overdischarging. This is when the electrodes inside the cell become reversed in charge, rendering the battery unable to store and supply energy. [47]

High Self Discharge will not cause catastrophic failure, unless it is to the extreme of an electrical short circuit. All batteries are affected by self-discharge, NiMH being one of the highest. Elevated self discharge occurs along with the growth of crystalline formation. As the crystalline forms out from the electrode, it begins to mar the separator, thus allowing for an easier path from one electrode to the other [50]. Accordingly, the higher the self-discharge, the lower the capacity of the battery.

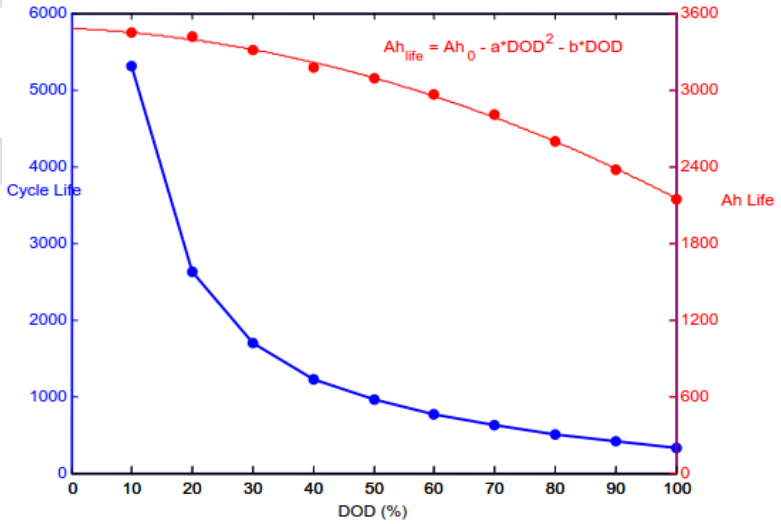

Figure 27 Comparison of cycle life and Ah life (the scale of Ah life is not accurate because it is based on an arbitrary value of nominal capacity. However the shape of the curve is independent from that value). **[48]**

The relationship between the cycle-life and the DOD of an NiMH battery is an exponential one as can be seen in Figure 28. Figure 28 shows that the cycle life is much greater when the DOD in each cycle is smaller. In this example, the battery can survive 5000 cycles if it is discharged by 10% in each cycle, or 500 cycles if the DOD

is 90%. It is important to understand that these results make sense only if the battery is discharged and charged hundreds or thousands of times with the same "current history", i.e. with subsequent identical cycles such as simple square waves or pulses. The model proposed in this paper, instead, is suitable for predicting the battery aging for applications in which the battery is aged with no pre-defined cycles. However, it takes into account the limitation imposed by typical HEV Control Strategies, which are engineered to keep the DOD of the battery above 50% [48].

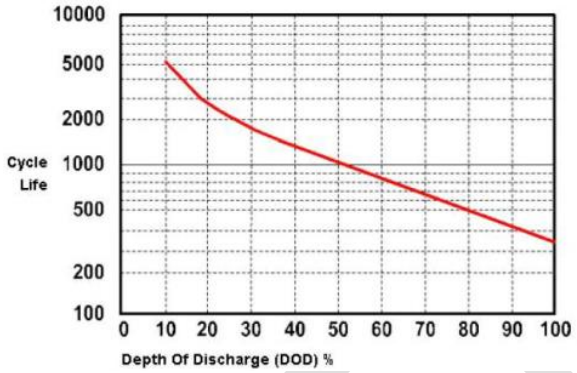

Figure 28 Example of the dependence of cycle life on DOD in a NiMH battery **[48]**

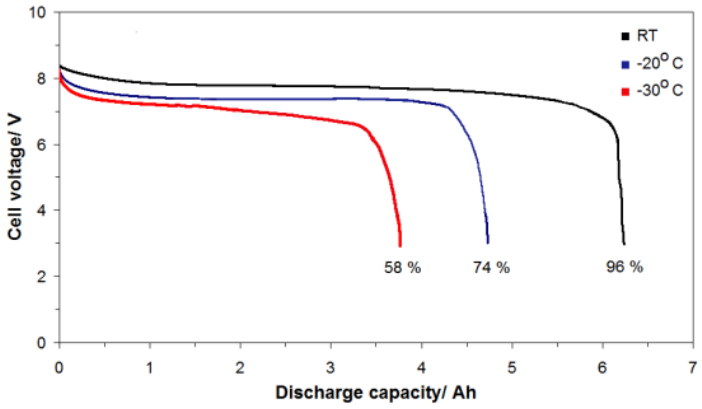

Figure 29. Discharged curves for a 6.5Ah NiMH prismatic battery module, recorded for a discharge rate of 0.15C at: room temperature (RT), -20, and -30°C **[51]**

Pierozynski [51] found that NiMH batteries undergo a dramatic deterioration of electrochemical performance at low operating temperatures, specifically for the temperature range below -20°C, as depicted in Figure 29. This proved to be the case not only for large battery modules as used in HEV applications, but also for advanced AA size battery cells. One of the key reasons for this phenomenon is the kinetics of the charge-transfer reaction at the negative (MH) electrode.

The NiMH chemistry degrades rapidly if cycled at higher ambient temperatures. Optimum battery life and cycle count are achieved at 20°C (68°F). Repeated charging and discharging at higher temperatures will cause irreversible capacity loss. For example, if operated at 30°C (86°F), the cycle life is reduced by 20 percent. At 40°C (104°F), the loss increases to as much as 40 percent. If charged and discharged at 45°C (113°F), the cycle life is only half of what can be expected if used at moderate room temperature [50].

Concluding Remarks on Degradation Mechanisms

The aging of Li-ion batteries is complex and determined by the operating conditions. In some cases it is possible to assign the observed capacity and power fade to a certain aging process. This is typically the case when the battery is used under extreme conditions such as elevated temperatures, high rate charging, or high SOC levels. However, in most applications where the conditions are controlled to optimize the total life the observed performance fade is the result of several processes of which some are coupled and others can be regarded as independent.

Generally, the capacity fade of Li-ion cells is due to a combination of three main processes:

- Loss of Li / loss of balance between electrodes
- Loss of electrode area
- Loss of electrode material / conductivity

The loss of cyclable lithium is in turn due to side reactions such as corrosion, Li-plating and solid electrolyte interface (SEI) formation at the graphite anode.

Since the graphite anode is the most widely used in present Li-ion batteries this study has set a particular interest in this electrode material. In contrast the aging properties of the cathode electrodes must be discussed from case to case depending on the particular cell design.

In addition, aging mechanisms that reduce capacity may also lead to changes in surface properties such as porosity and tortuosity. In this reasoning it is important to state that the available capacity might be reduced further by an increased voltage drop due to a rise in cell impedance that prevents the battery from being fully discharged (or charged) at a specific current. In most cases the capacity fade and impedance rise are clearly correlated. The aging processes are further complicated by the fact that many of the studied mechanisms are coupled to a rise in cell impedance, leading first and foremost to a notable reduction in maximum cell power.

An overview of the most significant mechanisms for power fade / impedance rise is summarized thusly:

- Surface film formation of both electrodes with low conductivity
- Loss of electrode area and electrode material leading to a higher local current density
- Lower diffusivity of lithium ions into active electrode particles and slower kinetics (increased charge transfer resistance) due to surface films
- Reduced conductivity between particles due to both surface films and degradation of binders, possibly in combination with a binder-Li reaction

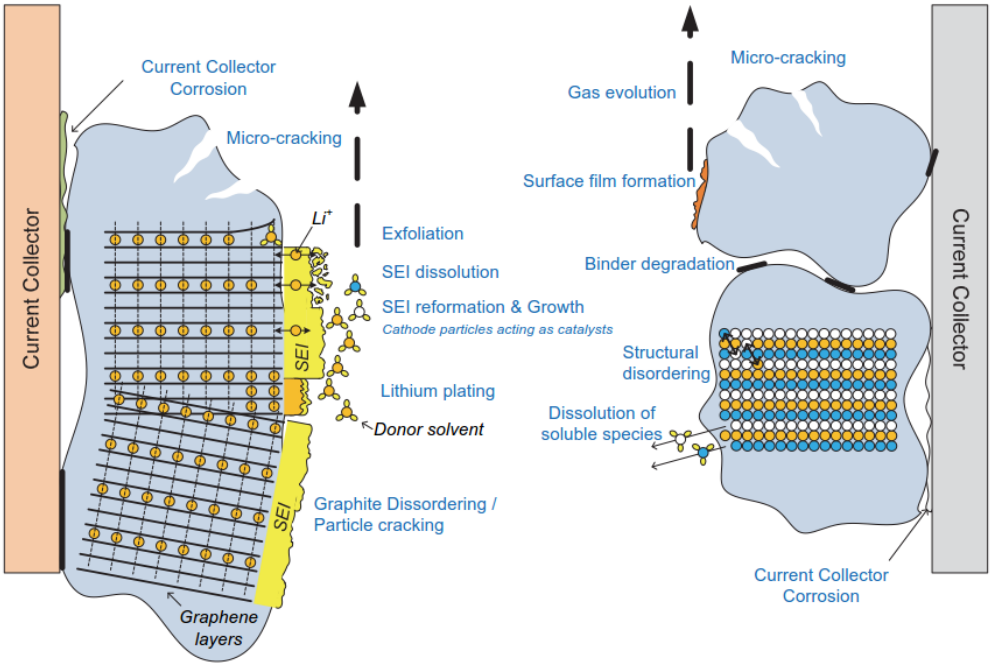

Figure 30 Aging mechanisms occurring at Li-ion battery electrodes **[52]**

A visual representation of the main electrode aging mechanisms, mainly described by Vetter et al. [18], is presented in Figure 30. Here, aging mechanisms can be categorized into mechanical changes (particle cracking, gas formation), surface film formation (SEI, lithium plating), bulk material changes (structural disordering), and parasitic reactions (binder degradation, localized corrosion). The aging mechanisms at the electrodes are directly dependent on the choice of the electrode material. However, there are several similarities between different electrode materials.

Testing Activities & Methodologies for Evaluating xEV Battery Durability

Introduction

In the previous section we have examined some of the electrochemical degradation mechanisms which affect battery durability in the various chemistries utilized for xEV applications. Although the studies from which such information comes involve testing, we now will focus on testing and evaluating durability at a vehicle-level or under vehicle-like conditions. In addition to road and dynamometer tests of vehicles, we shall also investigate laboratory tests of xEV batteries subject to simulated load conditions and model-based studies using vehicle and battery models derived from physical, empirical, and semi-empirical data.

The following categories will be examined:

- Charge Patterns and Optimization
- Climate and Thermal Effects
- Cycling and Depth-of-Discharge
- Fleet & On-Road Testing Activities

It should however be noted that, of course, we cannot consider the factors which impact battery lifetime and durability as being wholly independent of one another. However, the studies presented in this section will largely try to focus on a particular aspect, and observations related to other subsections will be identified and related. As shall be shown, the topic of battery durability, lifetime, and degradation is the result of the various factors working in tandem.

Charge Patterns and Optimization

Electrified vehicles with plug-in capabilities (PHEV, BEV) will by their very nature be subject to charging from external sources. As it presently exists, there are three charging levels, which are shown in Table 5. As part of the study on battery durability, we shall investigate the effect that the method of charging a battery has, including constant-current and smart charging.

Level	Location	V and I	Power (kW)	Approx. time to charge
1	Residential	110V, 15A	1.4	18 Hours
2	Residential / Public	220V, 15-30A	3.3	4-8 Hours
3	Commercial	480V, 167A	50-70	20-50 Minutes

Table 5. Charging Topologies **[53]**

Lacey et al. [54] examined charging under three scenarios: uncontrolled charging, delayed charging, and V2G. These are described thusly:

- Under uncontrolled charging, the BEV is charged up to 80% SOC upon being connected to charging at 6:00pm. The battery then holds this SOC until 8:00am on the following days.
- Under a delayed charging scenario, the EV remains at 40% SOC from 6:00pm until the time when it needs to charge for the next trip at 8:00am.
- In a V2G scenario, the EV is discharged to the grid from the point in time in which it is connected to the grid (6:00pm) until its SOC reaches 10%. It remains at this minimum until it is charged for the next trip at 8:00am. The resting SOC is therefore 10%.

	Charge only (3kW)	Delayed charge (3kW)	Charge only (7kW)	Delayed charge (7kW)	V2G (3kW)	V2G (7kW)
Average SOC	56.5%	51.6%	54.2%	34.6%	32.2%	27.2%
Change in SOC	40%	40%	40%	40%	70%	70%
C/D rate (A)	7.50	7.50	17.50	17.50	7.50	17.50
Degradation after 1000 cycles (%)	4.54%	4.46%	8.00%	7.71%	4.19%	7.63%
Degradation after 8 years (%)	13%	13%	23%	23%	12%	22%
Lifetime (years)	12.1	12.3	6.8	7.1	13.1	7.2

Table 6 Degradation factors for the different scenarios **[54]**

The effect of degradation due to fast weekly fast charging coupled with uncontrolled slow charges of 3kW or 7kW is shown in Table 7.

Battery charging pattern				Degradation	
Home charging per week		Fast charging per month		After 1000 cycles	Time (years) to 80% of new capacity
3kW	7kW	23kW	50kW		
6	0	0	0	1.5%	13.77
6	0	4	0	3.3%	6.09
6	0	0	4	5.7%	3.52
0	6	0	0	2.5%	8.01
0	6	4	0	4.3%	4.62
0	6	0	4	6.7%	2.97

Table 7 Effect of weekly fast charging on battery degradation in comparison with uncontrolled domestic charging **[54]**

The results from [54] demonstrate the effect of fast charging on battery degradation and lifetime. Even in Table 7 we see that charging at 3kW leads to a lifetime in excess of 10 years, going as far as to be in excess of 12

years for each of the 3kW cases, whereas with 7kW charging the battery lifetime is approximately 7 years or less. With fast charging at 23kW or 50kW, degradation is markedly faster, with the worst case shown being a combination of 7kW home charging with weekly fast charging of 50kW, resulting in a lifetime of less than 3 years [54].

A study at the Idaho National Laboratory conducted by Shirk and Wishart [55] looked at four Model 2012 Nissan Leaf vehicles and subjected two of these vehicles to Level 2 Charging (indicated as L2 in the report) and the other two vehicles were subjected to 50kW DC Fast Charging (indicated as DCFC in the report).

For on-road testing, the vehicles were typically driven six days per week, with each vehicle driven on public roads in Phoenix, Arizona, over a prescribed route twice per day. Each day of driving consisted of one route in the morning and the other in the evening for each vehicle. In order to minimize variation in drive-cycle and environmental variables, vehicles from the AC L2 group and DCFC groups were paired together and driven. Vehicle pairs alternated between early and late morning and evening groups daily, such that one pair of vehicles was not consistently driven during a cooler or hotter part of the day, or during rush-hour traffic. Drivers were also alternated so as to remove/reduce bias due to driver habits. Each vehicle was operated with the automatic climate control enabled and set at 72°F.

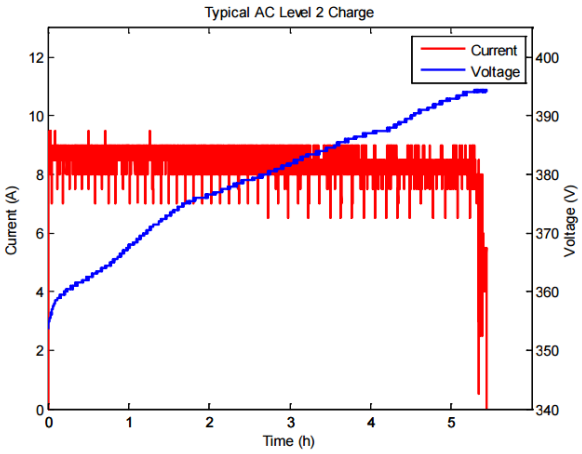

Figure 31 An AC level two charge is shown for a 2012 Nissan Leaf with a 3.3 kW onboard charger [55]

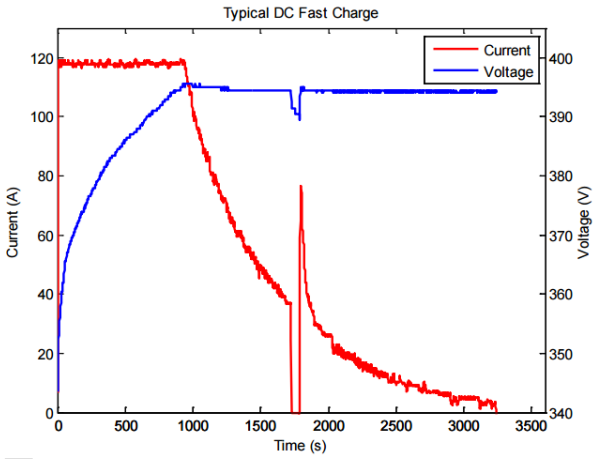

Figure 32 A DC fast charge is shown for a 2012 Nissan Leaf charged with a 50kW fast charger. The charge automatically ended after 1725 seconds, and another charge session was initiated shortly after the first one ended to fully charge the battery [55]

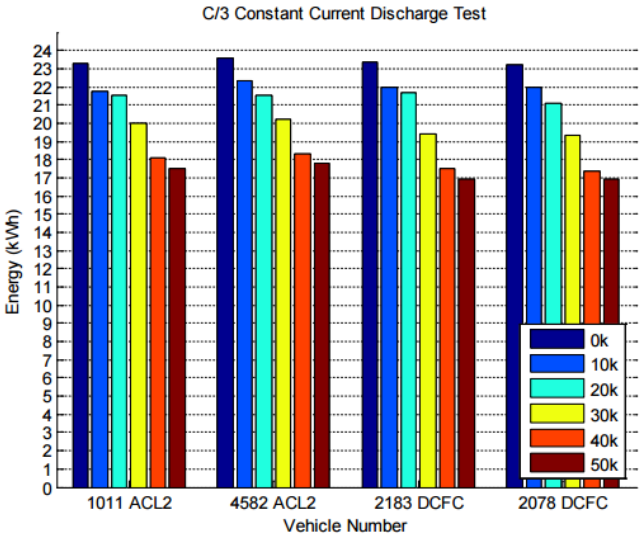

Figure 33 Battery capacity discharged for each pack at 10,000 mile intervals. Each result is the average of three 3-hour constant current discharge tests, falling within 2% of each other. **[55]**

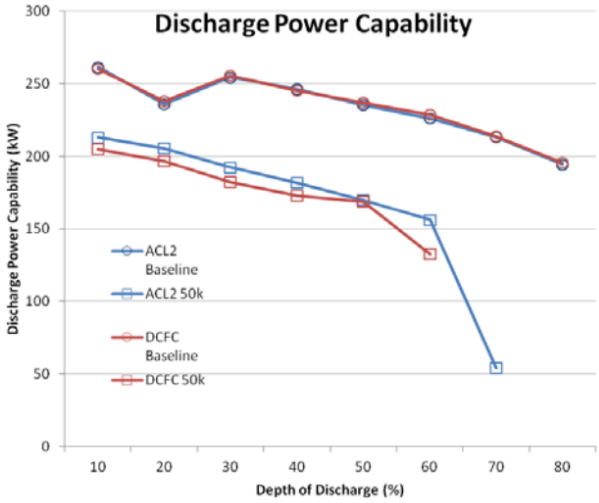

Figure 34 Average discharge power capability versus depth of discharge for ACL2 and DCFC groups at baseline and after 50,000 miles**. [55]**

As shown in Figure 33, the DCFC group shows distinct differences in capacity loss compared to the ACL2 group, noticeable beginning with the 30,000 mile test results. Figure 34 shows power capability vs. DOD for the baseline and 50,000 mile marks.

Despite exceeding the manufacturer-recommended amount of fast charging, the four BEVs operated without failure for 50 thousand miles. The vehicles which belonged to the group which underwent fast charging was observed to suffer from a greater loss in battery capacity when compared to L2-charged vehicles [55]. Being in Phoenix, Arizona meant that the high ambient temperatures also had an influence on the battery life. We will explore some of these effects in the section of the report which deals with Climate and Thermal Effects.

Bashash et al. [56] examined the problem of charge pattern optimization with PHEV applications for the purpose of optimizing energy cost and battery life. Specifically, they sought to simultaneously minimize (i) the total cost of fuel and electricity and (ii) the total battery health degradation over a 24-h naturalistic drive cycle.

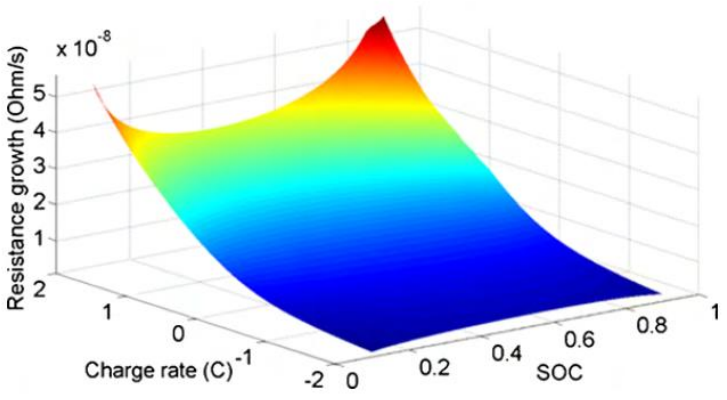

Figure 35 Battery degradation map **[56]**

To analyze degradation characteristics, the authors of [56] initialized their model at different SOC levels and applied currents at different rates to charge and discharge the battery. Average resistance growth is monitored. Figure 35 depicts the obtained map for an SOC range of 10–90% and a charging rate of −2C to 2C, with negative sign indicating discharge. The degradation map shows that at the low and high SOC ends the battery tends to degrade faster, especially when it is subject to high-rate charging. Additionally, battery degradation

takes place at a slower pace during charge depletion, compared to charging or storage. [56]. The optimization procedure is performed using the NSGA-II genetic algorithm. Some of the optimized solutions are shown in Figure 37.

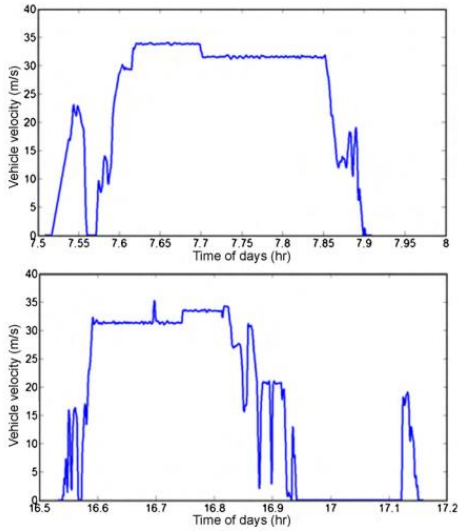

Figure 36. A sample suburban naturalistic drive cycle with two half trips, one in the morning and one in the afternoon (vehicle velocity is zero during the rest of the day) [56]

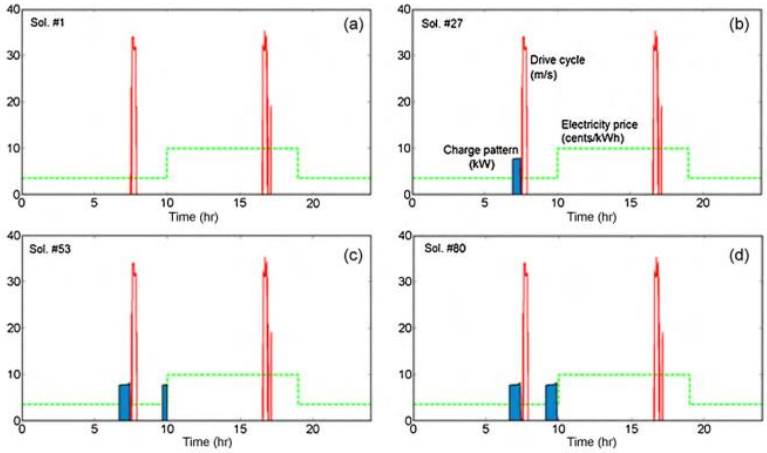

Figure 37. Four sample optimal PHEV charge patterns corresponding to: (a) Sol. #1 (least battery degradation), (b) Sol. #27, (c) Sol. #53, and (d) Sol. #80 (least energy cost). The red drive cycle spikes represent the drive cycles described in Figure 36 **[56]**.

The authors of [56] describe their obtained solutions thusly:

- The first solution shown, depicted in Figure 37(a) corresponds to the least battery degradation solution. There is no charge added to the battery, and thus, the SOC remains at the lowest limit for all time. The battery receives no external charge, and the PHEV operates as a conventional HEV.
- The second selected solution, i.e., Sol. #27, trades off the energy cost and battery health objectives with more preference towards battery health. As depicted in Figure 37(b), a charge amount of about 50% is added to the battery before the first trip only, and the charging is delayed until before the start of the trip. The reason for this delayed charging is to avoid the unnecessary degradation due to storage at high SOCs, and the best way to achieve this is to deplete the battery soon after charging.
- Solution #53 also trades off the optimization objectives, but with more weight on energy cost. As seen from Figure 37(c), both trips include charging, with the first trip receiving full charge (65%) while the second one receiving about 30% added charge. The first charging is delayed until the first trip departure time, while the second charging is delayed until the time of transitioning to on-peak electricity pricing. Therefore, PHEV charging takes place during off-peak hours only.
- The last solution, i.e., Sol. #80, corresponds to the charge pattern that results in the least energy cost. The only difference between this solution and Sol. #53 is that the PHEV receives full charge before both trips.

In another study by Hoke et al. [57], the focus on charging optimization was strictly on extending battery lifetime. The charge optimization method seeks to minimize the effects of three factors that lead to battery degradation: temperature profile, daily charge cycling (depth of discharge), and state of charge profile. To obtain driving data, a typical driving week for a Toyota Prius PHEV was sampled at 1Hz. This included five days of commuting 26-40 km (16-25 miles) round-trip, one longer trip of 65 km (40 miles), and one day on which the vehicle was not used [57]. Five charging scenarios are considered:

1. Full nightly charging at 6.6 kW (SAE level 2) to 90% SOC upon plug-in, without regard for battery degradation.
2. Full nightly charging to 90% SOC, with charge power profile optimized to reduce battery degradation.
3. Partial nightly charging as needed to provide for the next day's driving, optimized to reduce battery degradation. An ideal ability to perfectly predict the next day's energy requirement is assumed.
4. Partial nightly charging as needed to provide for the next day's driving with 16 km (10 mi) spare range, optimized to reduce battery degradation.
5. Partial nightly charging as needed to provide for the next day's driving one hour before departure and with 16 km spare range, optimized to reduce battery degradation.

The state of charge profiles for these scenarios are shown in Figure 38.

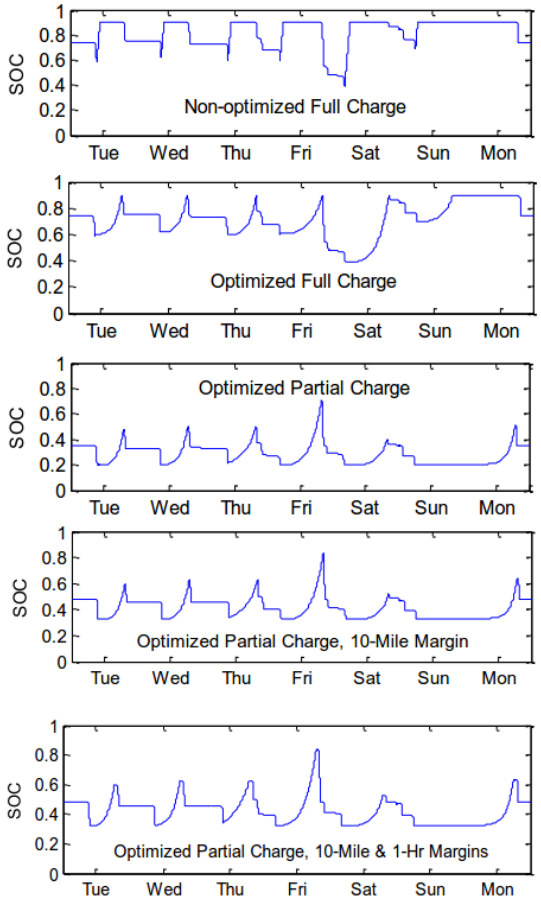

Figure 38 Weekly SOC profiles for the four charging methods. Horizontal axis labels indicate the beginning (midnight) of each day. **[57]**

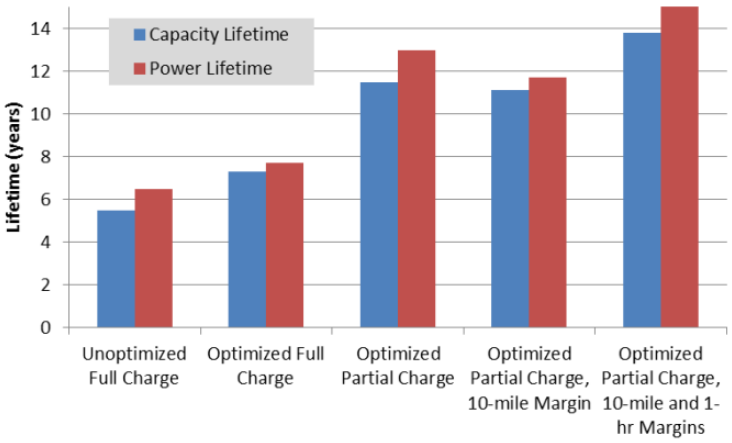

Figure 39 Comparison of battery energy and power lifetimes under the five charging scenarios. One power lifetime result over 15 years is truncated. **[57]**

As part of a NREL study, Neubauer and Wood [58] sought to assess the impact of realistic fast charging scenarios on BEV batteries, including thermal and degradation effects. The model-based experiment was conducted over a simulated 10 years of battery simulators for 180 driving profiles with added conditions for Level 2 home charging and Fast Charging station availability in two different climates (Seattle, WA and Phoenix, AZ). Additionally, the effects of battery thermal management systems were evaluated in three grades: passive cooling, high-power liquid cooling (active during driving), and high-power liquid cooling (active during both driving and charging).

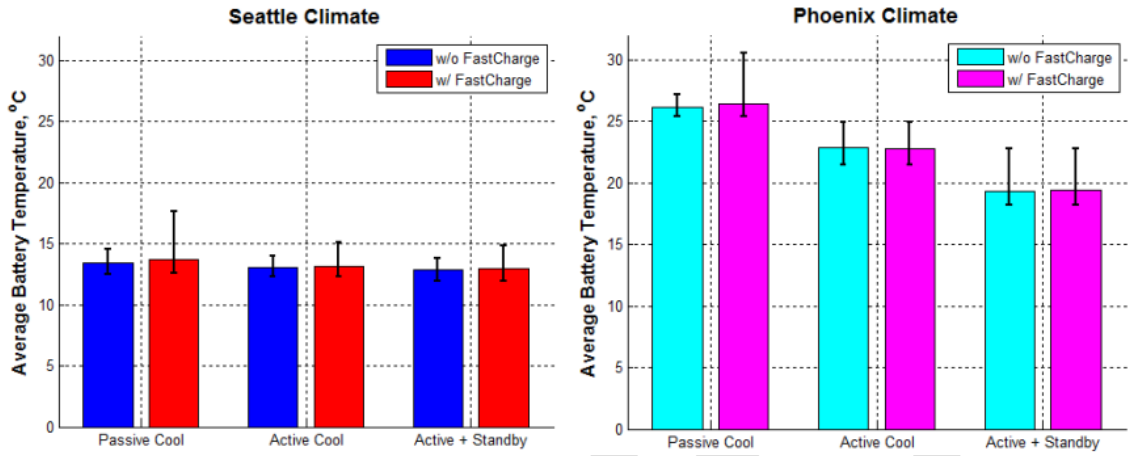

Figure 40 Effect of DCFCs and BTMSs on average battery temperature in Seattle (left) and Phoenix (right) **[59]**

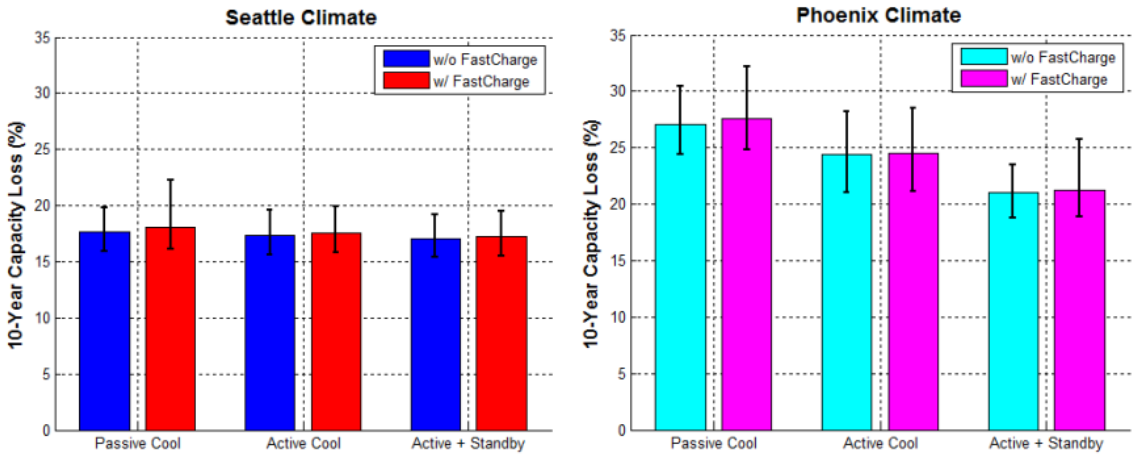

Conclusions from the study were that aggressive active battery cooling is important for constraining maximum battery temperatures, particularly for long fast-charge-enabled tours in hot climates, active battery cooling can also positively impact battery lifetime in hot climates when utilized while parked at a charger in addition to while driving [58]

A study by Krieger [29] presents a comparison of lead-acid, LCO-NMC, LCO and LFP cell degradation when charged with a wind-based current profile to evaluate the impact of variability on cell aging and consider alternative battery chemistries for off-grid renewable projects. Despite the goal of the author to apply these methods toward off-grid renewables, the effects observed here are nevertheless of relevance to automotive applications and offer comparisons of a wide range of battery chemistries utilized in automotive applications.

To perform a study on battery aging under variable conditions, Krieger [29] used the wind profile of a 150W wind turbine to collect 600 seconds worth of output current data with a resolution of 1s. The output sequence ranged from 0A to 6A with an average of 1.4A, as shown in Figure 41a. For the study, this pattern was scaled

such that the average charging current was C/5 for any cell, with the maximum current pulse being roughly 0.8C. This pattern was repeated until the battery was fully charged.

This wind profile is modified for the assessment of the impact of degradation as shown in Figure 41b. This is the same profile as in Figure 41a, but with 10s sampling as opposed to 1s, thereby creating what Krieger refers to as a low-frequency wind profile. This effectively becomes the drive cycle for this study.

Additional profiles are created by using sampling steps of 0.1s, shown in Figure 41c and a smoothed profile using a 5s moving average of the wind turbine output current, shown in Figure 41d, to replicate the smoothing from an ultracapacitor. The reasoning behind these modifications to the profile is in order to determine whether or not capacity fade is affected by the frequency of the oscillations, the power distribution, or both.

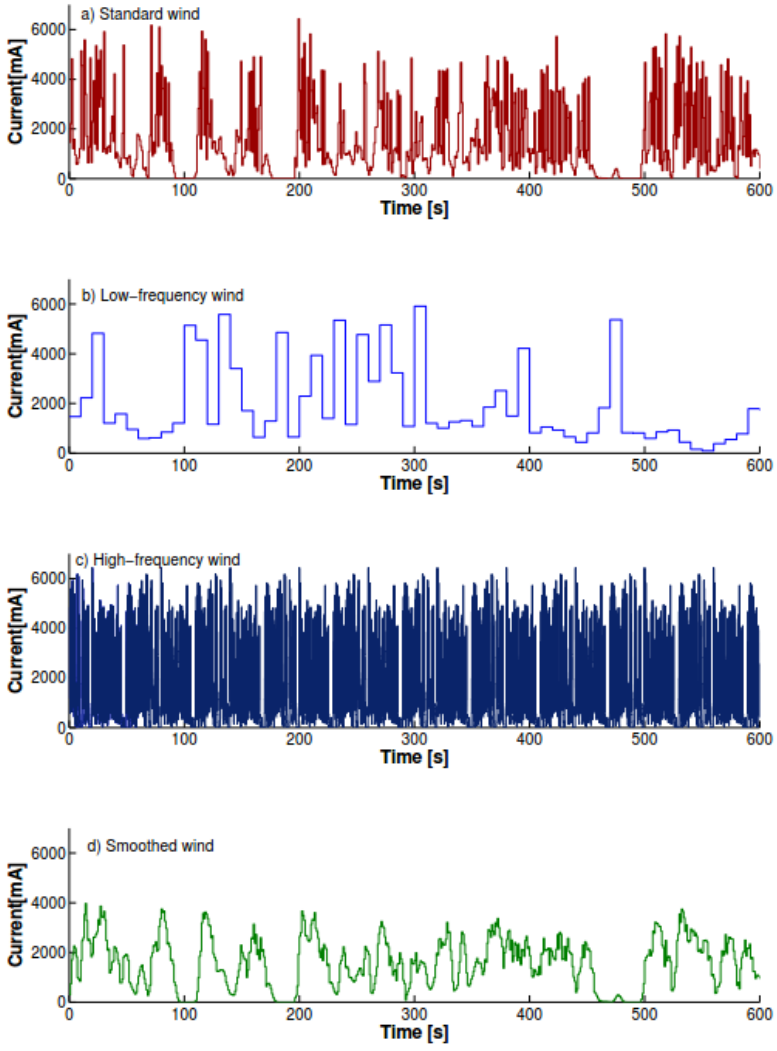

Figure 41: 600s data series of the a) standard wind, b) low-frequency wind, c) high-frequency wind, and d) smoothed wind current profiles, derived from the output current of a 150W wind turbine **[29]**.

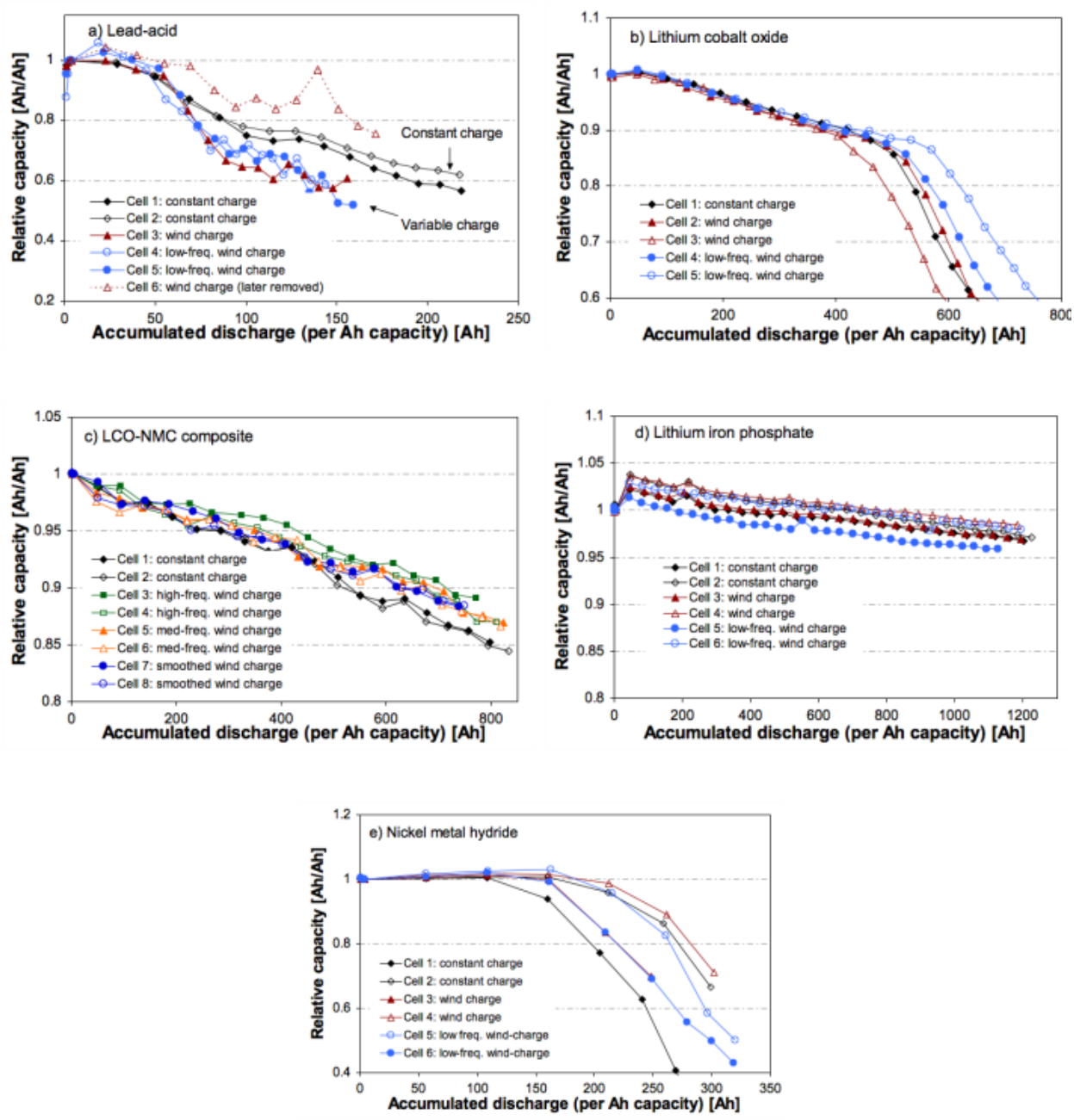

Figure 42. Capacity fade as a function of normalized discharge throughput in a) lead-acid, b) LCO c) LCO-NMC d) LFP cells and e) NiMH cells. **[29]**

Capacity fade in the lead-acid cells as a function of normalized accumulated discharge Ah is given in Figure 42a. The cells demonstrated a significant amount of variation, which the author of [29] attributed to both internal characteristics as well as fluctuations in ambient lab temperature. One cell charged with the standard wind profile exhibits erratic behavior and, while plotted in Figure 42a, was not considered in subsequent analysis. The cells charged at a constant rate show less degradation per processed Ah than the cells charged at a variable rate with the wind and low-frequency wind profiles.

Unlike the lead-acid cells, the LCO and LCO-NMC cells showed no aging benefit from the constant-charge profile. In Figure 42b, LCO cells charged with the low-frequency wind profile showed the least capacity fade, but these results may be within the noise of the system. In Figure 42c, the LCO-NMC cells charged at a

constant rate appear to lose capacity faster than those charged with any of the wind-based profiles, but the degradation trends have yet to fully differentiate after only 15% capacity loss. [29].

The LFP cells, shown in Figure 42d, show little aging after over 1200 cycles and nearly 1000 processed Ah per installed Ah. Capacity fade ranges from 1% to 3% loss from initial capacity. While the cells vary in total measured capacity fade, Krieger notes that this variance does not appear correlated with charge protocols and occurs primarily over the first fifty cycles; after this point, the degradation rate of all cells are similar. No variation in capacity fade between charge protocols could be identified from these plots.

The results of the capacity fade tests in the NiMH cells, seen in Figure 42e show no clear trends. After approximately 150 cycles, three of the batteries begin to rapidly lose capacity, and three maintain their capacity longer, but there is no correlation with battery charge profile. Krieger hypothesizes that the charging protocol for the NiMH results in overcharge, which is known to contribute heavily to NiMH degradation [48], due to the difficulty of ascertaining "end-of-charge" in these cells. Variations in the degree of overcharge due to the difficulty of test procedure standardization may result in the irregular degradation rates observed.

The discharge voltage curves for the standard wind-aged lead-acid, LCO, and LCO-NMC batteries are shown in Figure 43 along with a medium-frequency wind charged LCO-NMC cell, whose protocol most resembles the standard wind profile for this chemistry; the data plotted in these curves is collected following a full charge from a capacity test. The evolution of these curves highlights the relative aging mechanisms of these cells. Active material loss in all lithium-based cells is likely attributable to loss of cyclable lithium.

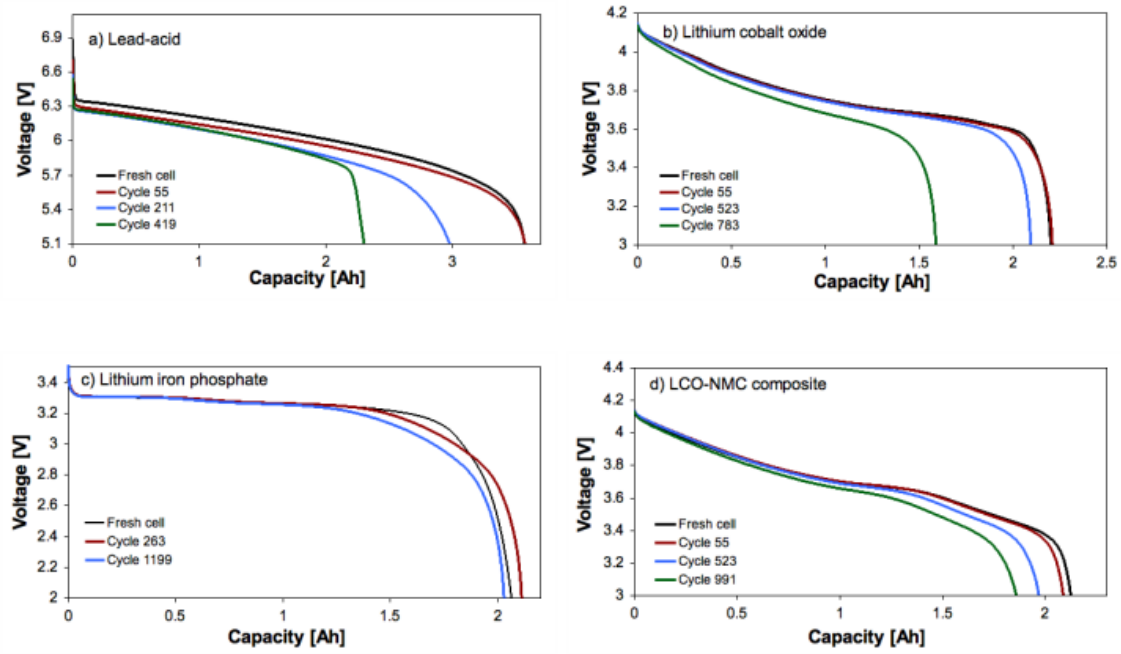

Figure 43 Discharge voltage curves after capacity tests in wind-aged a) lead-acid, b) LCO c) LFP and d) medium-frequency wind-charged LCO-NMC cells (Figure 4.2 from source) **[29]**.

The lead-acid cells studied showed rapid capacity fade which was characterized by an increase in internal resistance and loss of active material, with more rapid degradation in wind-charged cells than constant-charged cells. The lead-acid cells are also subject to severe partial charging when charged with a variable current; this latter effect is greater for longer pulses and reflects the poor pulse charge acceptance of these cells. Despite this capacity fade being reversible, it nonetheless greatly affects the operational performance of the cells. The LCO cells show better overall charge acceptance and, while variable charge results in greater partial charging, the

frequency of the variability does not affect charge acceptance. Variability does not increase capacity fade in the LCO cells. The LCO-NMC cells degrade slower than the LCO cells, and constant charge cells show initial signs of faster degradation than variable charge cells, which may be the result of incomplete charging limiting the side reactions induced by high SOC. Degradation in the LCO-NMC cells appears to be initially due to loss of active material, but ultimately shows an increase in resistance as well. The LFP cells show very little degradation under all charging protocols. No increase in resistance is seen, and the slight reduction in capacity observed appears to primarily stem from the loss of cyclable lithium. Partial charging in these cells does depend on pulse frequency, and 1s pulses are found to have greater charge acceptance than 10s pulses.

	Lead-acid	**LCO**	**LCO-NMC**	**LFP**
Characteristic cycle life	Poor	Good	Very good	Excellent
Effect of variability on lifetime	Decreases lifetime	No measured effect	Neutral or positive effect	No measured effect
Pulse length dependence of charge acceptance	Short pulses better than longer pulses	No measured effect	No measured effect	Short pulses better than longer pulses
Incomplete charge is a stressor	Yes	No	No	No
Charge power fade observed	Yes	Yes	Yes	No

Table 8 Summary of battery response to variable charging **[29]**

In another study on charging, Zhang [60] assessed the effect of the charging protocol on the cycle life of a $LiCoO_2$ cell using three methods: (1) constant current (CC) charging, (2) constant power (CP) charging, and (3) multistage constant current (MCC) charging. These patterns are shown in Figure 44. Fast charging resulted in an accelerated capacity fading due to the loss of Li+ ions and the related growth of a surface layer, which was associated with metallic lithium plating onto the anode and a high polarization at the electrolyte–electrode interface. Analyses of the cell electrochemistry showed that use of a reduced current to charge the initial 10% capacity and near the end of charge, respectively, was favorable for long cycle life.

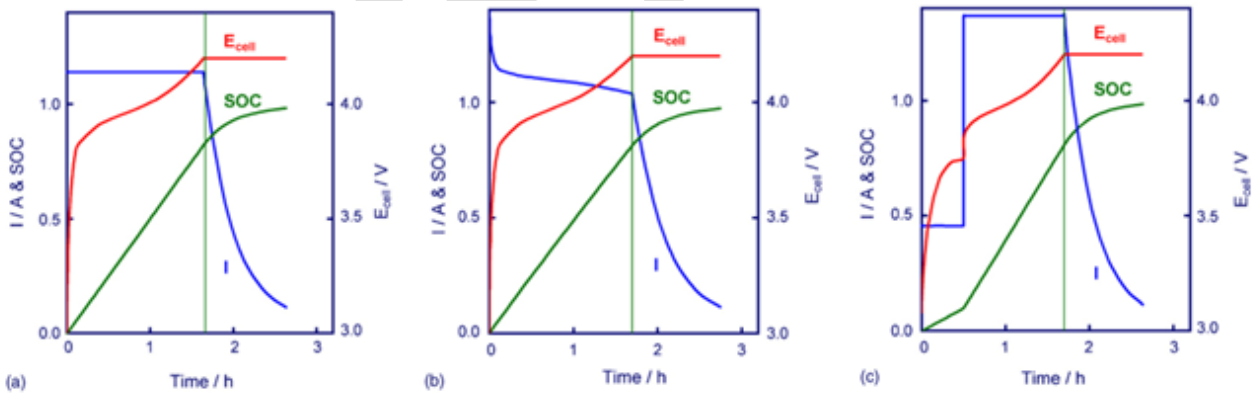

Figure 44. Characteristics of the charging protocols for a commercial 2.4Ah 18650 Li-ion cell using an averaged charging rate of 0.5C (a) Constant Current-Constant Voltage (b) Constant Power-Constant Voltage & (c) Multistage Constant Current – Constant Voltage. **[60]**

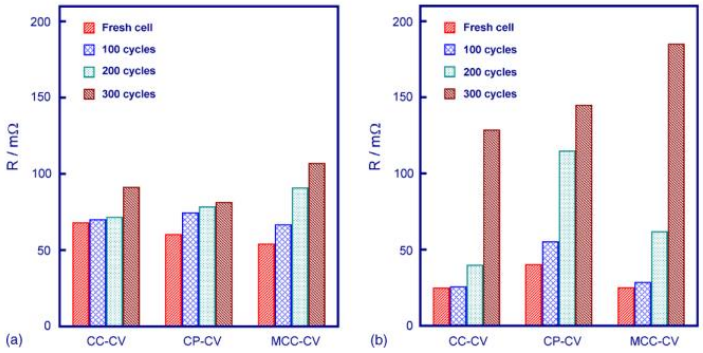

Figure 45 Comparison of the ohmic resistance (a) and charge-transfer resistance (b) for 18650 cells by different charging protocols. **[60]**

From the results of this work, it may be concluded that cycle life of Li-ion cells is significantly affected by the charging protocol even if the same charging rate is applied. A good charging protocol should strictly follow the cell chemistry. Impedance analysis shows that the cell with a low SOC (<0.1) has a much higher resistance, which suggests that a low charging rate be desirable for charging the initial 10% capacity. Potential monitoring indicates that due to electric polarization, the potential of the graphite anode may fall to below 0 V versus Li^+/Li near the end of charging so that metallic lithium plating can occur on the anode. Although the plated metallic lithium can continue to intercalate into the graphite, it inevitably reacts with the electrolyte solvents, which not only reduce charging efficiency but also promote progressive growth of the resistive surface layer. Therefore, a low charging rate is favorable for healthy charging near the end of charging. It is shown that the capacity loss of a Li-ion cell during cycling is associated with increased cell impedance and reduced charging efficiency relating to metallic lithium plating on the anode. [60]

	Total distance (km)	Urban distance (%)	Extra-urban distance (%)	Highway distance (%)	Avg. consumption (kWh_{AC}/100km)
EV1	8583	72.2	25.7	2.1	18.0
EV2	33919	40.3	43.5	16.2	20.9
EV3	25362	41.5	48.2	10.3	15.5
EV4	16712	24.3	40.4	35.3	18.1
EV5	5901	55.1	34.9	10.0	18.6

Table 9: Key data of the cars in **[61]**

A study by De Vroey et. al looked at the impact of charging on five vehicles over a period of three years [61]. The five vehicles under test were Peugeot iOn cars (equipped with 16kWh LMO batteries). The vehicles showed very different consumption profiles depending on their use. Designated EV1 through EV5, this consumption data is shown in Table 9.

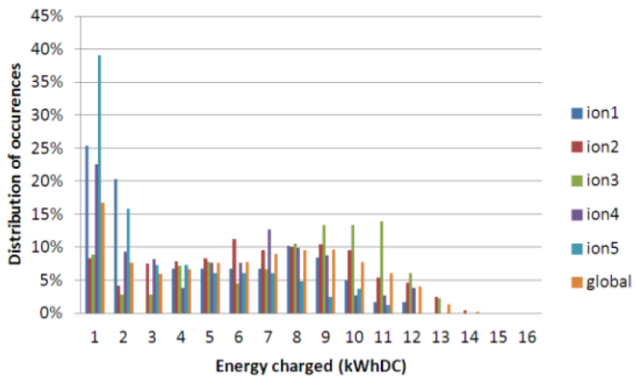

Figure 46. Distribution of the energy per charging cycle for the five cars **[61]**

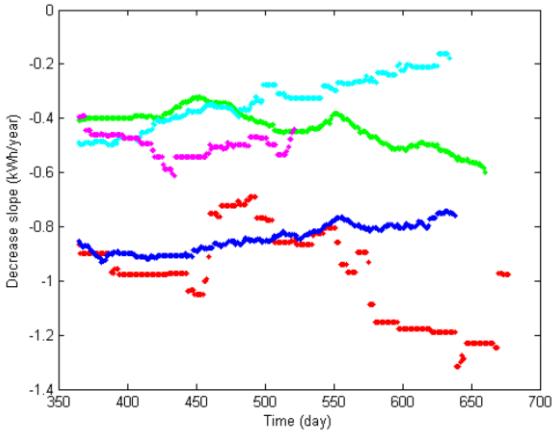

Figure 47. Average battery capacity evolution with a two-year sliding window centered with day mentioned on X-axis (red: EV1; green: EV2; blue: EV3; cyan: EV4; magenta: EV5) [61]

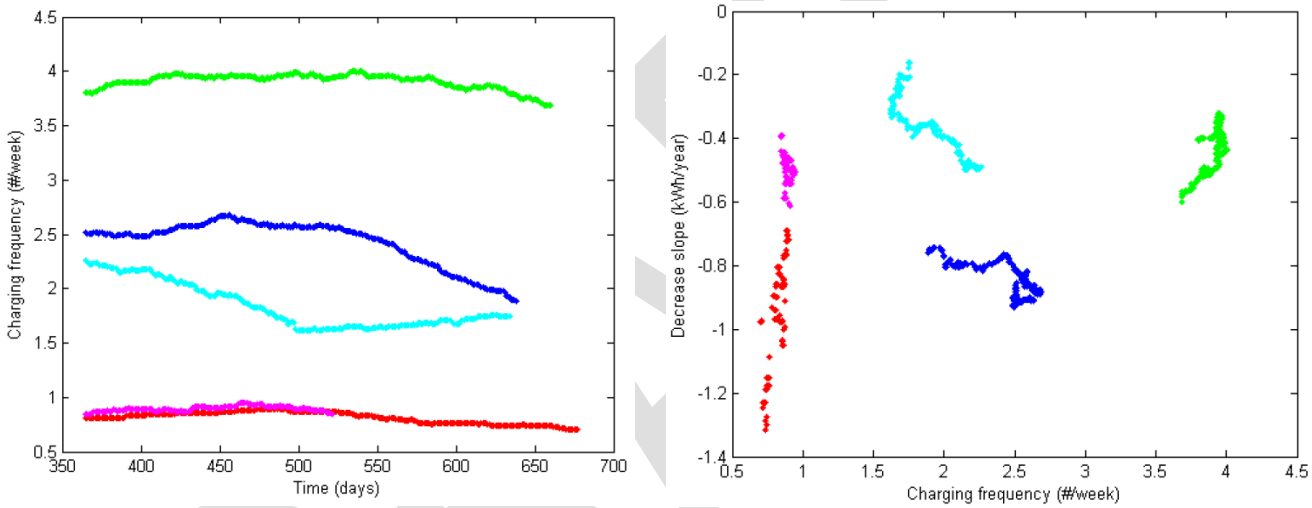

(a) (b)

Figure 48. (a) Time evolution of the charging frequency; (b) battery capacity evolution (kWh/year) in function of the charging frequency; two years sliding window centered on the day mentioned on X-axis (red: EV1; green: EV2; blue: EV3; cyan: EV4; magenta: EV5) **[61]**

Referring to Figure 48, for EV1 (red), EV2 (green) and EV5 (magenta) cars, an increasing charging frequency leads to a lower battery capacity decrease, while the EV3 (blue) and EV4 (cyan) cars show a stronger battery degradation when the charging frequency is higher.

The authors of [61] concluded that average state of charge had negligible impact on degradation over the period of three years. In the view of the authors, several factors were left with unclear impact, namely the frequency at which the vehicles were charged, as well as the power level of charging. This conflicts with the findings of [55] which showed a clear influence of high power charging on battery life. However, as shown in Figure 47, EV1 and EV2 both exhibit increasing degradation with time, despite EV1 not being subjected to 50kW charging.

Climate and Thermal Effects

In the previous section the study by Shirk and Wishart [55] set out with the goal of evaluating the effect of fast charging. However, as their study was conducted in Phoenix, Arizona, thermal effects had to be taken into consideration. It was observed that the average DC fast charging pack temperature rise during charging was 6.5°C, while the L2-charging pack average was 2.9°C, and the mean of difference between the two packs' temperatures at end-of-charge was 4.9°C. Figure 49 shows the cumulative distribution of temperatures for the study.

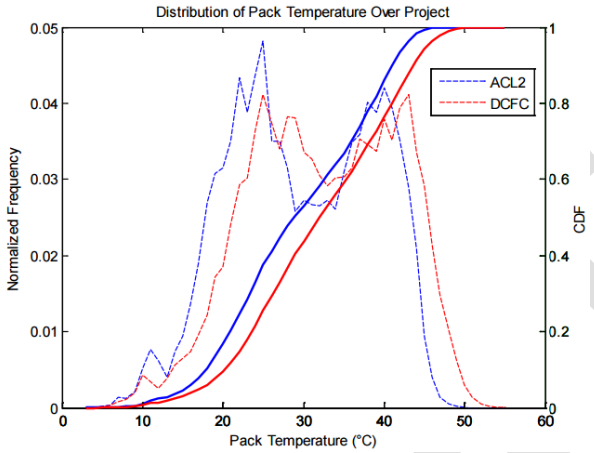

Figure 49 Battery pack temperature distribution for ACL2 and DCFC vehicles. The data represents 50,000 miles of driving, charging, and parking over more than 500 days **[55]**

Smith et al. [62] performed a study wherein they sought to analyze battery degradation in various geographic environments and driving scenarios. In exploring this topic, the authors apply a semi-empirical life model of the graphite / nickel-cobalt-aluminum (NCA) lithium-ion chemistry which is subjected to battery charge and discharge profiles from plug-in hybrid electric vehicles. 782 single-day driving cycles taken from a Texas travel survey are used to provide the drive cycle information. This work done in [62] specifically considers aging scenarios for plug-in hybrid electric vehicles (PHEVs) with 10 and 40 mile (16 and 64 km, respectively) nominal electric ranges.

To obtain geographic temperature distribution information, data was gathered from PHEV sales distributions within the United States, and the study was conducted around the median and hottest climates of the top 100 cities which exhibit a high likelihood for PHEV ownership. [62]

In addition to the above, three cases are considered:

- Battery aging under storage
- Aging at variable temperature, constant SOC
- Aging at variable temperature and variable SOC

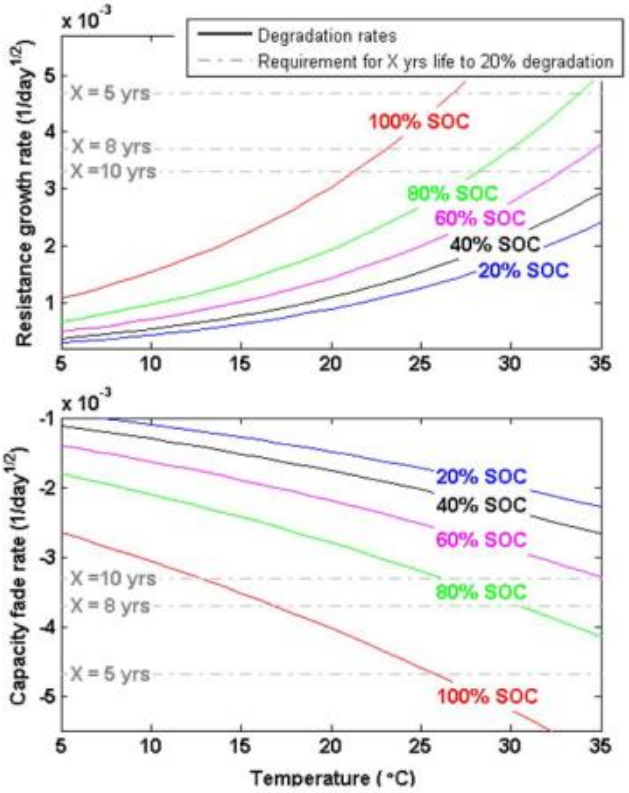

Figure 50 Typical graphite/NCA degradation rates for storage at constant SOC and temperature (solid lines). Dotted lines show maximum allowable degradation rates for example end-of-life requirements of 20% resistance growth and 20% capacity fade. [62]

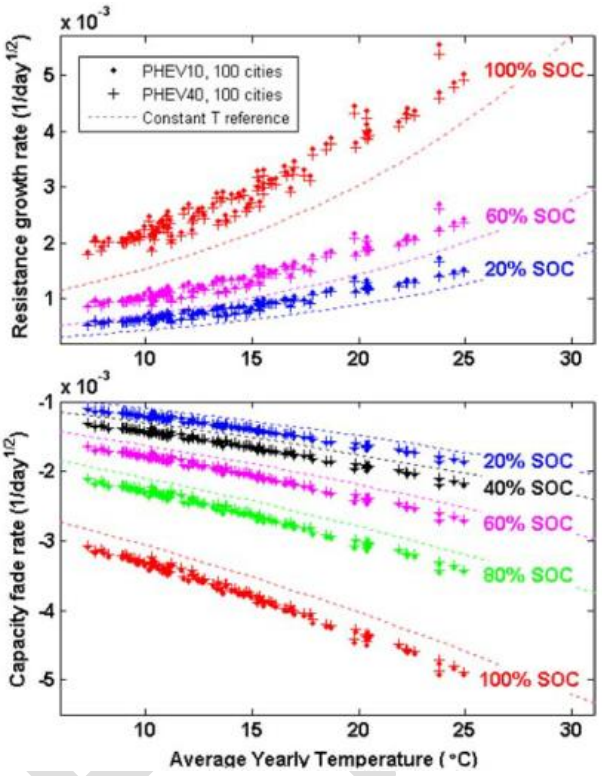

Figure 51 Resistance growth and capacity fade rates under storage at constant SOCs. Reference lines show results for constant temperature. Symbols show simulated results for PHEVs using hour-by-hour TMY ambient temperature and solar radiation data for 100 U.S. cities **[62]**

For the study conducted by Smith et al., the model did not take in to account degradation mechanisms such as fast charge-rates (with the exception of temperature rises as a result thereof), the effect of extreme temperatures (>50°C, < 0°C), damage done as a result of exceeding typical operating conditions, cell-to-cell manufacturing variations, and long term degradation effects which may manifest beyond 10 years of service life [62].

Subsequent analysis compares metrics of the Texas cycles to UDDS, HWY, and US06 standard drive-cycles. To achieve an appropriate mix of CD and CS operation, either four or five repetitions of the UDDS, HWY and US06 standard drive cycles are simulated so that each cycle's daily travel distance falls as close as possible to the Texas average of 38.9 miles/day. These UDDS, HWY, and US06 cycles are weighted with appropriate rest days such that the annual mileage of each is 12,375 miles/yr. The United States Advanced Battery Consortium (USABC) cycle-life test protocol is also simulated [23]. The PHEV10 USABC cycle simulated here uses both the CD and CS portions of the test protocol. The PHEV40 USABC cycle uses only the CD portion of the test. This is to keep the implied daily travel distance as close as possible to the Texas drive-cycle average.

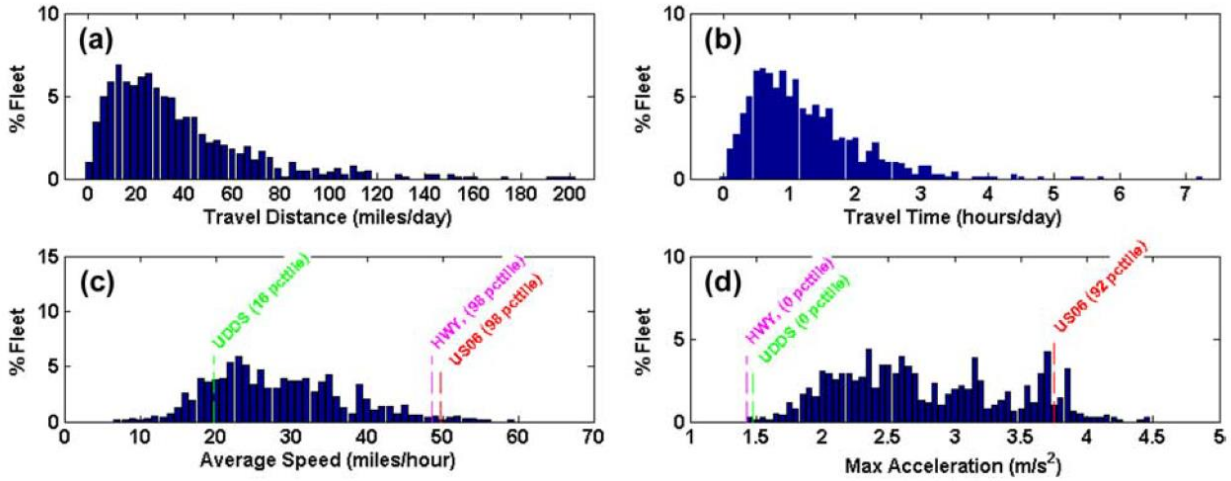

Figure 52 Drive-cycle metrics (a) distance-traveled per day, (b) travel time per day, (c) average speed while driving, and (d) maximum acceleration. Blue histograms represent 782 drive-cycles from Texas survey **[62]**.

Figure 52 shows histograms representing the 782 drive cycles used from the Texas survey. Averages speeds and maximum acceleration figures are compared against UDDS, HWY, and US06 drive cycles. Daily travel distance results (Figure 52a) show 66% of the Texas driving trips are less than 40 miles per day and 14% of drive cycles are less than 10 miles per day [62].

The authors of [62] assume resistance growth and lithium capacity loss to be proportional to the square-root of time, as this factor is typical of diffusion-limited film growth processes. At SOC $\geq$ 80% there is a greater sensitivity to temperature [62] shown in

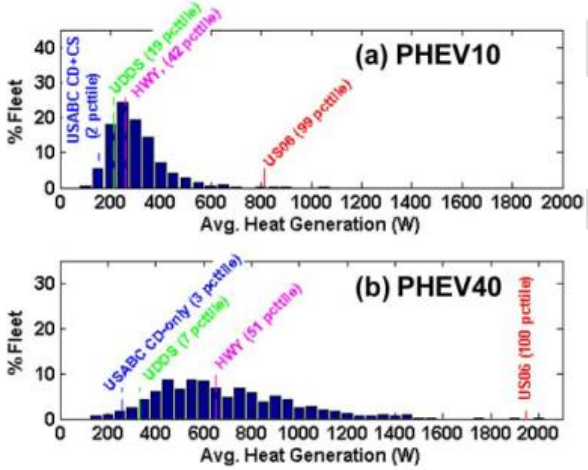

Figure 53 Model-predicted 100% DOD-equiv. cycles per day. [62]

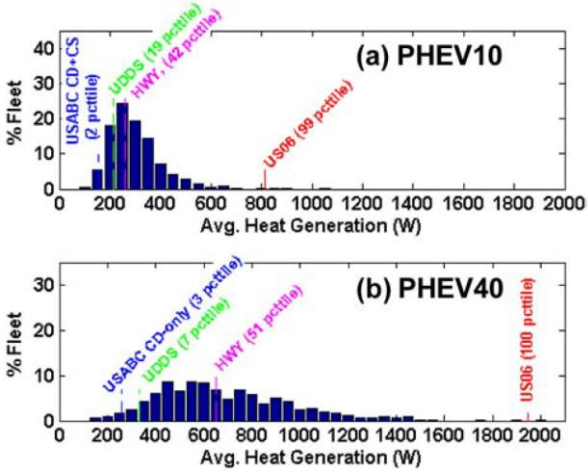

Figure 54 Model-predicted average heat generation rate during driving **[62]**

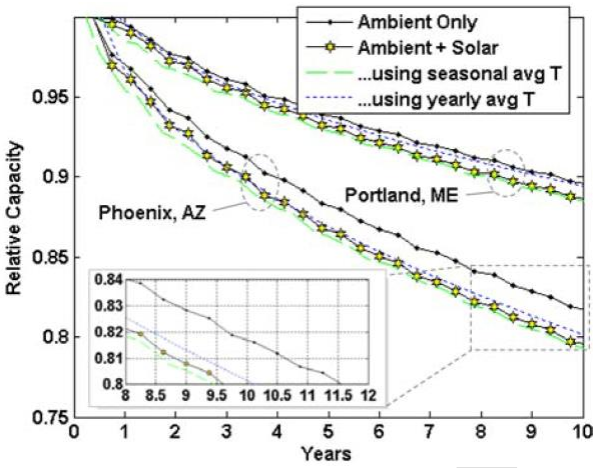

Figure 55 Capacity fade under storage at 90% SOC for two geographic locations with and without impact of solar loading on the parked vehicle **[62]**

The results of the study in [62] suggest that storage degradation in worst-case temperatures is negatively affected by high SOC. Therefore, part of a worst-case durability testing procedure should combine high SOC with high temperature in order to observe faster degradation. Furthermore, analysis of cycling-related degradation by comparing attributes of UDDS, HWY, US06 and USABC cycles to 782 single-day drive-cycles demonstrate the importance of factors such as the charge/discharge cycles and heat-generation as a by-product of such. Worst-case PHEV driving and charging patterns are those with high utilization of charge-depletion mode of operation.

Similar testing was conducted on the Nissan Leaf at Argonne National Laboratory, with testing being performed in a thermal chamber at temperatures of 20°F, 72°F, and 95°F (-7°C, 22°C, and 35°C respectively) [63]. For these thermal tests, the vehicles were operated using drive cycles such as UDDS, HWY, and US06. Data showing the impact of temperature on energy consumption and range are shown in Figure 56 and Figure 57 respectively.

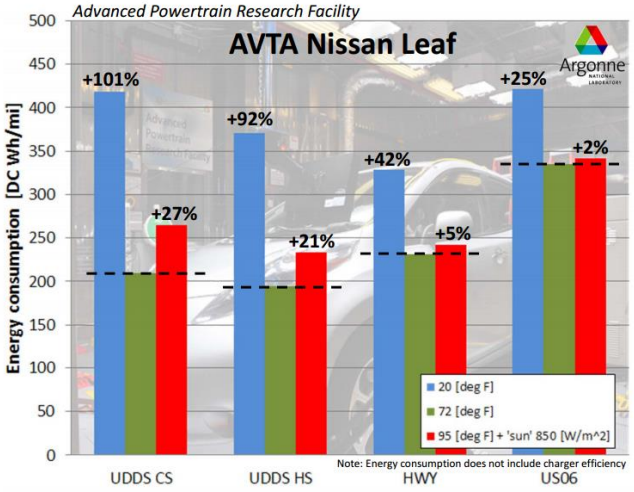

Figure 56 Impact of Temperature on Energy Consumption **[63]**

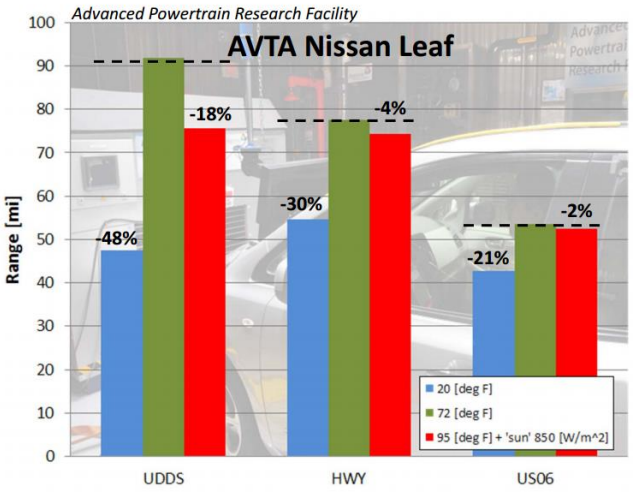

Figure 57 Impact of Temperature on Range **[63]**

It should of course be noted that in the cases of the 20°F and 95°F tests that the vehicle's cabin climate control was set to 72°F [63]. Such an approach in vehicle testing is warranted as it assumes the desire of the vehicle occupants to maintain a comfortable climate. Due to the Leaf being a BEV, the energy consumed to power heating contributes directly to the increased energy consumption and lower range [63].

Song et al [64] examined the impact of pre-heating a battery in low temperature climates on the performance and lifetime of the battery. Four cases were considered:

1. a reference test fixed at room temperature (+25°C)
2. preheating to +25°C (from the minimum of -20°C)
3. preheating to +10°C (from the minimum of -20°C)
4. no pre-heating at low temperature (fixed at -20°C)

A 6.9 kWh, 20Ah lithium polymer battery pack was connected to a battery HIL which was using a mid-sized BEV model supplied by Argonne National Laboratory. After the temperature soak, the battery was subjected to three UDDS cycles. The results of each of the cases are shown in Table 10:

	Case 1	Case 2	Case	Case 4
Remaining capacity (Ah)	7.47	7.32	7.26	6.82
SOC(%)	36.10	35.45	35.16	33.03
Room temperature contrast ratio(%)	-	0.73	1.02	3.15

Table 10 Comparison of remaining capacity for temperature profiles **[64]**

The results of [64] demonstrate that in a low temperature environment, the battery is able to retain greater capacity under a preheat / preconditioning scenario.

Barnitt et al. [65] performed a study similar to that of [64], showing effects for temperature pre-conditioning at both low and high temperatures. Here, three simulated vehicle types are considered:

1. PHEV15—a blended PHEV with an approximately 15-mile (23.4-km) all-electric range (AER) under certain usage conditions.
2. PHEV40s—a series PHEV designed to provide up to 40 miles (64 km) of AER, then operate in charge-sustaining (CS) mode using a range-extending gasoline engine.
3. BEV—a BEV designed to provide up to 100 miles of AER.

Additionally, the following scenarios for these vehicles are considered:

Climate Control Scenario	**Ambient Temp.**	**Thermal Preconditioning**	**Initial Battery Temp.**
A/C on (hot)	35°C	Yes	26.7°C
		No	35°C
Heat on (cold)	-6.7°C	Yes	1.7°C
		No	-6.7°C
Neither A/C nor heat on	20°C	N/A	20°C

Table 11 Climate Control, Temperature Scenarios **[65]**

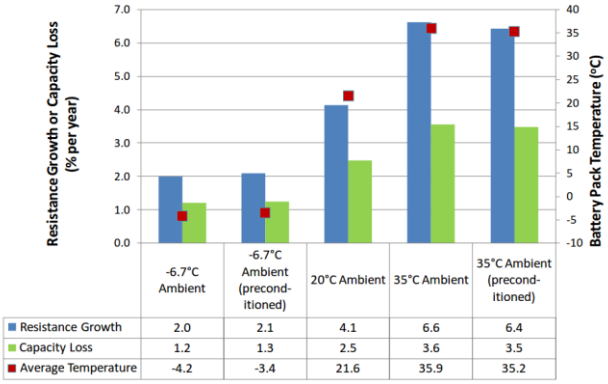

Figure 58 PHEV15 battery degradation rates (left axis) and average temperature (right axis) **[65]**

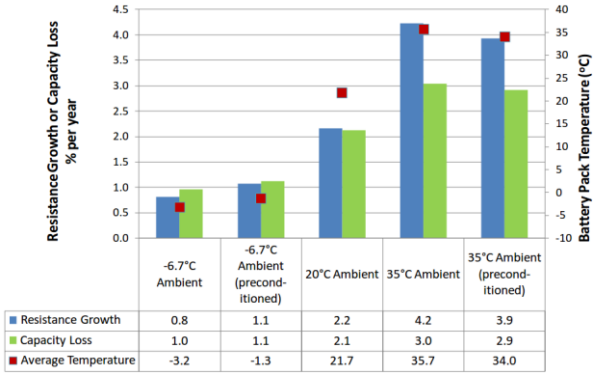

Figure 59 PHEV40s battery degradation rates (left axis) and average temperature (right axis) **[65]**

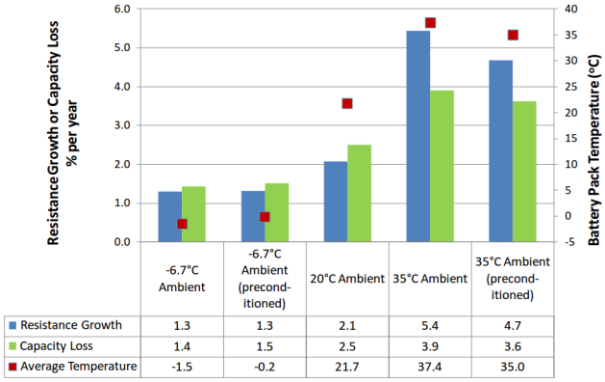

Figure 60 EV battery degradation rates (left axis) and average temperature (right axis) **[65]**

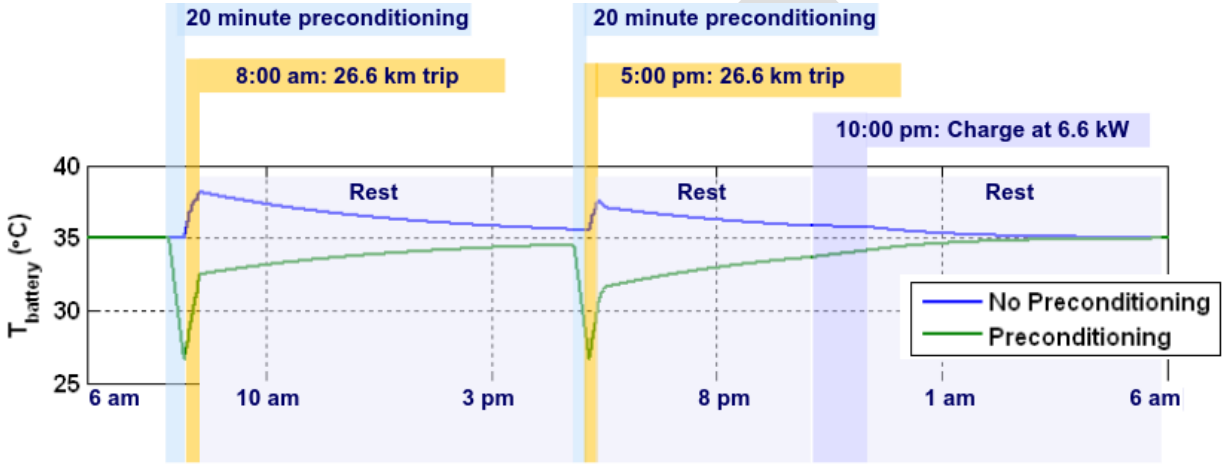

Figure 61 Battery temperature and SOC profiles for PHEV40s, 35°C ambient temperature, with and without thermal preconditioning **[65]**

From figures Figure 58 to Figure 60 we are able to observe the battery degradation results. From these results, pre-cooling of electric-drive vehicle batteries is predicted to reduce capacity fade by 2.1% to 7.1% and resistance growth by 3.0% to 13.8% in hot (35°C) ambient conditions when compared to the baseline configuration of no pre-conditioning [65].

A summary of the fuel consumption and CD range impact is given in Table 12.

EDV Platform (Climate Control)	Fuel Consumption Impact	CD Range Impact
PHEV15 (heat)	-1.4%	+19.2%
PHEV15 (A/C)	-0.6%	+5.2%
PHEV40 (heat)	-2.7%	+5.7%
PHEV40 (A/C)	-1.5%	+4.3%
BEV (heat)	N/A	+3.9%
BEV (A/C)	N/A	+1.7%

Table 12 Impact of thermal preconditioning as compared to scenarios without thermal preconditioning **[65] [39]**

As can be seen in Table 12, the effect of thermal preconditioning of the battery is able to offer benefits to both fuel consumption and to range, in addition to extending battery life as shown in Figures Figure **58** - Figure **60**.

A study performed by Vatanparvar and al-Faruque was conducted to develop an automotive climate control methodology which manages the vehicle's HVAC power consumption so as to improve battery lifetime and

driving range. In effect, the lifetime-aware HVAC system decreases power consumption of the HVAC when electric motor power consumption is high, and when the electrical motor is consuming less or generating, the HVAC may consume more in order to maintain the temperature and precool/preheat the cabin. [66]. The other methodologies examined where those of On/Off management and a fuzzy-based methodology. The modeling of these methodologies is outside of the scope of this review, but may be referenced within [66].

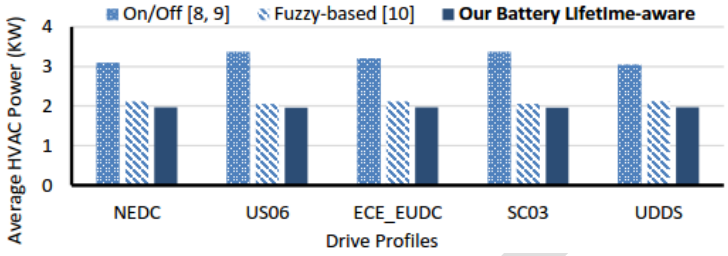

Figure 62 HVAC Power Consumption Analysis for Different Drive Profiles **[66]**

Yuksel & Michalek [67] also studied thermal management methods as they relate to battery life in a PHEV. The battery chemistry which formed the focus of the study was $LiFePO_4$/graphite. Drive cycles used are UDDS and US06, with a fan On/Off control strategy wherein ambient or cabin air is used to cool the battery. Climates considered for the study are Phoenix and Miami.

Conclusions drawn suggested that thermal management increases life by 5% to 53%, depending on the scenario. Variation in driving conditions from the UDDS cycle to the US06 cycle has a dramatic effect on battery life if there is no thermal management, reducing life by about 60%. With air cooling, US06 decreases life by only 20%. Thus, driving conditions are important for battery longevity, and thermal management mitigates the effects of aggressive driving. One observation was that batteries have a 20% shorter life in Phoenix than in Miami (reduced to 11% with thermal management) due to higher summer peak temperatures in Phoenix even though Miami has higher average temperatures, demonstrating the impact of sustaining high temperatures for a time. Use of ambient inlet air vs. pre-conditioned cabin air for battery cooling has a minor effect on degradation for the base control strategy. However, variation in control parameters (fan on-off temperatures) can increase battery life by 53% or more [67].

A study conducted by Smith, Earleywine, Wood, and Pesaran performed a study for the evaluation of PHEV10 (16km AER) and PHEV40 (64km AER) vehicles using a lithium ion graphite / nickel-cobalt-aluminum battery model. The analysis of battery lifetime was conducted using 782 different duty cycles obtained from travel survey data, using climate and geographic data as well.

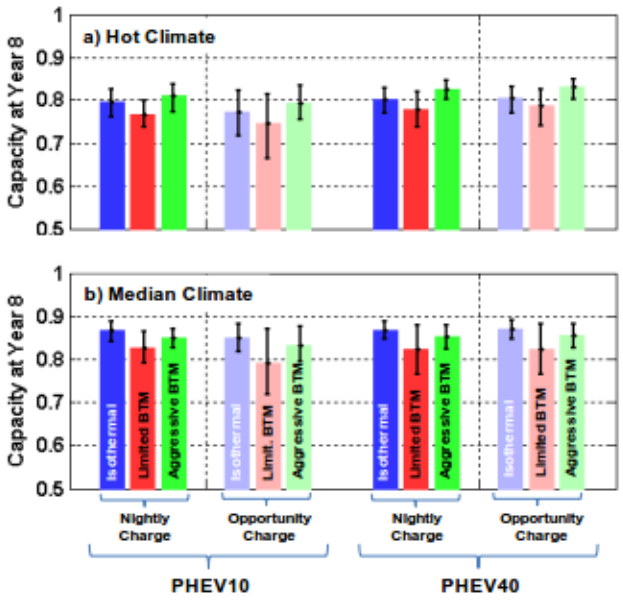

Figure 63 Remaining capacity at the end of 8 years for various BTM and charging scenarios. Colored bars show average result for all 782 drive cycles. Error bars show result for 5th and 95th percentile drive cycles. **[68]**

The drive cycle distribution in the study presented in [68] is identical to that of [62], namely, that the experiment's drive cycles are derived from 782 individual light-duty drive cycles.

The authors of [68] state that battery aging is caused by combination of the phenomena related to both cycling and time. Battery degradation noted to accelerate with the DOD and frequency of cycling, elevated temperature, and elevated voltage exposure, among other factors. At the battery terminals, degradation manifests itself as an increase in resistance and a reduction in capacity. These two effects can be correlated with power and energy losses that cause battery end-of-life in an application.

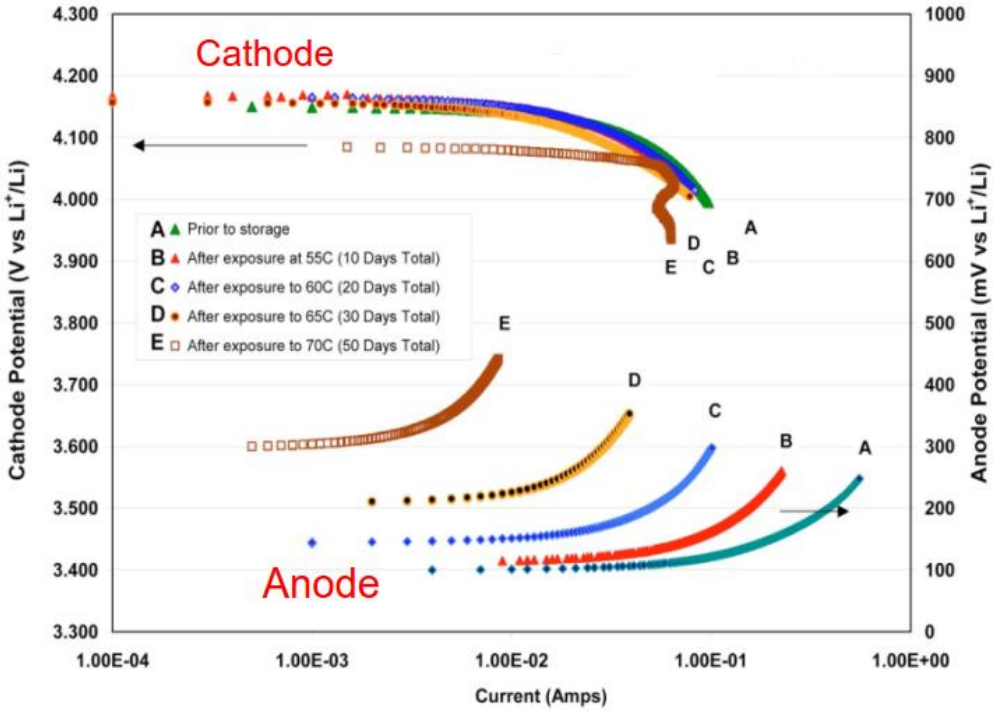

Figure 64 Half-cell Potentials from cells subjected to aging at different temperatures: Side reactions happen faster on the electrode surface with increase in the temperature – resulting in faster build-up of the resistance at the electrode surface **[69]**

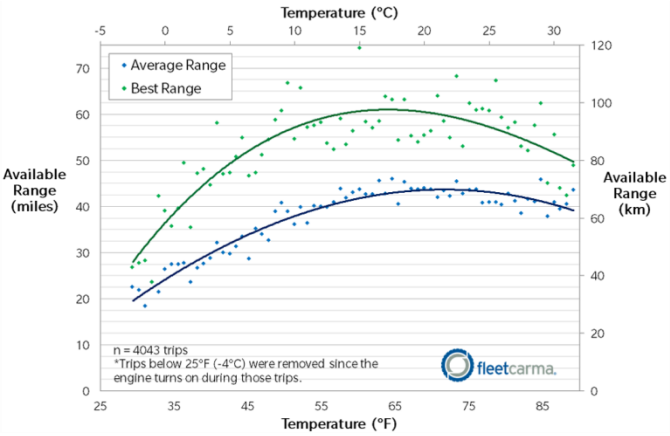

Figure 65 Chevrolet Volt: Electric Range vs. Temperature spanning all model years in the FleetCarma database [70]

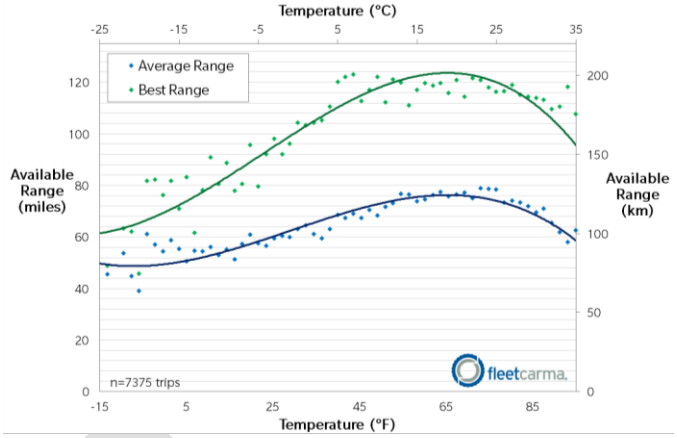

Figure 66 Nissan Leaf: Range vs. Temperature spanning all model years in the FleetCarma database **[70]**

From Figure 65 and Figure 66 we see that optimal range characteristics for the Volt and Leaf lie between 15°C and 25°C. It should be noted however as per Figure 65 that performance below -4°C is not shown for the Chevrolet Volt as the ICE is activated at this temperature. Nevertheless, we see a clear trend as far as decreases in range at concerned at these temperatures. The same can be said of both vehicles as ambient temperatures approach 30°C. A further comparison between the two vehicles is presented in Figure 67.

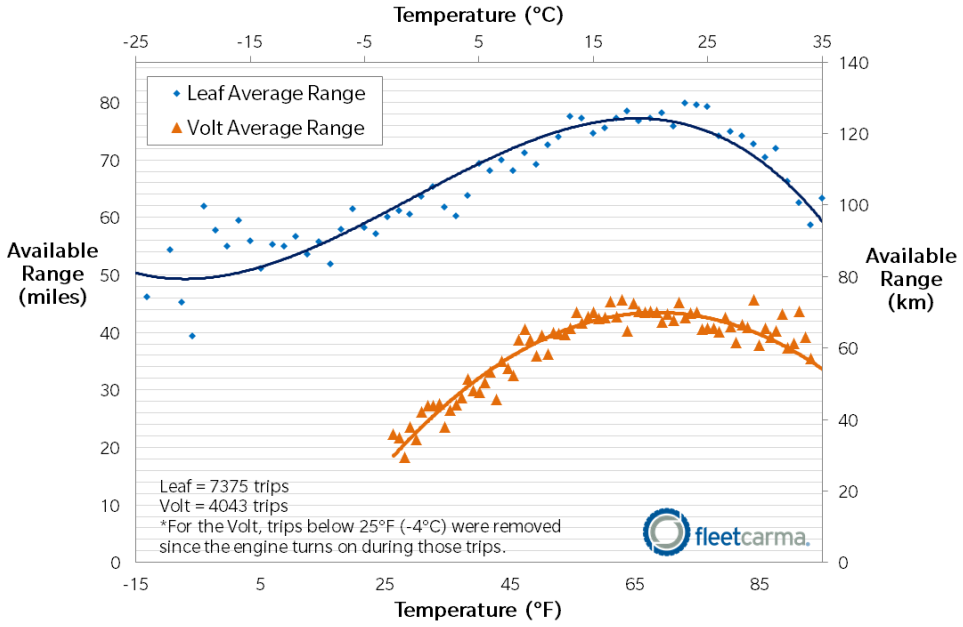

Figure 67 Nissan Leaf & Chevrolet Volt: Range vs. Temperature **[70]**

A study under taken by Santhanagopalan et. al [71] sought to create life models of lithium-ion cells based on obtained experimental data. Specifically, the study investigated capacity fade in cells (and related cell degradation) for cycling at different temperatures (5°C, 15°C, 25°C, 35°C, and 45°C). Each cycle consisted of a constant current charging at the C/2 rate (where in this case C-rate = 1.656A) until the voltage reached 4.1V, followed by constant charging at 4.1V until the current reduced to 50mA, and then a constant discharge at the C/2 rate until the cells reached a cutoff of 3.3V. Additionally, rate capability tests were performed before

cycling and at the end of every 100 cycles. These rate capability tests consisted of measuring the charge-discharge capacity of the cell at different rates, with these being C/33, C/2, and C, in that order. [71]

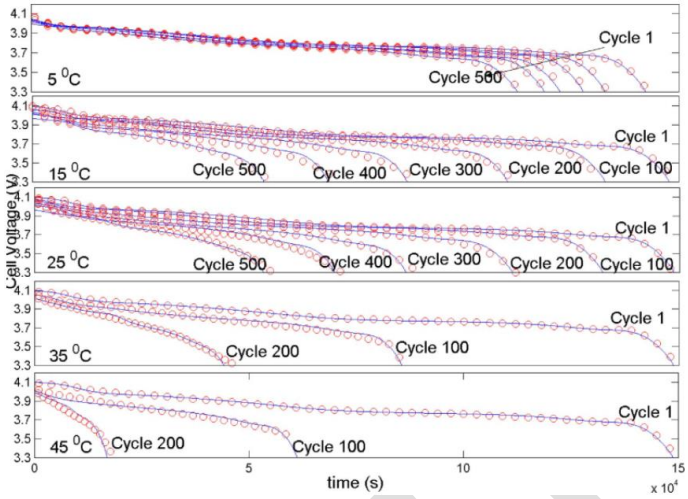

Figure 68: Degradation of cell voltage for increasing cycles at various temperatures **[71]**

Comparison of the predictions from the single particle model to the experimental data at the C/33 rate. Solid lines indicate experimental data and the symbols indicate the model predictions. At 35 and 45°C, the cycling was stopped after 200 cycles since the remaining capacity was very low.

	Fresh	Cycle 100	Cycle 200	Cycle 300	Cycle 400	Cycle 500
5°C	1.8867	1.7454	1.6723	1.6031	1.5522	1.4705
15°C	1.9870	1.7891	1.6094	1.4227	1.2143	0.9730
25°C	1.9667	1.7367	1.4567	1.1867	0.9467	0.7367
35°C	1.9667	1.3466	0.6667	--	--	--
45°C	1.9667	0.8667	0.2467	--	--	--

Table 13. Experimental capacities (Ah) measured after every 100 cycles for five different cells cycled at 5, 15, 25, 35, and 45°C [71]

From the data shown in Figure 68 and Table 13 we are able to see the evident loss of capacity as a result of the combination of both temperature and cycling, with temperature here as the main variable in the experimentation. Beyond 25°C we see significant degradation, as is also corroborated by Figure 65 and Figure 66, for example.

In the study by Keil & Jossen with regard to the impact of regenerative braking on battery degradation, temperature and state of charge were both varied. As concerned

At 40 °C, the Li-ion cells cycled within the low and medium SOC window show almost no dependency on the level of regenerative braking. All curves lie closely together. At the end of the cycling process, cells at low SOC exhibit a capacity loss of almost 6 % and cells at medium SOC of almost 7 %. The additional capacity loss at medium SOC can be attributed to increased calendar aging. Thus, the capacity loss supplementary to calendar aging due to cycling is considered identical for both SOC levels and accounts for about 2.5 % after the total charge throughput of 1,400 Ah. Regarding the high SOC level at 40 °C, Fig. 7 demonstrates a dependency on regenerative braking, as the capacity curves diverge. A trend becomes apparent: A higher level of regenerative braking reduces the capacity loss. At the end of the test, the capacity loss supplementary to calendar aging is about 2.5 % for the cell with the maximum level of regenerative braking and more than 4 % for the cell with no regenerative braking.

Our aging study also demonstrates that the contributions of calendar aging and cyclic aging vary with temperature. Fig. 9 compares calendar aging with the aging results of one level of regenerative braking for all three temperatures. Calendar aging increases substantially with elevated temperature:

After five months at 40 °C, the capacity fade is about 2 percentage points higher than at 25 °C and about 2.5 percentage points higher than at 10 °C. In contrast, cyclic aging decreases with temperature. At low SOC, cyclic aging at 40°C is approximately 1 percentage point lower than at 25°C and 10°C. Cyclic aging at medium SOC is comparable to low SOC for 40°C and 25°C, whereas it increases by 1 percentage point at 10°C. At high SOC, lower temperatures exhibit intensified aging. Fig. 9 illustrates that cyclic aging has increased by about 1 percentage point at 25°C and by about 2 percentage points at 10 °C compared to medium SOC.

Cycling and Depth-of-Discharge

Wood et al. [73] performed a study which sought to improve understanding of battery wear in xEVs by implementing a predictive battery wear model (developed by the National Renewable Energy Laboratory) that is capable of capturing the effects of multiple cycling and storage conditions in a representative lithium chemistry. In particular, Wood et al. explored the sensitivity of battery wear rates to ambient conditions, maximum allowable depth of discharge, and vehicle miles traveled. The analysis focuses on two midsize vehicle platforms: a battery electric vehicle (BEV) with a nominal range of 75 mi (121 km) and a plug-in hybrid electric vehicle (PHEV) with 40 mi (64 km) of nominal charge-depleting range.

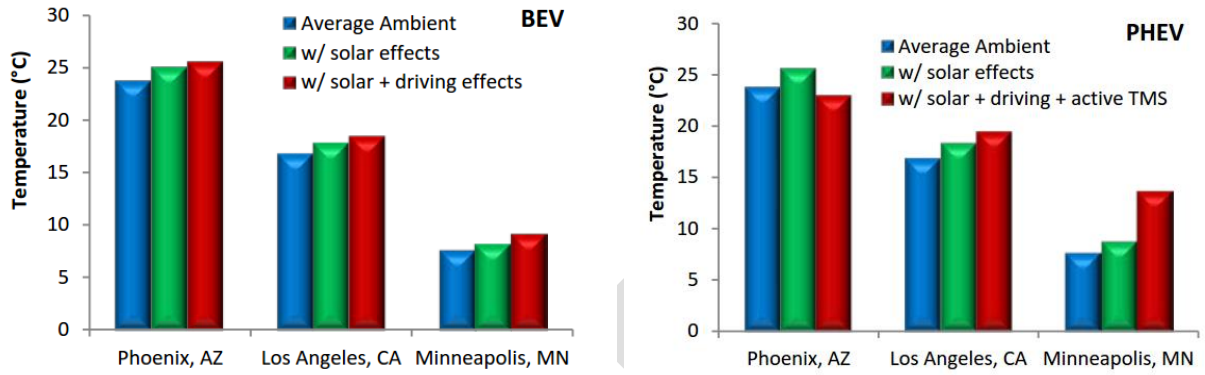

Figure 69 Average yearly battery temperature contributions from ambient, solar loading, and internal heat generation for simulated (a) BEV and (b) PHEV. **[73]**

The effect of maximum allowable DOD on battery wear is explored for both the BEV and the PHEV. Each vehicle was assigned a nominal value for maximum allowable DOD and maximum state of charge (SOC). These values are adjusted over a feasible range for both the BEV and PHEV to explore the effect on wear (80%–94% and 55%–87% maximum allowed DOD, respectively). The SOC window of the pack is adjusted relative to total energy to ensure that the available energy in the pack remains constant for all maximum allowable DODs. By adjusting the maximum allowable DOD and maximum SOC, the life model will capture the wear effects of deep cycling and operation at high voltages [73].

In the case of the BEV, increasing the maximum allowable DOD of the pack from 80% to 94% causes 8-year resistance growth and capacity fade values to increase by 6% and 8% respectively. For the PHEV, increasing the maximum allowable DOD window of the PHEV from 55% to 87% increased resistance growth by 18% while capacity loss increased by 8% over the same range. [73]

Adjusting pack energy has an impact on vehicle mass (and cost) and is subsequently related to CD range, efficiency, and acceleration.

It was determined that maximum allowable DOD was found to significantly impact battery wear. Reductions to the maximum allowable DOD leads to a subsequent reduction in resistance growth rates and capacity fade. However, the tradeoff which allows a reduced DOD window to physically occur means that a larger overall battery pack will be required. The authors of [73] estimate that the extra battery capacity required for n 80% vs. 94% DOD window will lead to a $2800 increase in pack cost. Similarly, for the PHEV, adjusting the DOD for a 55% vs. 87% DOD window represents roughly a $4900 increase in pack cost.

Y. Zhang et al. [74] performed a study on the degradation of $LiFePO_4$ cells at various temperatures.

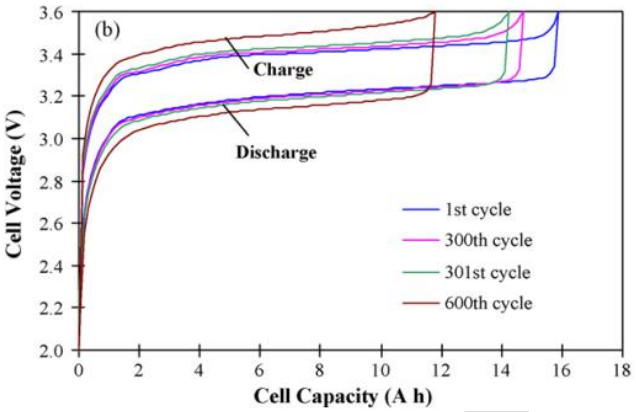

Figure 70 Cycling performance at 3C rate between 3.6 and 2.0 V at 50°C: charge–discharge loops for the beginning and last cycles of the 1st 300 cycles (1st and 300th cycles) and the 2nd 300 cycles (301st and 600th cycles). **[74]**

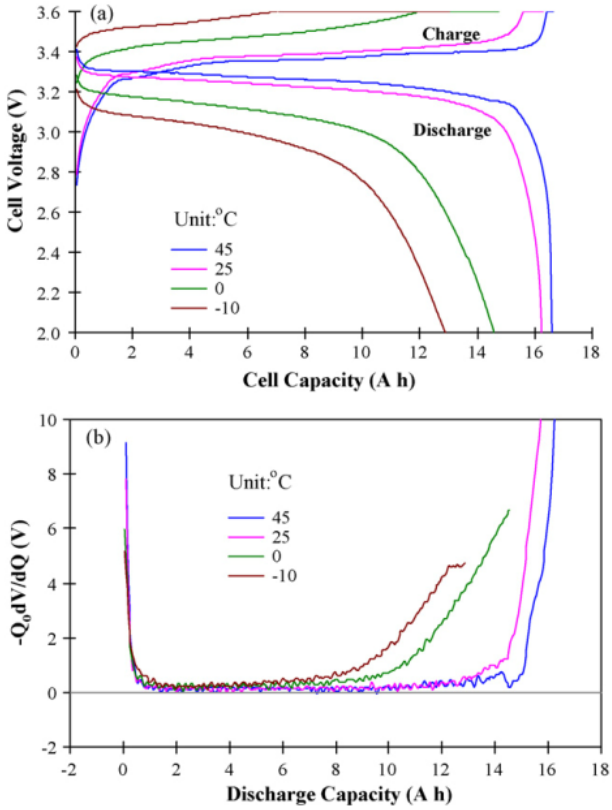

Figure 71 (a) Charge–discharge curves at 1C rate measured at different temperatures for a fresh cell and (b) the corresponding differential voltage ($-Q_o dV/dQ$) versus discharge capacity. [74]

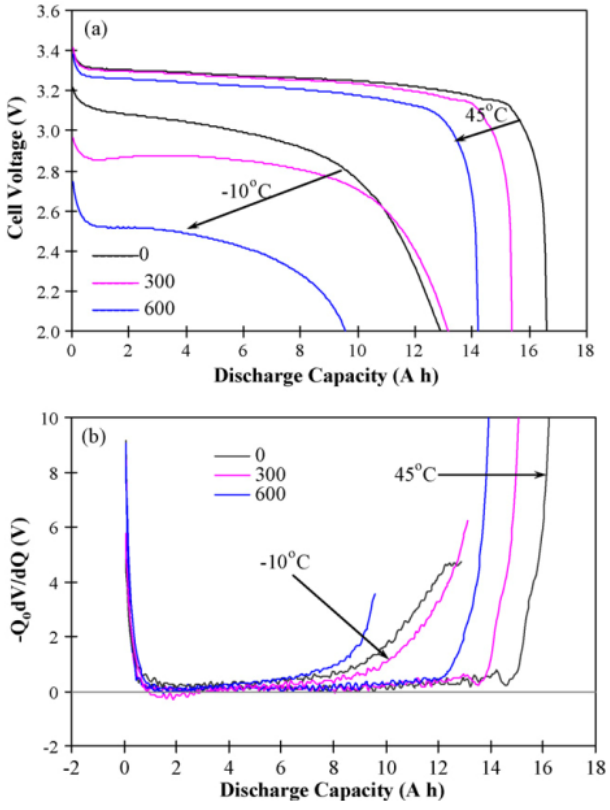

Figure 72 (a) Discharge curves at 1C rate measured at 45 and −10°C after different cycles and (b) the corresponding differential voltage ($-Q_o dV/dQ$) with respect to discharge capacity. [74]

An interesting result from [74] is that for testing temperatures of 25°C and 45°C, discharge capacity decreases linearly over the range of cycles 0 to 600. In the case of cycling at 0°C and -10°C, however, capacity fade is linear up to cycle 300, however, at 600 cycles, this has fallen drastically such at in the case of -10°C, a capacity fade of 25.8% at 600 cycles is noted [74].

Testing for power fade in [74] is done with an HEV focus, specifically evaluating using discharge resistance and discharge pulse power capability as derived from [75].

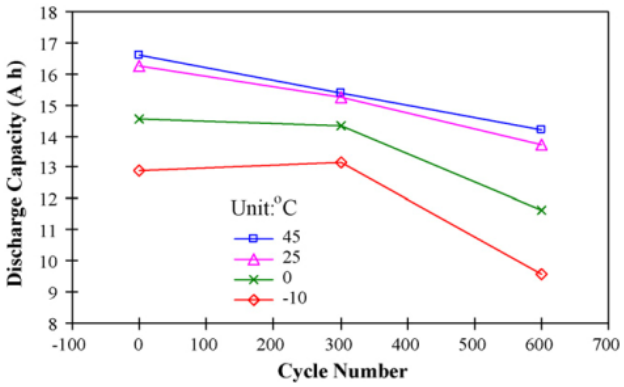

Figure 73 Discharge capacity measured at different temperatures varying with cycle number.

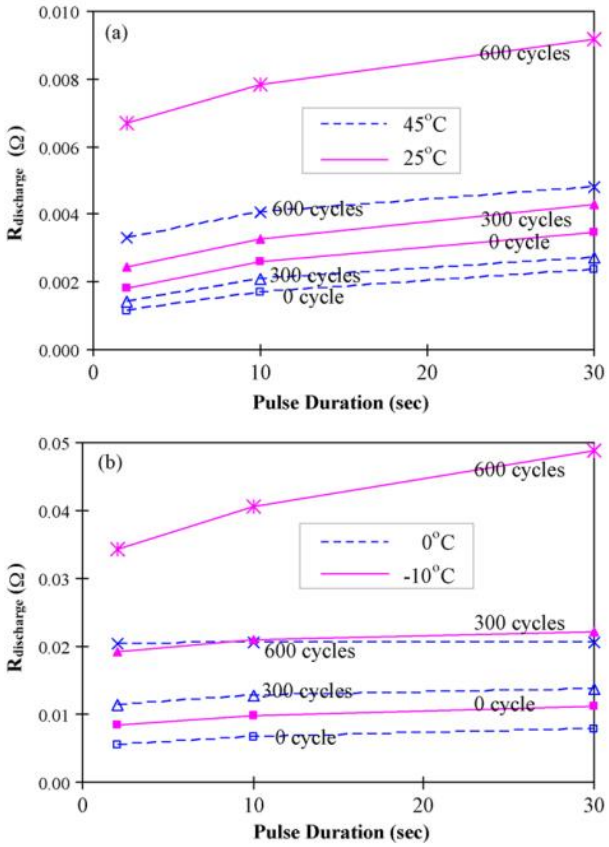

Figure 74 Discharge resistance changes with pulse duration after different cycles (a) at 45 and 25°C, and (b) at 0 and −10°C.

Degradation of a high capacity $LiFePO_4$ cell with deep cycling at elevated temperature of 50°C is studied by characterizing capacity fade, power fade and impedance rise at different test temperatures (45, 25, 0 and −10 °C). Capacity fade after 600 cycles is 14.3% at 45°C and 25.8% at −10°C [74]. The discharge pulse power capability at 45°C does not decrease with cycling (namely, there is little power fade) from 0 to 600 cycles, whereas the power fade after 600 cycles is 61.6% and 77.2%, respectively, at 0 and −10°C [74]. Increases in cell resistance at lower temperatures leads to more severe capacity and power fade. In particular, the power fade at low temperatures (e.g., 0 and −10°C) rather than capacity loss is a major limitation of the $LiFePO_4$ cell.

It was found from variations of the impedance spectra that the ohmic resistance (R_o) clearly rises in conjunction with the lowering of temperature and upon cycling. The activation energy increases from 4.3 kJ mol^{-1} for a fresh cell to 20.9 kJ mol^{-1} after 300 cycles, which suggests that the electronic resistance of electrode particles is dominant in R_o for a fresh cell and increasing electrolyte resistance has become dominant in R_o after 300 cycles. Accordingly, the increase of ohmic resistance with cycling comes mainly from increase in electrolyte resistance resulting from the lithium loss within the electrolyte due to lithium-consuming SEI layer growth and side reactions that also lead to loss of cyclable lithium. Evidence therefore suggests that the loss of cyclable lithium is the primary mechanism for capacity fade, as supported by the narrowing of close-to-zero plateaus in the differential voltage curves. Mid-frequency arc width (R_w) evidently increases (by 2.5–6 times) from 300 to 600 cycles due to SEI layer growth on the graphite anode with a catalytic effect from iron impurities that deposit from the dissolved iron on the $LiFePO_4$ cathode, but does not greatly increase (0.9–1.5 times) from 0 to 300 cycles because there is no catalytic effect of iron deposition in this period. Consequently, the increased interfacial resistance due to the catalytic growth of SEI layer on the anode and increased electrolyte resistance in Ro are the main sources for power fade, leading to very poor discharge pulse power capability at low temperatures (0 and −10°C) after cycling and even very small electric-only range due to power capability too low to surmount a high discharge peak power under the UDDS driving schedule. [74]

Anseán et al. [5] subjected $LiFePO_4$ (LFP) cells from five different manufacturers to a series of tests for evaluating cycle life, energy efficiency, power capability, and internal resistance. The results were compared against the USABC targets for xEV applications. The various cells are described in Table 14.

	Cell 1	Cell 2	Cell 3	Cell 4	Cell 5
Nominal capacity	2.3Ah	16 Ah	42 Ah	60 Ah	100 Ah
Maximum continuous discharge	70A (30C)	160A (10C)	126A (3C)	180A (3C)	300A (3C)
Maximum continuous charge	10A (4C)	80A (5C)	42A (2C)	180A (3C)	300A (3C)
Cell weight	70g	500g	1000g	2000g	3200g
Cell geometry	Cylindrical	Cylindrical	Pouch	Prismatic	Prismatic
DC internal resistance	8 mΩ	< 8 mΩ	N/A	< 2 mΩ	< 0.9 mΩ
Country of Origin	USA	China	Finland	China	China

Table 14 Summary of the main characteristics of the batteries tested in [5]

The above cells were tested in accordance with USABC guidelines.

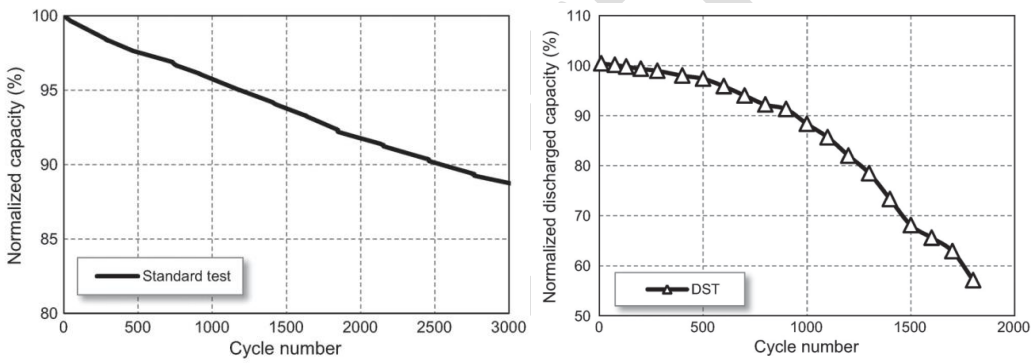

Figure 75 Cell 1 from [5] subjected to standard tests and USABC DST tests

The results of cycling tests for Cell 1 from Table 14 are shown in Figure 75. Under nominal conditions, the battery was tested for 3000 cycles, which corresponds to roughly 13 months of continuous testing. Under these conditions, 11% of capacity was lost. When subjected to more stressful testing, namely USABC DST tests, the cell was shown to meet EOL goals, losing 20% of capacity after approximately 1200 cycles [5].

The authors of [5] concluded that although the USABC long-term goal for cycling is achieved on both the nominal and the fast charge/DST, there are important differences in terms of capacity fade and power capability. Testing under standard conditions is usually well tolerated by the batteries. On the other hand, stressful conditions, as the ones that can be found on an actual EV, are more detrimental to the battery life. This helps to understand the importance of developing an adequate set of testing protocols and diagnosis tools that can simulate and predict the battery performance in real-life EV applications.

In terms of performance, the LFP cells tested by [5] fail to meet the long-term goals set by the USABC in terms of specific energy. All cells were able to meet the requirements for cycle life as specified.

Wood et al. [76] performed a study to understand the effect of battery degradation and the need for battery replacement in PHEVs through the experimental measurement of lithium-ion battery lifetime under PHEV-type driving and charging conditions. The work presented by [76] was a critique of the USABC manuals which were present at the time of [76]'s publication (2011). At the time, the work conducted was with respect to the 1996 USABC standards, whereas today there is a June 2015 revision (Rev. 3) of these USABC documents [77].

The test profile used by Wood et al. was adapted by Southern California Edison (SCE) to the test equipment at their Electric Vehicle Technical Center (EVTC). The 7.3 h cycle was applied to 3 PHEV battery modules

continuously from March 2005 to August 2009 for a total of 4323 cycles. Reference Performance Tests (RPTs) were conducted before the start of the life cycle test, and at periodic intervals every 240 test cycles (equivalent to approximately 2 months of testing) to characterize the performance of the battery. The following tests are included in each RPT:

- Constant current discharge at a rate of C/1.
- Constant current discharge at a rate of C/3.
- Peak power test.
- Hybrid Pulse Power Characterization (HPPC) Test (performed in the dual mode configuration).

The first three tests were performed using the methods of the USABC Electric Vehicle Test Procedure Manual, 2nd Revision (1996) ; the HPPC test was performed using the methods the PNGV Battery Test Manual [16]. A preliminary cycle, including a discharge at a constant current rate of C/3 down to 60% DOD and a full recharge, was performed prior to each RPT. A 30 min rest was included in between each charge and discharge.

The authors of [76] examine both SOC and t-SOC, where t-SOC is defined as being the thermodynamic state of charge. This is defined as a characterization of the battery with respect to its instantaneous chemical composition. An example of how this relates to the capacity of the battery is shown in Figure 76.

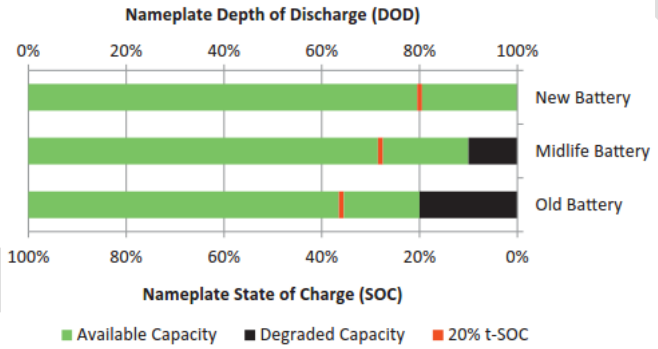

Figure 76 Variation of t-SOC as a result of capacity degradation. As the battery degrades, the degraded capacity occupies a greater fraction of nameplate SOC, whereas t-SOC is normalized to the available capacity. **[76]**

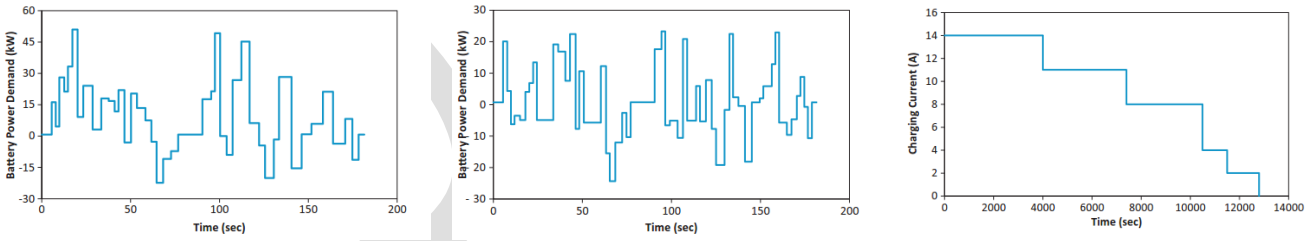

(a) (b) (c)

Figure 77 Degradation test procedure profiles for (a) PHEV CD test, (b) PHEV CS test, and (c) PHEV charging profile **[76]**

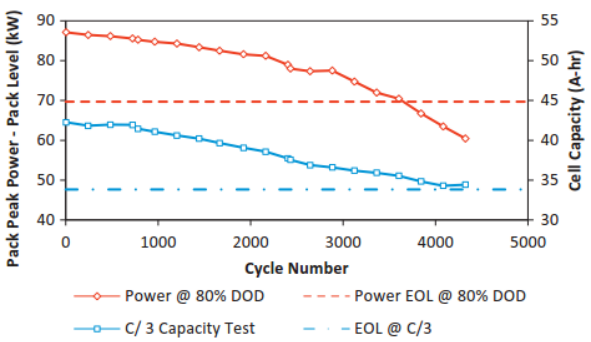

Figure 78 Energy and power measurements as a function of cycle number (fig5) **[76]**

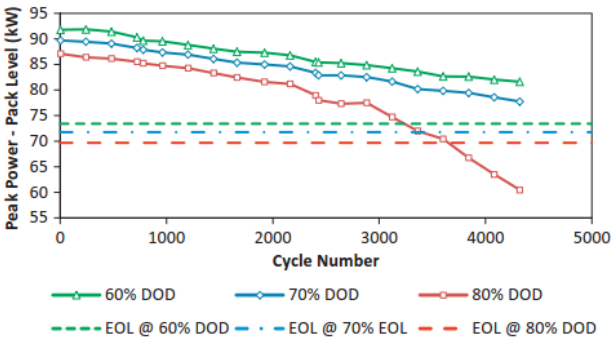

Figure 79 Power degradation at various levels of capacity based DOD as a function of cycle number (fig6) **[76]**

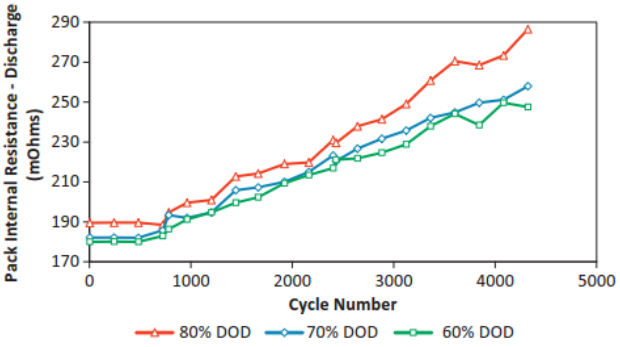

Figure 80 Pack internal discharge resistance as a function of cycle number **[76]**

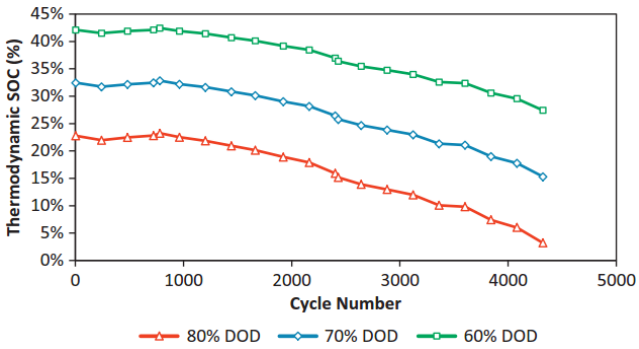

Figure 81 Thermodynamic SOC relative to capacity based DOD as a function of cycle number **[76]**

The results of the experimental battery degradation tests show that PHEVs can increase their battery cycle life and power capability by implementing a degradation control strategy (DCS) which allows the battery to reduce its maximum capacity-based DOD during operation so as to maintain a constant minimum t-SOC. These changes to the battery DCS should minimize increases in fuel consumption, performance and lifecycle cost of the PHEV. To determine the effects of battery degradation and DCS on these PHEV attributes, a light commercial vehicle was modeled and simulated as a blended-mode capable, parallel PHEV20. A vehicle simulation environment was used to relate battery degradation to changes in vehicle performance. These simulations assume that calendar life degradation in practice is insignificantly different from calendar life degradation in the laboratory, that module-level performance degradation dominates over pack level effects such as module imbalance, and that the rate of battery degradation is independent of control strategy.

Simulations were performed using two DCSs: a “Static DCS” and a “Dynamic DCS”. The Static DCS maintained the SOC window in the battery such that the energy available for discharge remained constant over the battery’s life (equivalent to maintaining a constant, minimum capacity-based SOC over the lifetime of the vehicle). The

Dynamic DCS allowed for a constant percentage of thermodynamic capacity to be utilized in CD mode such that the energy available for discharge was a function of the actual energy available in the battery instead of rated capacity (equivalent to measuring and recalibrating the minimum t-SOC continuously over the lifetime of the vehicle). The Dynamic DCS ensured that the vehicle entered charge sustaining mode at 25% t-SOC.

The vehicle model employed in these simulations represents a limited-production vehicle which was designed so that the battery was not oversized in terms of its power output, thereby minimizing incremental costs. As such, any loss of battery power from original specifications would be immediately visible at the vehicle level. Modern PHEVs are designed with some battery power margin to allow for battery degradation without affecting the electrical power capability of the drivetrain. As such, these degradation simulations represent a worst-case scenario.

The question of charge patterns is specifically addressed in [56] and [53] [29] [78] [57]

Hoke et al. [78] performed a study using a simplified lithium-ion battery lifetime model (which includes effects due to temperature, state of charge profile, and daily depth of discharge) with the goal of developing an optimized charge pattern which would account for electricity cost and degradation. The chemistry utilized for this study was that of nickel-cobalt-aluminum (NCA) cathode and graphite anode. The optimized charging

algorithm as described in [78] was run simultaneously for three vehicles with different plug-in times, initial SOCs, and charge target times. Each vehicle had a 30-kWh battery pack with a minimum SOC of 20% and a maximum SOC of 90%. Ambient temperature for this experiment was set at 25°C.

Name	Description
Optimized	Optimized per Section III of [78]
Early 3.3 kW	Upon plug-in at 3.3 kW
Early 6.6 kW	Upon plug-in at 6.6 kW*
12am 6.6 kW	At midnight at 6.6 kW*
Late 6.6 kW	As late as possible at 6.6 kW*
Late 24 kW	As late as possible at 24 kW

Table 15. Charge Profiles; * SAE Level II maximum

In order to ascertain whether or not their charge optimization method actually reduced battery degradation, Hoke et al. looked at experimental driving data from a large scale usage study of Toyota Prius PHEVs and combined these with several simulated charge profiles described in Table 15. For the simulation, a typical driving week was selected involving five days of commuting 26-40 km (16-25 miles) round-trip, one longer trip of 65 km (40 miles), and one day on which the vehicle was not used. These data provided the driving SOC profiles, time windows available for charging, and initial SOC values for each charge. Simulations were performed for three battery sizes: the 3.5 kWh battery in the Prius, a 19 kWh battery, and a larger 35 kWh battery. The authors scaled the Prius data in order to obtain hypothetical simulated SOC profiles for the larger batteries.

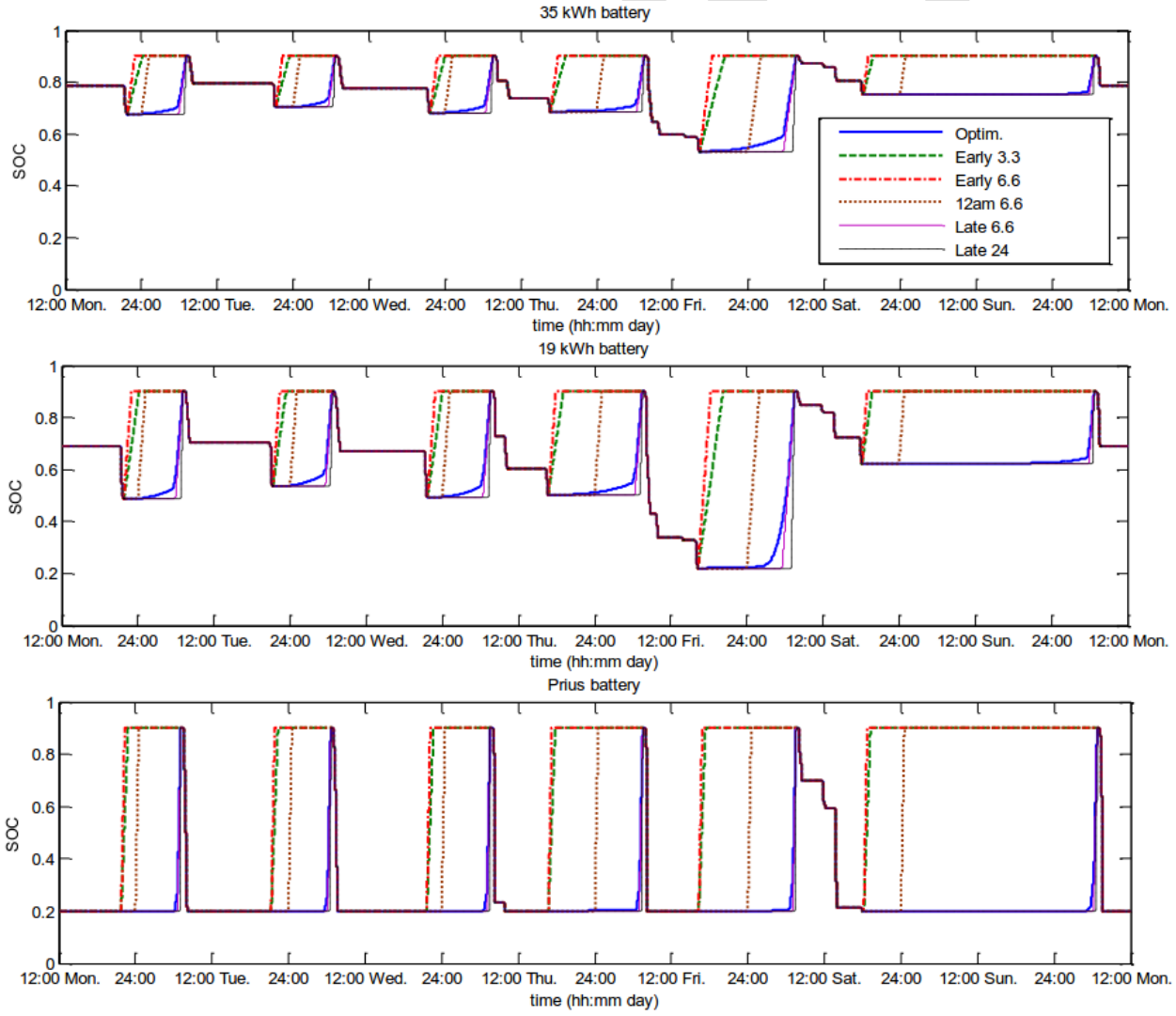

Figure 82. Weekly SOC profiles for three battery sizes under various charging scenarios

Six charging scenarios, described in Table 15, were imposed upon each experimental driving SOC profile. Figure 82 shows weekly SOC profiles for all three batteries under each charge scenario. The charge scheme labeled "Optimized" uses the charge optimization method described in [78] , with flat cost of electricity so that battery life is maximized. The two "Early" schemes begin charging 5 minutes after the vehicle is plugged in. The two "Late" schemes reach full charge 30 minutes before the vehicle leaves. The "Late 24 kW" scheme requires a DC fast charger.

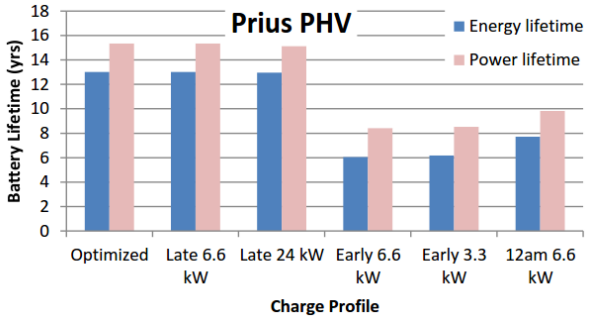

Figure 83. Prius battery lifetime under various charge scenarios

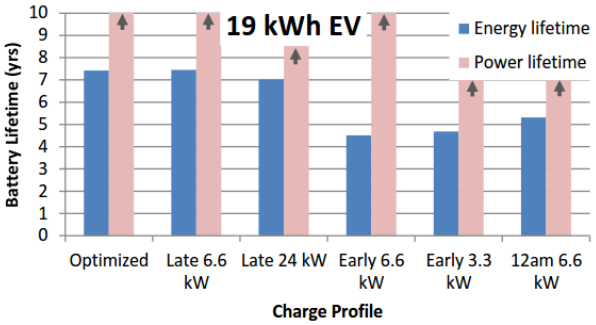

Figure 84. 19 kWh battery lifetime under various charge scenarios. Power lifetimes truncated.

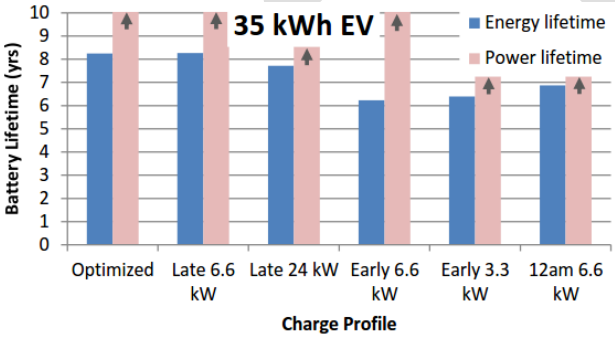

Figure 85. 35 kWh battery lifetime under various charge scenarios. Power lifetimes truncated. **[78]**

This charging data was fed into NREL's model to compute the estimated battery lifetime for each scenario, assuming the charge cycle is repeated weekly. Figure 83 through Figure 85 show battery lifetime for each scenario. For each of the three battery sizes, the optimized charge resulted in longer battery life than all but the "Late 6.6 kW" scenario, which resulted in almost the same battery life (within the accuracy of the model). The estimated lifetime under optimized charging is between 1% and 115% longer than the lifetime under the other scenarios considered. The gains in lifetime from optimized charging are largest for the smallest battery.

The authors of [78] note of course that the benefits of charging late in the available window must of course be balanced with the utility of the vehicle: having the vehicle unavailable for unexpected late-night trips may be unacceptable to some drivers. This consideration is most important for BEVs and may not be a concern for PHEV drivers.

Niikuni et al. [79] sought to construct a test method for the evaluation of battery degradation, using load conditions that reflect the situation of an actual vehicle. In this study, the degrees of influence of two load terms, both a specific charge/discharge load (corresponding to the cycle life) and a thermal load (corresponding to the calendar life), in the capacity reduction were compared and a condition for an accelerated test was also discussed [79]. Four sets of three batteries each were tested at temperatures of 25°C, 40°C, 55°C, and 70°C.

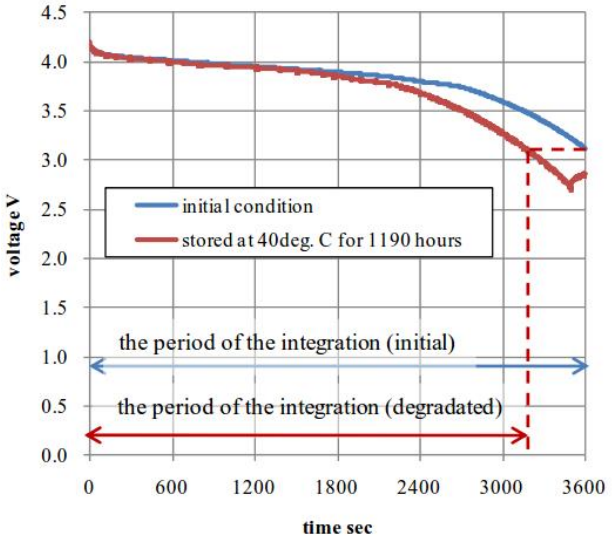

Figure 86 Comparison of the discharge characteristics of a battery which was initially not stored at 40°C at beginning of testing and after 1190 hours of storage at 40°C **[79]**.

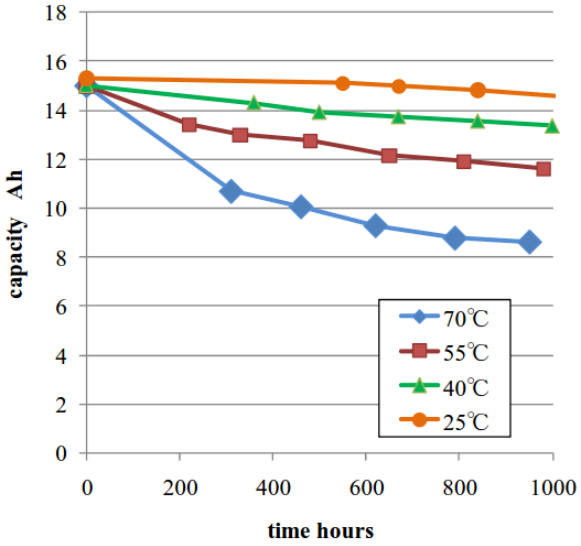

Figure 87 decrease of Ah capacity in each of the temperature conditions **[79]**

Capacity under a strictly thermal load was examined. The results showed that for ambient temperatures below 55°C, the capacity loss of test battery cells was proportional to the square root of days. Although the test battery cells had relatively short lifetime, the characteristic of the capacity loss against thermal load was same as that of other typical lithium ion batteries. Only the variation of the capacity loss under the condition of 70°C was not proportional against the square root of days and it suggested that other degradation processes, for example the degradation in the electrolyte, might be influenced.

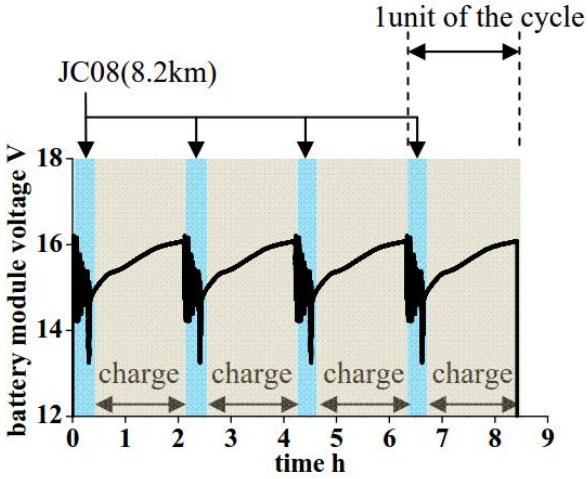

Figure 88 Voltage variation of the test battery module with the JC08 charge/discharge patterns **[79]**

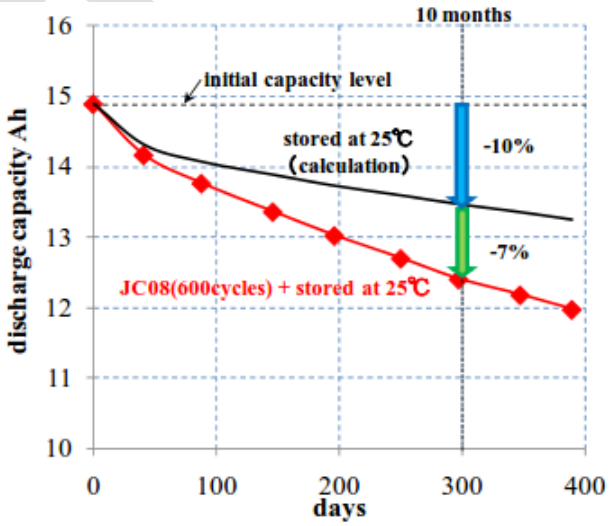

Figure 89 Variation of the discharge capacity against time in days [79]

The degree of influence of two load terms both the JC08 pattern cycle (corresponding to the cycle life) and the thermal load (corresponding to the calendar life) on the capacity reduction was compared. From the results, it was observed that there was a 7% difference in the capacity reduction between the specific pattern and the thermal-only load. In addition, the potential of a thermally accelerated test under the condition that consists of both the JC08 charge/discharge load and thermal load was shown. This methodology will contribute to evaluate battery degradation in a short period.

Niikuni et al. also offer an accelerated testing solution as part of their study in [79]. Coupling the JC08 cycling with an increase in temperature to +39°C (as opposed to +25°C as depicted in Figure 89), they were able to achieve the 17% loss from the initial level in 1.7 months as opposed to 10 months of testing.

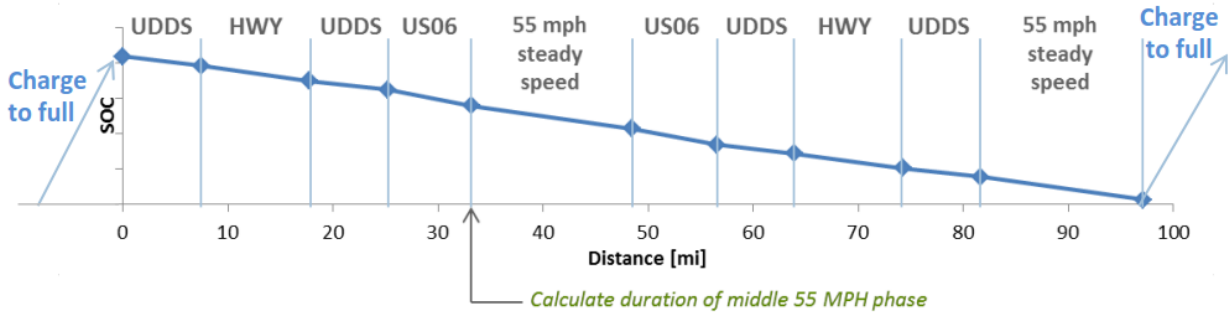

Figure 90 Multi-Cycle Test for BEV used by Argonne National Laboratory (Simplified) **[80]**

One method of charging a vehicle during its on-road operation is by way of regenerative braking, which offers short periods of recharging. A study by Keil & Jossen set out to address the impact of regenerative braking on the aging of lithium-ion batteries in electric vehicles [81]. As part of their study, lithium ion cells with NCA chemistry and a minimum nominal capacity of 2.8 Ah were used.

	Duration (min)	**Average Velocity (km/h)**	**Discharged Ampere-hours (Ah)**	**Maximum Charge Recovery**
ARTEMIS Urban	16.5	16.2	0.151	25%
ARTEMIS Road	18.0	57.5	0.354	17%
ARTEMIS Motorway 130	17.8	96.9	0.773	8%
NYCC	10.0	11.4	0.063	21%
FTP72	22.8	31.5	0.244	19%
LA92	23.9	39.7	0.401	20%
HWFET	12.8	77.7	0.277	6%
US06	10.0	77.3	0.369	15%

Table 16 Comparison of eight European and American driving cycles including the maximum amount of charge recovered in the driving simulation with vehicle A **[81]**

From the data in Table 16, it is shown that the amount of energy that can be recovered by regenerative braking in highway driving cycles amounts to 8 % for the Artemis Motorway 130, 6 % for the HWFET, and 15 % for the US06 driving cycle. Since the American US06 driving cycle recovers substantially more charge than the other two highway driving cycles and since it contains a considerable percentage of regenerative braking events with a current magnitude above 2A (see Figure 91), it was selected for the cycle life study in [81]. In this cycle life study, different influencing factors are investigated: temperature, SOC, and the magnitude of regenerative braking. For each factor, at least three values were tested. Different magnitudes of regenerative braking were implemented by varying the maximum recharge current rate of the load profile.

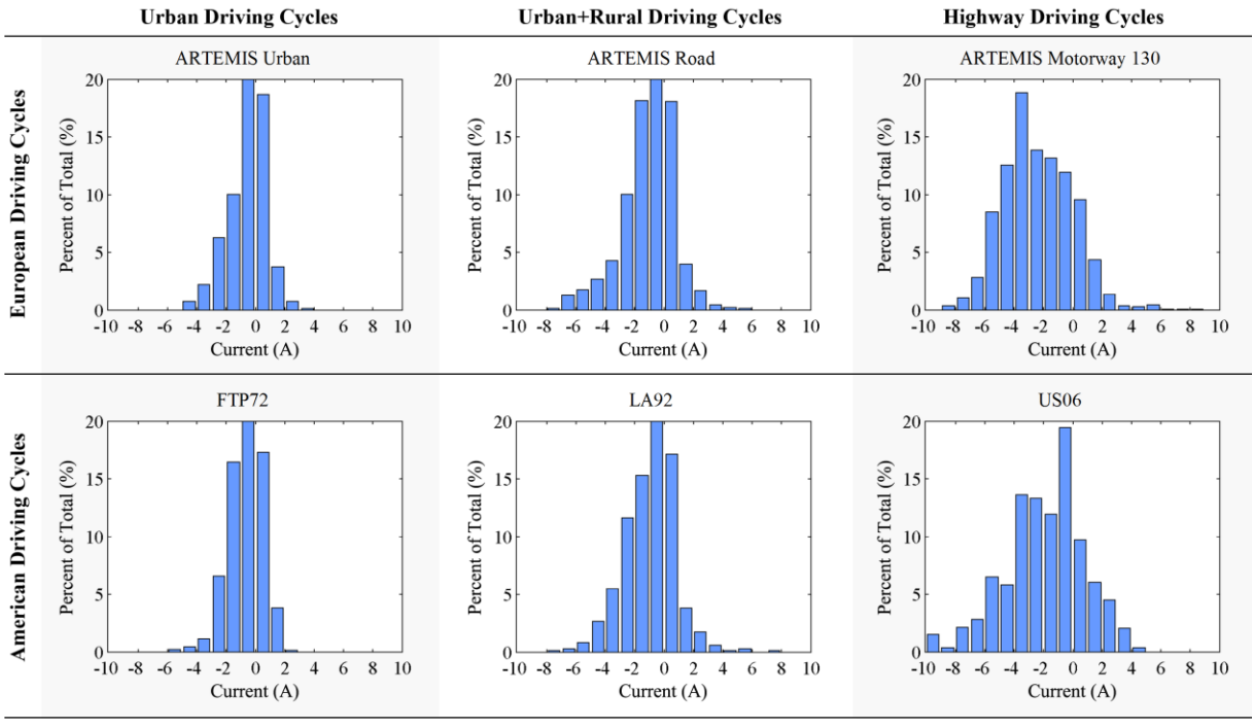

Figure 91. Distribution of cell currents for different European and American driving cycles as percent of total driving cycle duration [81]

Keil & Jossen employed a cycle life testing approach which was defined as follows: After placing the cell in its temperature chamber, it would be charged with a constant current of 0.7 A (= 0.25 C), until it reached its dedicated charging voltage as defined by the low (3.7V), medium (3.9V), and high (4.1V) SOC values defined for the experiments. It should however be noted that for testing at 10°C, the low and medium SOC states were set to 3.75V and 3.925V, respectively. This correction was applied due to internal resistance growth at low temperature. Following a pause of 5 minutes, two consecutive driving cycle runs were performed with a pause of 1 minute between each run. The combination of constant-current charging and two driving cycle runs is repeated 400 times. As each of the 400 cycles depletes about one fourth of the cell's capacity, each cell has been charged and discharged approximately 100 times its nominal capacity (= 280 Ah) between two checkups. The authors of [81] focused on capacity changes as a result of cycling. In doing so, they found that after five months of cycle life testing, the lithium-ion cells were exposed to a charge throughput of 1400 Ah, corresponding to 500 equivalent full cycles and roughly 50000 km of distance traveled.

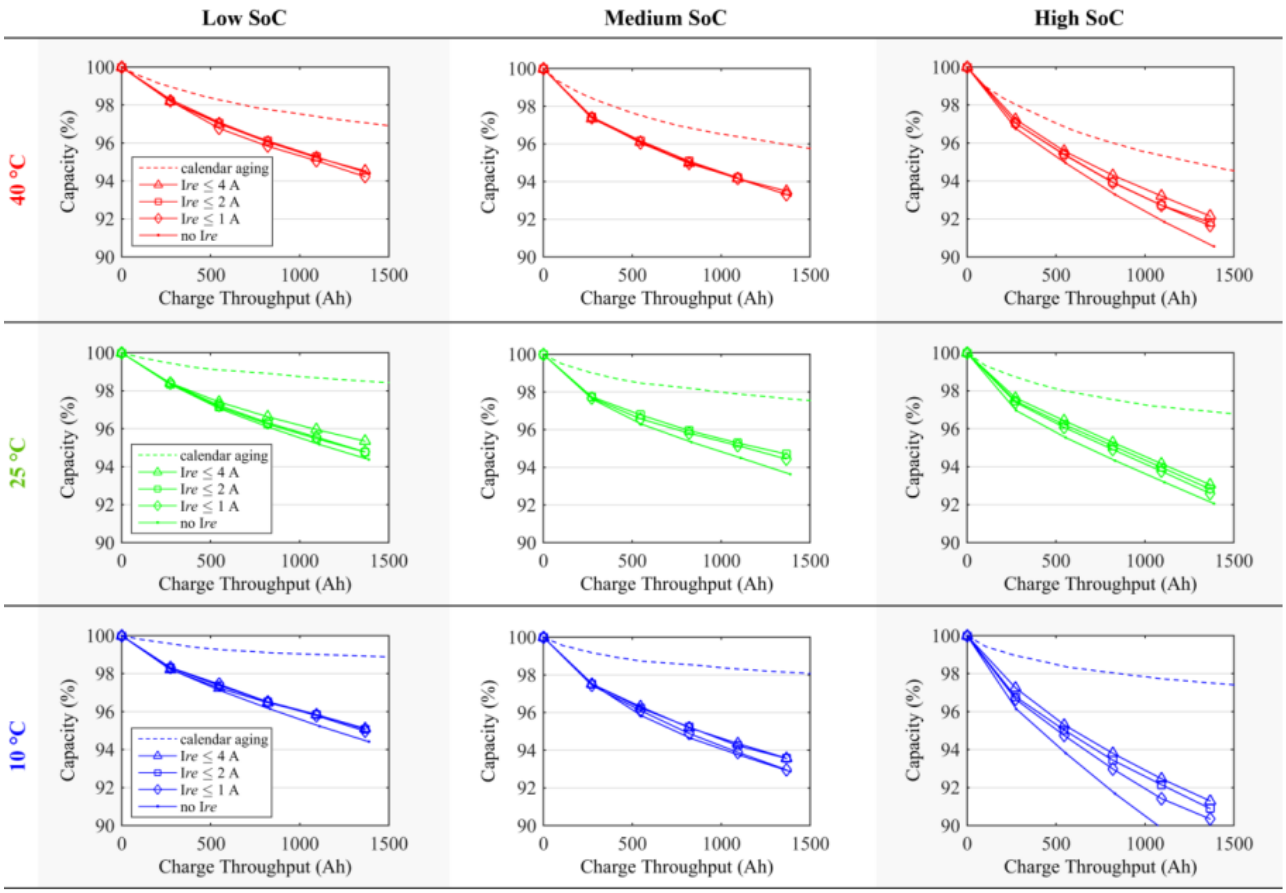

Figure 92. Cell degradation during the cycle life experiment for the four magnitudes of regenerative braking at different temperatures and SoC. The checkup measurements have always been performed after a total charge throughput of about 280 Ah (= 280 Ah charged + 280 Ah discharged), which represents a driven distance of 10,000 km. The calendar aging curves are scaled accordingly to the about four weeks of cycling between two consecutive checkups. I*re* refers to maximum allowable regenerative current. **[81]**

The authors found that for higher levels of regenerative braking, battery aging was reduced. Referring to Figure 92, it can be seen that this has a more pronounced effect for high SOC and low temperature. This can be attributed to lithium plating, which is typically aggravated under these conditions. The results of the cycle life testing also suggest that regenerative braking helps to reduce lithium plating. The authors reason that this is explained by a decreased DOD after driving cycles as charge recovered from regenerative braking leads to higher ending SOC following a driving cycle. Consequently, the amount of constant-current charging required is reduced.

Fleet & On-Road Testing Activities

The Advanced Vehicle Testing Activity (AVTA) of the Idaho National Laboratory has the stated purpose of providing benchmark data for technology modeling, and research and development programs, by benchmarking and validating the performance of light-, medium-, and heavy-duty vehicles that feature one or more advanced technologies. Published on their website one is able to find test reports for a number of xEVs, with many models of vehicles having multiple unique vehicles (given by VIN) evaluated.

Vehicle models for which battery testing information is available is shown in below in Table 17.

Battery Electric Vehicles (BEVs)	Hybrid Electric Vehicles (HEVs)	Plug-In Hybrid Electric Vehicles (PHEVs)
• 2015 Chevrolet Spark • 2015 KIA Soul • 2014 BMW i3 • 2014 Smart Electric Drive Coupe • 2013 Ford Focus • 2013 Nissan Leaf • 2012 Mitsubishi i-MiEV • 2012 Nissan Leaf • 2011 Nissan Leaf	• 2015 Honda Accord • 2014 Volkswagen Jetta • 2013 Ford C-Max • 2013 Chevrolet Malibu • 2013 Honda Civic • 2011 Hyundai Sonata • 2011 Honda CRZ • 2010 Toyota Prius Gen III • 2010 Ford Fusion • 2010 Honda Insight • 2008 Chevrolet Tahoe • 2007 Nissan Altima • 2007 Saturn Vue • 2007 Toyota Camry • 2006 Honda Civic • 2006 Lexus RX400H • 2005 Ford Escape • 2005 Honda Accord • 2004 Chevrolet Silverado • 2004 Toyota Prius • 2003 Honda Civic • 2002 Toyota Prius • 2001 Honda Insight	• 2014 BMW i3 REx • 2013 Ford Fusion Energi • 2013 Ford C-Max Energi • 2013 Toyota Prius PHEV • 2013 Chevrolet Volt • 2011 Chevrolet Volt • 2011 Chrysler Town & Country

Table 17 Vehicle Models with Battery Testing Results from INL [82] [83] [84]

For testing the vehicles in Table 17, they are operated on-road for a minimum mileage accumulation of 160,000 miles. Vehicle characteristics are then weighed against the existing DOE End of Life criteria using tests for acceleration, hybrid pulse power characterization, and static capacity. Degradation values are evaluated at initial laboratory and final laboratory tests. It should be noted that some of the later models in Table 17 have only undergone their initial tests, and degradation figures are not yet available.

Degradation of Battery Over Test Periods		
Vehicle	**Hybrid Pulse Power Characterization Test**	**Static Capacity Test**
2011 Honda CR-Z 4466 [85]	ΔPeak Pulse Discharge Power @ 10s: -0.32kW (-3.7%) ΔPeak Pulse Charge Power @ 10s: -0.94kW (-11%)	Measured Average Capacity: -0.68Ah (-12%) Measured Average Energy Capacity: -70 Wh (-12%)
2011 Hyundai Sonata 3539 [86]	ΔPeak Pulse Discharge Power @ 10s: -25.5kW (-52%) ΔPeak Pulse Charge Power @ 10s: -4.8kW (-14%)	Measured Average Capacity: -1.14Ah (-22%) Measured Average Energy Capacity: -334Wh (-24%)
2010 Toyota Prius 0462 [87]	ΔPeak Pulse Discharge Power @ 10s: -5.3kW (-26%) ΔPeak Pulse Discharge Power @ 1s: -4.4kW (-16%) ΔPeak Pulse Charge Power @ 10s: -0.5kW (-3.0%) ΔPeak Pulse Charge Power @ 1s: -6.2kW (-26%)	Measured Average Capacity: -1.25Ah (-20%) Measured Average Energy Capacity: -200Wh (-15%)
2010 Ford Fusion 4757 [88]	ΔPeak Pulse Discharge Power @ 10s: -1.8kW (-8.0%) ΔPeak Pulse Discharge Power @ 1s: -1.5kW (-4.9%) ΔPeak Pulse Charge Power @ 10s: -2.6kW (-17%) ΔPeak Pulse Charge Power @ 1s: -5.9kW (-23%)	Measured Average Capacity: -0.20Ah (-3.8%) Measured Average Energy Capacity: -110Wh (-8.0%)
2010 Honda Insight 0141 [89]	ΔPeak Pulse Discharge Power @ 10s: -0.34kW (-3.7%) ΔPeak Pulse Discharge Power @ 1s: -1.9kW (-12%) ΔPeak Pulse Charge Power @ 10s: -0.39kW (-4.7%) ΔPeak Pulse Charge Power @ 1s: -0.5kW (-3.6%)	Measured Average Capacity: -0.03Ah (-0.5%) Measured Average Energy Capacity: -10Wh (-1.7%)
2010 Toyota Prius 6063 [90]	ΔPeak Pulse Discharge Power @ 10s: -2.5kW (-13%) ΔPeak Pulse Discharge Power @ 1s: -1.9kW (-4.9%) ΔPeak Pulse Charge Power @ 10s: +0.39kW (+36%) ΔPeak Pulse Charge Power @ 1s: +4.1kW (+18%)	Measured Average Capacity: -1.15Ah (-0.5%) Measured Average Energy Capacity: -260Wh (-20%)

Table 18 INL 160,000 mile tests

Each of the vehicles in shown in Table 18 was operated over 160,000 miles (approx. 257,500km). On-road fleet testing was performed by ECOtality North America (in conjunction with EZ-Messenger courier services). The vehicles in these tests are subjected to a combination of city and highway routes using several different drivers in order to expedite the mileage accumulation and reach the vehicle end of life. For example, the 2011 Honda Insight, 45.2% of the driving was considered to be city driving and 54.8% was highway driving [89], where city routes are determined as being those with an average speed of less than 42mph. The Toyota Prius, with VIN 6063 [90], experienced 18.9% degradation in battery capacity and stayed below DOE targets for all aspects of the HPPC test over the duration of approximately 160,000 miles of fleet testing. In this case, the vehicle was driven 30.5% in city routes and 69.5% on highway routes. The other Prius in the fleet, with VIN 0462, was subjected to 29.4% city and 70.6% highway routes, exhibiting degradation of 20% of the battery, reaching EOL [87].

On-road testing of a 2012 Chevrolet Volt [91] was performed during the winter and spring months in order to determine the impact of cold temperature on driving and charging efficiency. A single test vehicle was parked and charged overnight in an unsheltered parking stall and operated by a single driver in the morning hours, following a specified route which included rural, city, and highway roads. Throughout the testing process, the climate control was set to 72°F.

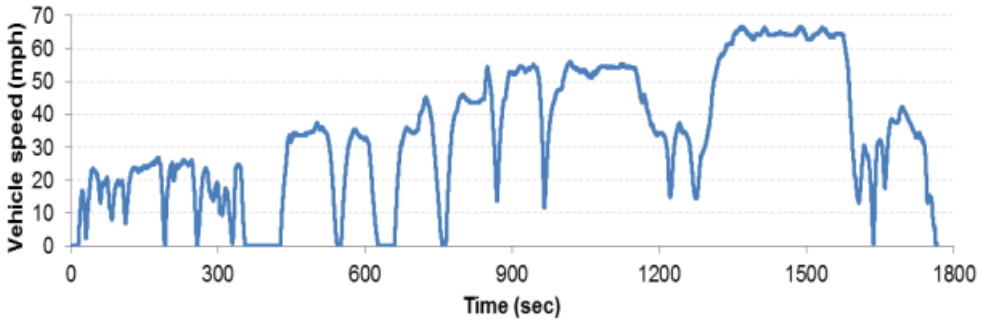

Figure 93 A selected vehicle speed profile for the Idaho Falls cold weather test route [91]

Tests were repeated until the vehicle's battery was depleted to the point that the operating mode transitioned from CD to CS mode. Ambient temperatures ranged from -17°F (-27°C) to +70°F (+21°C). However, as has

been noted earlier in [70], for example, at approximately 27°F, the Volt's ICE will begin to start periodically, consuming fuel. The coldest CD test which was recorded was performed with an average ambient temperature of -15°F. Electrical energy efficiency across all CD tests with cold starts ranged from 246 DC Wh/mi to 452 DC Wh/mi. The Volt's full-charge EV range dropped from 42.0 miles at 70°F to 19.7 miles at -15°F, a reduction of 53%.

Test Standards & Procedures for xEV Batteries

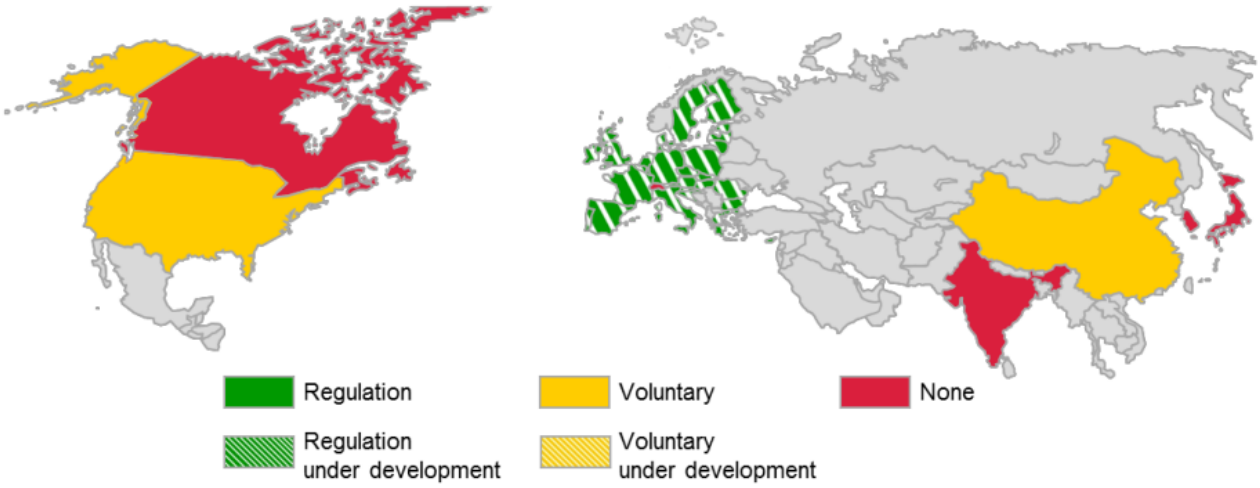

Figure 94 Battery durability requirements, world-wide view **[9]**

According to EVE-IWG [9] battery durability is somewhat unaddressed by present standards, with some exceptions being partial coverage in US and Canadian laws and optional Automotive Industry Standards in China. The activity level is expected to increase however with plans to develop battery durability requirements within the framework of the WLTP, which will be subsequently adopted into EC law (2015/2016). These requirements will not only address battery lifecycle determination, but the impact of partially deteriorated batteries on CO_2 emissions / fuel economy. [9]

The US EPA/NHTSA specifies a procedure for measuring the deterioration of PHEV batteries. This is to ensure that the CO_2 emissions from the vehicle do not increase excessively over the useful life of the vehicle. The regulation requires that CO_2 deterioration not exceed 10% of a vehicles certified value at full useful life. There are no regulations in place to address the durability of battery packs in BEVs, but the USABC has voluntary test procedures that can be followed for testing these so-called rechargeable energy storage devices (RESSs) [92]. There also exist voluntary SAE standards for battery module life cycle testing (J2288) and vibration testing (J2380). It should be noted that SAE J2288 is functionally identical [93] is the USABC Baseline Life Cycle Test Procedure. In order to earn California ZEV credits, the California Air Resources Board (ARB) stipulates a durability requirement for HEVs and PHEVs which is enforced through a 10 year, 150,000 mile warranty of "zero-emission energy storage device used for traction power" that automakers must provide in conjunction with the sale of these vehicles [94]. Canadian Federal law has included the US procedure for PHEVs, but does not presently have anything in place with regard to BEVs. China has established voluntary guidelines for the determination of battery reliability and durability through the QC/T 743-2006 Automotive Industry Standard. The European Commission does not presently have battery durability requirements, but will adopt into law durability test requirements that are planned to be developed within the framework of the WLPT. Voluntary standards ISO 12405-1:2011 (International Standards Organization) and IEC 62660-2 (International Electrotechnical Commission) both address durability testing of Lithium Ion batteries. Japan, India, South Korea, and Switzerland do not presently have requirements relating to battery durability. [9]

As we consider durability to relate battery lifetime, from a combination of calendar life and cycle life standpoints, we shall examine components of standards and test procedures which specifically target these factors, with an emphasis on State of Health. Certain abuse and safety tests, such as penetration, shock, crush, etc. are not considered as part of the scope encompassing durability.

In its PHEV Battery Test Manual, the Idaho National Laboratory (INL) identifies three phases of testing, with those being characterization, life, and reference performance testing. As part of the scope of this review, we shall focus on both life and reference performance testing as it is derived from the INL PHEV Battery Test Manual. Characterization testing establishes the baseline performance and includes static capacity, hybrid pulse power characterization, self-discharge, cold cranking, thermal performance, and efficiency tests. Life testing establishes behavior over time at various temperatures, states of charge and other stress conditions and includes both cycle life and calendar life testing. Reference Performance Tests establish changes in the baseline performance and are performed periodically during life testing, as well as at the start- and end-of-life testing.

Life Testing Procedures

Per the U.S. Department of Energy and Idaho National Laboratory [77] [75], life testing consists of cycle-life and calendar-life aging to ensure the device can meet EOL targets. Cycle-life testing consists of repeating a test profile continuously for a sustained period of time until the appropriate amount of energy has been depleted specified by EOL. Cycle life testing as defined per ISO 12405-1

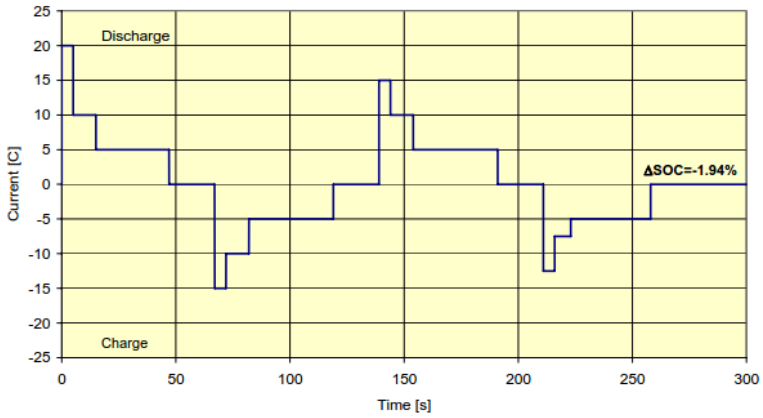

Figure 95 ISO 12405-1 — Current profile for cycle life test — Discharge-rich profile **[95]**

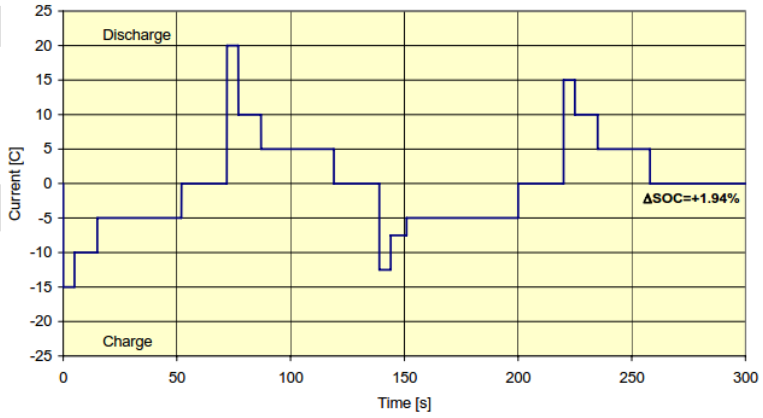

Figure 96 12405-1 — Current profile for cycle life test — Charge-rich profile **[95]**

As shown in Figure 95 and Figure 96, ΔSOC is -1.94% and +1.94%, respectively, over a period of 300 seconds. These cycles are combined in Figure 97 to present a cycle wherein the battery SOC goes from 80% to 30% and is then charged back up to 80%. Operating within this SOC range is a good way to ensure battery longevity, as deep-discharges from 100%-0% are shown to negatively impact battery SOH.

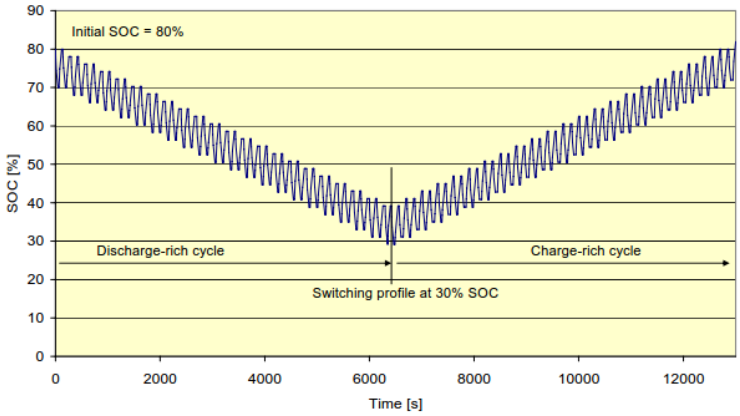

Figure 97 12405-1 — Typical SOC swing for combined cycles in Figure 95 and Figure 96 **[95]**

In the case of ISO 12405-2, SOC swing is from 100% to 20%. As above, there are two procedures which are combined to form a full cycle, and in this instance these are

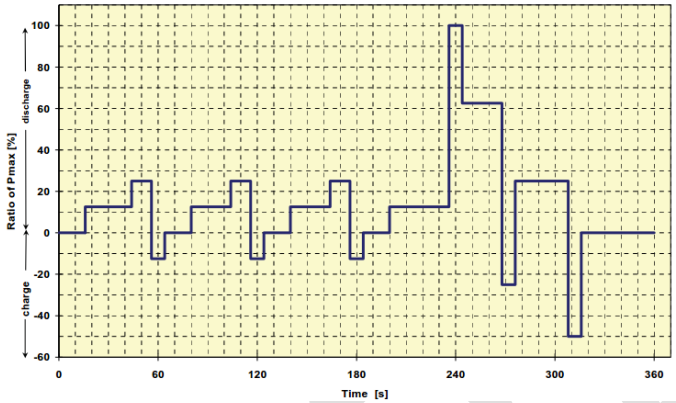

Figure 98 ISO 12405-2 Profile for cycle life test — Dynamic discharge power profile A **[96]**

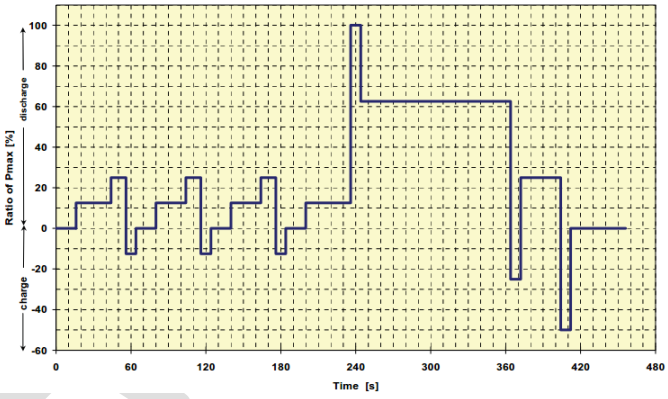

Figure 99 ISO 12405-2 Profile for cycle life test — Dynamic discharge power profile B **[96]**

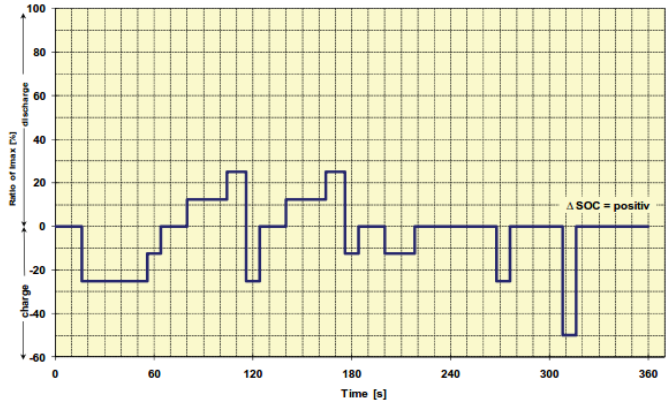

Figure 100 ISO 12405-2 Profile for cycle life test — Plug-in charge-rich current profile **[96]**

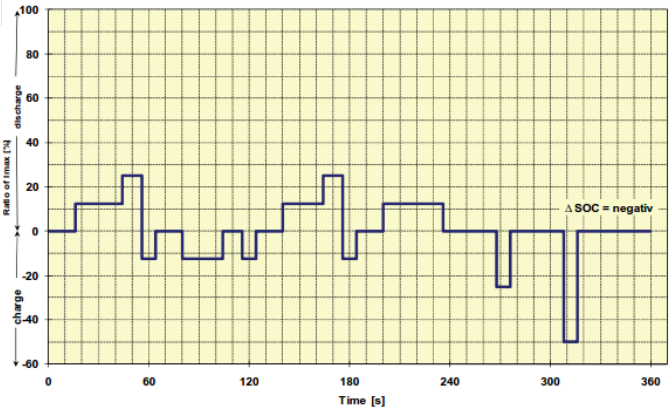

Figure 101 ISO 12405-2 Profile for cycle life test — Plug-in discharge-rich current profile **[96]**

Calendar-life testing generally consists of resting the device under test at OCV using elevated test temperatures with a pulse profile applied once per day. Calendar life tests are therefore more of an evaluation of degradation due to the passage of time. The specification for calendar life has the battery being charged and stored at 30°C.

This provides an adequately high temperature when compared to some of the findings for average temperature as determined by the climate data used in [73], [65], [63], [62], and [58].

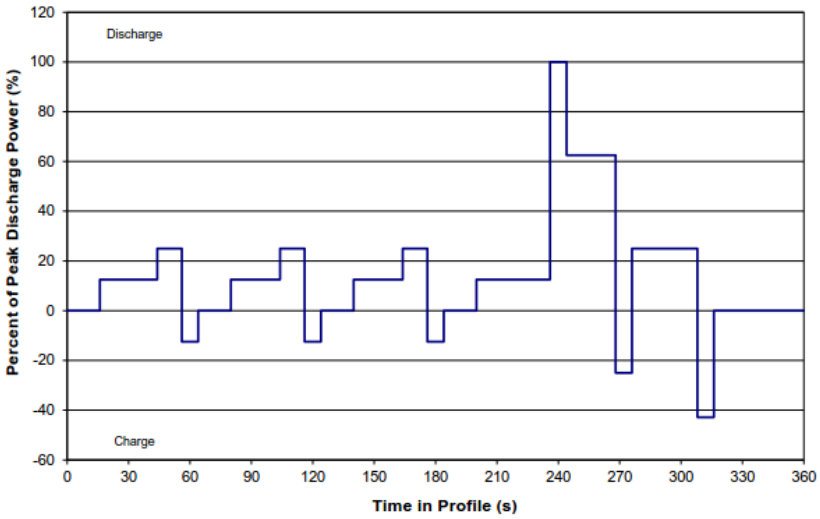

Figure 102 Charge-Depleting Cycle Life Test Profile for the BEV Battery **[77]**

One set of standards which may not have been considered for commercial electric vehicle applications are those from the United States Department of Defense [97], specifically for Group 31 and Group 34 lithium-ion batteries. These feature a range of performance and environmental tests which may be useful for determining some standards for xEV testing. Some of these specified tests are:

1. **Deep Cycle Life**: The batteries shall maintain at least 80% capacity rating after >1000 100% depth of discharge cycles at 35°C. Each cycle shall consist of a 1C rate charge and 1C rate discharge.
2. **High Temperature Cycle Life Test**: The batteries shall maintain at least 80% capacity rating after 250 100% depth of discharge cycles at 60°C. Each cycle shall consist of a 1C rate charge and 1C rate discharge.
3. **Battery Storage and Charge Retention (capacity fade)**: The batteries shall have a capacity fade of no more than 10% over a 90 day period at 40°C. The battery shall have a shelf life of at least 30 months. Shelf life is defined as the battery stored at 100% state of charge and not dropping below 20% state of charge at 25°C.
4. **Calendar Life**: The batteries' calendar life shall be at least 5 years when properly maintained in storage and when not exceeding cycle life.

From the above requirements, we can already see a divergence from commercial vehicle requirements (for example, a calendar life of five years as opposed to fifteen years per the USABC). Environmental standards which govern the military requirements are referenced in [97] and defined in [98]. Of these, the only that may be of use to commercial xEV battery systems from a durability standpoint are humidity and sand & dust. Depending on how xEVs are deployed in the coming years, we may see vehicles in humid environments / tropics or deserts.

SAE J2464 [15]		
Mechanical Abuse Tests	**Thermal Abuse Tests**	**Electrical Abuse Tests**
• Shock Tests • Drop Test • Penetration Test • Roll-over Test • Immersion Test • Crush Test	• High Temperature Hazard Test • Thermal Stability Test • Cycling without Thermal Management • Thermal Shock Cycling • Passive Propagation Resistance Test	• Short Circuit Tests • Overcharge Test • Overdischarge Test • Separator Shutdown Integrity Test

ISO-12405 [95] [96]		
Performance Tests	**Reliability Tests**	**Abuse Tests**
• Energy and capacity at RT • Energy and capacity at different temperatures and discharge rates • Power and internal resistance • No load SOC loss • SOC loss at storage • Cranking power at low temperature • Cranking power at high temperature • Energy efficiency • Cycle Life	• Dewing (temperature change • Thermal shock cycling • Vibration • Mechanical shock	• Short circuit protection • Overcharge protection • Overdischarge protection

DOE/INEEL Tests		**FreedomCAR**
Battery Test Manual For Electric Vehicles	**Battery Test Manual For Plug-In Hybrid Electric Vehicles**	**Battery Test Manual For Power-Assist Hybrid Electric Vehicles**
• Static Capacity Test • High Rate Charge • Hybrid Pulse Power Characterization Test • Peak Power Test • Self-Discharge Test • Thermal Performance Test • Life Testing • Cycle Life Dynamic Stress Tests • Calendar Life Test	• Static Capacity Test • Constant Power Discharge Tests • Hybrid Pulse Power Characterization Test • Self-Discharge Test • Cold Cranking Test • Thermal Performance Test • Energy Efficiency Test • Life Testing • Charge-Sustaining Cycle Life Tests • Charge-Depleting Cycle Life Tests • Calendar Life Test	• Static Capacity Test • Hybrid Pulse Power Characterization Test • Self-Discharge Test • Cold Cranking Test • Thermal Performance Test • Energy Efficiency Test • Operating Set Point Stability Test • Cycle Life Tests • Calendar Life Test • Thermal Management Load • System-Level Combined Life Verification Test

Stress Factor	Number of Stress Levels	Suggested Stress Levels
Temperature (°C)	3 to 4	Max (e.g. 55-60°C) High (e.g. 50-55°C) Medium (e.g. 45-50°C) Reference (e.g. 30°C)
State of Charge (%) (maximum operating)	3	High (e.g. 80%) Medium (e.g. 60%) Low (e.g. 40%)
Discharge energy throughput rate (mph)	3	High (e.g. 25mph) Medium (e.g. 20mph) Standby (zero) / Calendar
Fraction of Pulse Power Rating (%)		
Discharge pulses	3	High (e.g. 100%) Medium (e.g. 80%) Low (e.g. 60%)
Regenerative pulses	3	High (e.g. 100%) Medium (e.g. 80%) Low (e.g. 60%)

Table 19 Basic stress factors and suggested stress levels for accelerated life testing. **[92]**

The FreedomCAR Manual for Power-Assist Hybrid Electric Vehicles posits what it calls a **Combined Life Verification Test**. This is the closest type of test which FEV is able to call a durability test. Specifically, it suggests that after the cycle life and calendar life have been individually verified, that the two be verified concurrently. It is stated that such a procedure combine cycling operation and storage at elevated temperatures, with the objective of validating a battery system life model at accelerated stress conditions [99].

In principle such a test regime consists of a calendar life test described by in section 3.10 Calendar Life Test of [99] , interspersed with periodic (typically daily) intervals of life cycling. The number of life cycles to be performed each day is determined by dividing the total cycle life goal by the predicted calendar life (in days) at the test temperature. For example, if the projected calendar life of a battery at 50°C is 300 days, the 300,000-cycle life goal could be demonstrated by performing 1000 cycle life test profiles each day.

Additionally, the authors of the Life Verification Manual put forth the null hypothesis that battery operation (within accepted performance constraints) at low temperatures does not adversely affect battery life [92]. Although such may be considered to be true when considering the same drive cycles as at the reference or high temperatures, this neglects to take into consideration the effect of the vehicle HVAC system, or, for example, battery degradation at low temperatures as a result of fast charging regimens.

In order to perform durability tests, FEV GmbH has a facility intended solely for durability testing located in Brehna, Germany. The FEV Durability Test Center (Ger: *FEV Dauerlaufprüfzentrum*) [100]. The second and third expansions of the Durability Test Center (DLP-II and III) are fully capable of supporting hybrid and fully electric vehicles. In total, there are 58 engine test cells (of which 10 are equipped for deep freeze and thermal shock). Additionally, there are 8 powertrain test cells (2WD and 4WD) along with 10 dummy test benches. Each of the 76 test benches mentioned support battery simulation environments, with FEV able to provide high voltage capabilities of 400 to 600V.

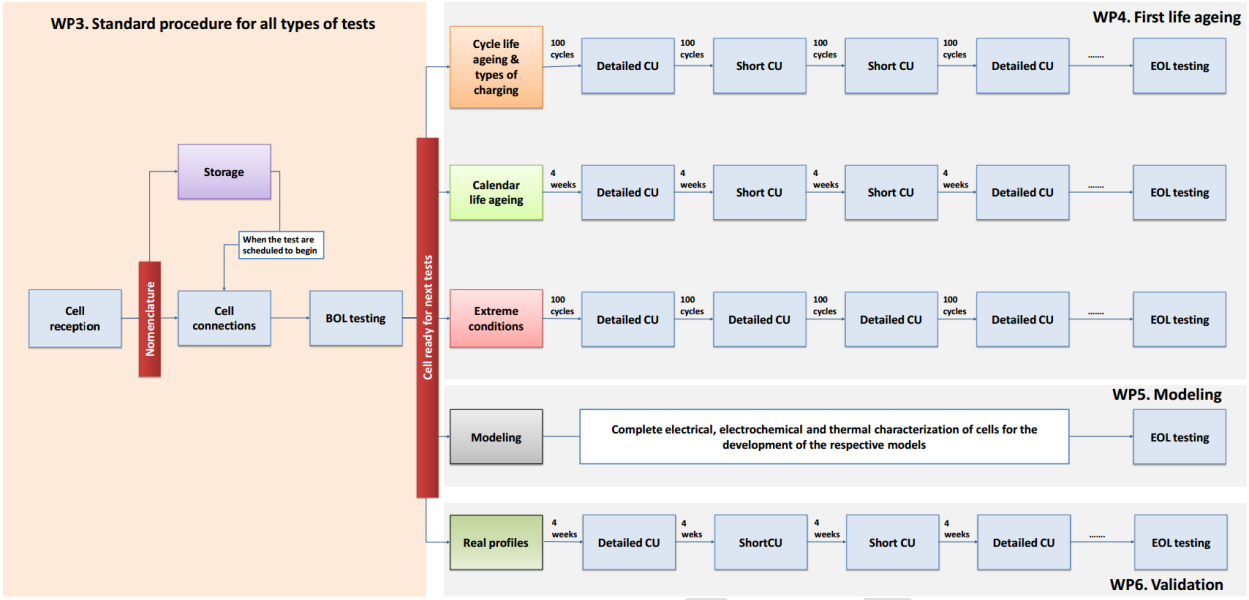

Figure 103 Proposed battery testing sequence from Batteries2020. CU stands for check-up or characterization tests to be done at different State-of-Health levels of the cells. **[101]**

A European initiative, "Batteries 2020" seeks to obtain a thorough understanding of aging and degradation through a combination of tests, models, and prediction focused in one system. Additionally, a complete characterization of the cells will be carried out to be used as the basis for the development of electrical, electrochemical, thermal and lifetime models. Although publications focused on the work package which concerns itself with first life (xEV usage) aging are not available as of the writing of this document, the details of the standardized begin-of-life tests were presented at the 28th International Electric Vehicle Symposium and Exhibition. These procedures are however intended only for characterization. Figure 103 shows a proposed battery testing protocol from Batteries 2020.

Of note is that the intended aging procedures are divided in to three paths. These correspond to cycle life, calendar life, and extreme conditions. It is the opinion of FEV that durability testing should be related to the first two categories but with greater emphasis on cycle life, which will more closely represent consumer usage scenarios.

Recommendations and Future Work

Having examined the literature related to battery degradation & durability, testing procedures & methodologies, and existing international standards, FEV has identified several areas which the EVE-IWG may consider for investigation in developing standards for battery durability as part of its drive to establish harmonized testing programs for Electrified Vehicles. Ultimately, the decision to implement these recommendations, and the means by which they may be integrated into or utilized with the WLTP, are the sole discretion of the EVE-IWG and associated international regulatory bodies.

The key figure when determining the End of Life of an Electrified Vehicle is the capacity of the battery as a percentage of the initial or nameplate capacity. Upon reaching 80% of the initial state of charge, the battery is said to have reached its End of Life. Consequently, the combination of factors which lead to this figure must be considered as part of a whole when evaluating battery durability. Specifically, we shall look to improvements in Cycle Life and Calendar Life procedures, along with environmental factors. In order to have a proper durability test, it will be necessary to combine these facets such that a comprehensive durability test can be created.

Cycle Life Testing

The number of cycles specified for PHEV and BEV EOL is 1000 [12] [13]. Some battery chemistries, such as $LiFePO_4$ have shown good cycle life performance as per the studies in [5], [29], and [74]. Temperature and the ΔSOC window / DOD in operation are, in addition to chemical considerations, large contributors to the degradation of batteries when combined with cycling. FEV recommends as part of cycle life testing a procedure which involves the following:

- Temperatures intended to indicate seasonal changes over the useful life of the vehicle. Testing should therefore allow for approximately three temperature grades: hot, average, and cold. Preliminary recommendations can be on the order of 35°C, 25°C, and -10°C for hot, average, and cold temperatures. Furthermore, one quarter of each year equivalent of cycling shall be hot, one quarter shall be cold, and one half shall be average.
- In instances where ambient temperature deviates sufficiently enough from room temperature values, cabin climate control functionality should become engaged.
- Inclusion of a mixture of fast and slow charging such that approximately four of every five cycles are charged using slow charging and the remainder is fast charged. This will give an idea of how the vehicle will react to the charging infrastructure.
- Determination of drive cycle duration and which of the stages of the WLTP shall be applied throughout should be derived from consumer patterns, indicating, for example, daily morning and evening commutes throughout a typical work-week, with the potential for longer duration, higher speed drive cycles reserved for a lesser part of the overall cycle pattern.

Calendar Life Testing

- Vehicles at rest undergo passive degradation as a function of temperature, time, and state of charge. Worst-case combinations of these factors should be considered alongside ideal cases (very high or low temperatures coupled with very high or low SOC as opposed to room temperature & mid-range SOC).

Additional Environmental Considerations for Testing

- In seeking to develop a Worldwide harmonized Light vehicle Testing Procedure, it may be prudent to seek to develop test conditions which may mimic future markets for xEVs. It may be worthwhile to adapt some of the environmental MIL standards for commercial usage such as humidity, sand/dust, etc.

References

[1] S. E. de Lucena, "A Survey on Electric and Hybrid Electric Vehicle Technology".

[2] MIT Electric Vehicle Team, "Electric Powertrains," 2008.

[3] C. C. Chan, A. Bouscayrol and K. Chen, "Electric, Hybrid, and Fuel-Cell Vehicles: Architectures and Modeling," *IEEE Transactions on Vehicular Technology,* vol. 59, no. 2, 2010.

[4] M. A. Kromer and J. B. Heywood, "Electric Powertrains: Opportunities and Challenges in the U.S. Light-Duty Vehicle Fleet," Laboratory for Energy and the Environment, Cambridge, MA, 2007.

[5] D. Ansean, M. Gonzalez, V. M. Garcia, J. C. Viera, J. C. Anton and C. Blanco, "Evaluation of LiFePO4 Batteries for Electric Vehicle Applications," *IEEE Transactions on Industry Applications,* vol. 51, no. 2, pp. 1855-1863, 2015.

[6] National Petroleum Council, "Advancing Technology for America's Transportation," 2012.

[7] F. Niedermayr, "Akku4Future: Report for Workpackage 2," Fraunhofer Italia, 2013.

[8] Nationale Plattform Elektromobilität, "Die deutsche Normungs-Roadmap: Elektromobilität - Version 1," 2010.

[9] The United Nations Economic Commission for Europe, "Electric Vehicle Regulatory Reference Guide, First Draft".

[10] S. Boulos, A. Sousanoglou and L. Evans, "The Durability of Products: Standard assessment for the circular economy under the Eco-Innovation Action Plan," Ricardo-AEA, 2014.

[11] "USABC Goals for Advanced Batteries for 48V Hybrid Electric Vehicle Applications," 2014.

[12] "USABC Goals for Advanced Batteries for PHEVs for FY 2018 to 2020 Commercialization," 2014.

[13] "USABC Goals for Advanced Batteries for EVs - CY 2020 Commercialization," 2014.

[14] Oxford University Press, "Oxford Dictionaries," [Online]. Available: http://www.oxforddictionaries.com/us/definition/english/durability.

[15] SAE International, "SAE J2464 Surface Vehicle Recommended Practice: Electric and Hybrid Electric Vehicle Rechargeable Energy Storage System (RESS) Safety and Abuse Testing," SAE International, 2009.

[16] G. M. Ehrlich, "Lithium-Ion Batteries," in *Handbook of Batteries, 3rd Edition*, McGraw-Hill, 2001, pp. 1074-1167.

[17] S. Zhang, K. Xu and T. Jow, "EIS study on the formation of solid electrolyte interface in Li-ion battery,"

Electrochimica Acta, vol. 51, pp. 1636-1640, 2006.

[18] J. Vetter, P. Novák, M. Wagner, C. Veit, K.-C. Möller, J. O. Besenhard, M. Winter, M. Wohlfahrt-Mehrens, C. Vogler and A. Hammouche, "Ageing mechanisms in lithium-ion batteries," *Journal of Power Sources,* vol. 147, pp. 269-281, 2005.

[19] V. Agubra and J. Fergus, "Lithium Ion Battery Anode Aging Mechanisms," *Materials,* no. 6, pp. 1310-1325, 2013.

[20] P. Kubiak, M. Wolfahrt-Mehrens, K. Edström and M. Morcrette, "Review on ageing mechanisms of different Li-ion batteries for automotive applications".

[21] K. Kumaresan, Q. Guo, P. Ramadass and R. E. White, "Cycle life performance of lithium-ion pouch cells," *Journal of Power Sources,* vol. 158, pp. 679-688, 2005.

[22] M. Broussely, S. Herreyre, P. Biensan, P. Kasztejna, K. Nechev and R. Staniewicz, "Aging mechanism in Li ion cells and calendar life predictions," *Journal of Power Sources,* Vols. 97-98, pp. 13-21, 2001.

[23] F.-M. Wang, M.-H. Yu, Y.-J. Hsiao, Y. Tsai, B.-J. Hwang, Y.-Y. Wang and C.-C. Wan, "Aging Effects to Solid Electrolyte Interface (SEI) Membrane Formation and the Performance Analysis of Lithium Ion Batteries," *International Journal of Electrochemical Science,* vol. 6, pp. 1014-1026, 2011.

[24] L. Kanevskii and V. Dubasova, "Degradation of Lithium-Ion Batteries and How to Fight It: A Review," *Russian Journal of Electrochemistry,* vol. 41, no. 1, pp. 1-16, 2005.

[25] M. Koltypin, D. Aurbach, L. Nazar and B. Ellis, "More on the performance of LiFePO4 electrodes—The effect of synthesis route, solution composition, aging, and temperature," *Journal of Power Sources,* vol. 174, p. 1241–1250, 2007.

[26] J. Morales, R. Trócoli, S. Franger and J. Santos-Pena, "Cycling-induced stress in lithium ion negative electrodes: LiAl/LiFePO4 and and Li4Ti5O12/LiFePO4 cells," *Electrochimica Acta,* vol. 55, pp. 3075-3082, 2010.

[27] V. Etacheri, R. Marom, R. Elazari, G. Salitra and D. Aurbach, "Challenges in the development of advanced Li-ion batteries: a review," *The Royal Society of Chemistry,* 2011.

[28] SECONDARYSOURCE, J. Vetter, P. Novák, M. Wagner, C. Veit, K.-C. Möller, J. O. Besenhard, M. Winter, M. Wohlfahrt-Mehrens, C. Vogler and A. Hammouche, "Ageing mechanisms in lithium-ion batteries," *Journal of Power Sources,* vol. 147, pp. 269-281, 2005.

[29] E. M. Krieger, "Effects of Variability and Rate on Battery Charge Storage and Lifespan," Princeton University, 2013.

[30] K. Amine, J. Liu and I. Belharouak, "High-temperature storage and cycling of C-LiFePO4/graphite Li-ion cells," *Electrochemistry Communications,* vol. 7, no. 7, pp. 669-673, 2005.

[31] D. Aurbach, B. Markovsky, G. Salitra, E. Markevich, Y. Talyossef, M. Koltypin, L. Nazar, B. Ellis and D. Kovacheva, "Review on electrode-electrolyte solution interactions related to cathode materials for Li-ion batteries," *Journal of Power Sources,* vol. 165, pp. 491-499, 2007.

[32] M. Maccario, L. Croguennec, F. L. Cras and C. Delmas, "Electrochemical performances in temperature for a C-containing LiFePO4 composite synthesized at," *Journal of Power Sources,* vol. 183, no. 1, pp. 411-417, 2008.

[33] H.-F. Jin, Z. Liu, Y.-M. Teng, J.-k. Gao and Y. Zhao, "A comparison study of capacity degradation mechanism of LiFePO4-based lithium ion cells," *Journal of Power Sources,* vol. 189, no. 1, pp. 445-448, 2009.

[34] K. Striebel, J. Shim, A. Sierra, H. Yang, X. Song, R. Kostecki and K. McCarthy, "The development of low cost LiFePO4-based high power lithium-ion batteries," *Journal of Power Sources,* vol. 146, pp. 33-38, 2005.

[35] G. Chen, X. Song and T. J. Richardson, "Electron Microscopy Study of the LiFePO4 to FePO4 Phase Transition," *Electrochemical and Solid-State Letters,* vol. 9, no. 6, pp. A295-A298, 2006.

[36] M. Dubarry, V. Svoboda, R. Hwu and B. Y. Liaw, "Capacity and power fading mechanism identification from a commercial cell evaluation," *Journal of Power Sources,* vol. 165, pp. 566-572, 2007.

[37] D. Abraham, J. Liu, C. Chen, Y. Hyung, M. Stoll, N. Elsen, S. MacLaren, R. Twesten, R. Haasch, E. Sammann, I. Petrov, K. Amine and G. Henriksen, "Diagnosis of power fade mechanisms in high-power lithium-ion cells," *Journal of Power Sources,* Vols. 119-121, pp. 511-516, 2003.

[38] SECONDARYSOURCE, D. Aurbach, B. Markovsky, A. Rodkin, E. Levi and Y. Cohen, "On the capacity fading of LiCoO2 intercalation electrodes: the effect of cycling, storage, temperature, and surface film forming additives," *Electrochimica Acta,* vol. 47, no. 27, p. 4291–4306, 2002.

[39] J. P. Rugh, A. Pesaran and K. Smith, "Electric Vehicle Battery Thermal Issues and Thermal Management Techniques," 2013.

[40] R. G. Jungst, G. Nagasubramanian, C. C. Crafts, D. Ingersoll and D. H. Doughty, "Analysis of Lithium-Ion Battery Degradation During Thermal Aging," Sandia National Laboratories, 2010.

[41] T. Finley, "Battery Degradation Modeling for Vehicle Applications," 2015.

[42] J. P. Sullivan, K. R. Fenton, F. E. G. Marquez, C. T. Harris, C. C. Hayden, N. S. Hudak, K. L. Jungjohann, C. J. Kliewer, K. Leung, K. McCarty, A. H. McDaniel, G. Nagasubramanian and J. D. Sugar, "The Science of Battery Degradation," Sandia National Laboratories, 2015.

[43] J. Shim, R. Kostecki, T. Richardson, X. Song and K. Striebel, "Electrochemical analysis for cycle performance and capacity fading of a lithium-ion battery cycled at elevated temperature," *Journal of Power Sources,* vol. 112, pp. 222-230, 2002.

[44] J. A. Jeevarajan, "Hazards Associated with High Voltage High Capacity Lithium-ion Batteries," *ECS Transactions,* vol. 33, no. 22, pp. 1-6, 2011.

[45] D. H. Doughty and A. A. Pesaran, "Vehicle Battery Safety Roadmap Guidance," 2012.

[46] E. P. Roth, "Abuse Response of 18650 Li-Ion Cells with Different Cathodes Using EC:EMC/LiPF6 and EC:PC:DMC/LiPF6 Electrolytes," *ECS Transactions,* vol. 11, no. 19, pp. 19-41, 2008.

[47] J. Kopera, "Considerations for the Utilization of NiMH Battery Technology in Stationary Applications," Cobasys, Orion, MI, 2005.

[48] L. Serrao, Z. Chehab, Y. Guezennec and G. Rizzoni, "An Aging Model of Ni-MH Batteries for Hybrid Electric Vehicles," 2005.

[49] L. L. Guenne and P. Bernard, "Life durations of Ni-MH cells for high power applications," *Journal of Power Sources,* vol. 105, no. 2, pp. 134-138, 2002.

[50] I. Buchmann, Batteries in a Portable World, Cadex Electronix, 2001.

[51] B. Pierozynski, "On the Low Temperature Performance of Nickel-Metal Hydride (NiMH) Batteries," *International Journal of Electrochemical Science,* vol. 6, pp. 860-866, 2011.

[52] J. Groot, "State-of-Health Estimation of Li-ion Batteries: Cycle Life Test Methods," Chalmers University of Technology, Göteborg, Sweden, 2012.

[53] A. Bandyopadhyay, L. Wang, V. K. Devabhaktuni, R. Yang and R. C. G. II, "Assessing the Effect of Fast Charging on the Battery Health of Plug-in Hybrid Electric Vehicles," IEEE, Toledo, OH, 2012.

[54] G. Lacey, T. Jiang, G. Putrus and R. Kotter, "The Effect of Cycling on the State of Health of the Electric Vehicle Battery," in *Power Engineering Conference (UPEC), 2013 48th International Universities*, 2013.

[55] M. Shirk and J. Wishart, "Effects of Electric Vehicle Fast Charging on Battery Life and Vehicle Performance," 2015.

[56] S. Bashash, S. J. Moura and H. K. F. Joel C. Forman, "Plug-in hybrid electric vehicle charge pattern optimization for energy cost and battery longevity," Ann Arbor, MI, 2010.

[57] A. Hoke, A. Brissette, D. Maksimovic, D. Kelly, D. Boundy and A. Pratt, "Maximizing Lithium Ion Vehicle Battery Life Through Optimized Partial Charging".

[58] J. Neubauer, E. Wood, E. Burton, K. Smith and A. Pesaran, "FY14 Milestone: Simulated Impacts of Life-Like Fast Charging on BEV Batteries," 2014.

[59] J. Neubauer and E. Wood, "Will Your Battery Survive a World With Fast Chargers?," 2015.

[60] S. S. Zhang, "The effect of the charging protocol on the cycle life of a Li-ion battery," *Journal of Power Sources 161,* vol. 161, pp. 1385-1391, 2006.

[61] L. D. Vroey, R. Jahn, N. Omar and J. V. Mierlo, "Impact of smart charging on the EV battery ageing - Discussion from a 3 years real life experience," 2015.

[62] K. Smith, M. Earleywine, E. Wood, J. Neubauer and A. Pesaran, "Comparison of Plug-In Hybrid Electric Vehicle Battery Life Across Geographies and Drive Cycles," 2012.

[63] H. Lohse-Busch, M. Duoba, E. Rask and M. Meyer, "Advanced Powertrain Research Facility AVTA Nissan Leaf Testing and Analysis," 2012.

[64] H.-S. Song, J.-B. Jeong, B.-H. Lee, D.-H. Shin, B.-H. Kim, T.-H. Kim and H. Heo, "Experimental Study on the Effects of Pre-Heating a Battery in a Low-Temperature Environment," in *IEEE Vehicle Power and Propulsion Conference*, Seoul, Korea, 2012.

[65] R. A. Barnitt, A. D. Brooker, L. Ramroth, J. Rugh and K. Smith, "Analysis of Off-Board Powered Thermal Preconditioning in Electric Drive Vehicles," 2010.

[66] K. Vatanparvar and M. A. Al-Faruque, "Battery Lifetime-Aware Automotive Climate Control for Electric Vehicles," San Fransisco, CA, 2015.

[67] T. Yuksel and J. Michalek, "Evaluation of the Effects of Thermal Management on Battery Life in Plug-in Hybrid Electric Vehicles".

[68] K. Smith, M. W. E. Earleywine and A. Pesaran, "Battery Wear from Disparate Duty-Cycles: Opportunities for Electric-Drive Vehicle Battery Health Management," 2012.

[69] M. C. Smart, B. V. Ratnakumar, J. F. Whitacre, L. D. Whitcanack, K. B. Chin, M. D. Rodriguez, D. Zhao, S. G. Greenbaum and S. Surampudi, "Effect of Electrolyte Type upon the High-Temperature Resilience of Lithium-Ion Cells," *Journal of the Electrochemical Society,* vol. 152, no. 6, pp. A1096-A1104, 2005.

[70] M. Allen, "Electric Range for the Nissan Leaf & Chevrolet Volt in Cold Weather," fleetcarma, [Online]. Available: http://www.fleetcarma.com/nissan-leaf-chevrolet-volt-cold-weather-range-loss-electric-vehicle/. [Accessed 27 July 2015].

[71] S. Santhanagopalan, Q. Zhang, K. Kumaresan and R. E. White, "Parameter Estimation and Life Modeling of Lithium-Ion Cells," *Journal of the Electrochemical Society,* vol. 155, no. 4, pp. A345-A353, 2008.

[72] M. Conte, F. V. Conte, I. D. Bloom, K. Morita, T. Ikeya and J. R. Belt, "Ageing Testing Procedures on Lithium Batteries in an International Collaboration Context," in *25th World Battery, Hybrid, and Fuel Cell Electric Vehicle Symposium & Exhibition*, 2010.

[73] E. Wood, J. Neubauer, A. D. Brooker, J. Gonder and K. A. Smith, "Variability of Battery Wear in Light Duty Plug-In Electric Vehicles Subject to Ambient Temperature, Battery Size, and Consumer Usage," in *International Battery, Hybrid and Fuel Cell Electric Vehicle Symposium 26*, Los Angeles, California, 2012.

[74] Y. Zhang, C.-Y. Wang and X. Tang, "Cycling degradation of an automotive LiFePO4 lithium-ion battery," *Journal of Power Sources,* vol. 196, pp. 1513-1520, 2011.

[75] Idaho National Laboratory, "Battery Test Manual For Plug-In Hybrid Electric Vehicles (Rev. 3)," United States Department of Energy, 2014.

[76] E. Wood, M. Alexander and T. H. Bradley, "Investigation of battery end-of-life conditions for plug-in hybrid electric vehicles," *Journal of Power Sources,* vol. 196, pp. 5147-5154, 2011.

[77] Idaho National Laboratory, "Battery Test Manual for Electric Vehicles, Rev. 3," 2015.

[78] A. Hoke, A. Brissette, K. Smith, A. Pratt and D. Maksimovic, "Accounting for Lithium-Ion Battery Degradation in Electric Vehicle Charging Optimization," 2013.

[79] T. Niikuni, K. Koshika and T. Kawai, "Evaluation of the influence of JC08-based cycle stress on batteries in plug-in hybrid electric vehicle," 2010.

[80] M. Duoba, H. Lohse-Busch, K. Stutenberg and E. Rask, "HEV, PHEV, EV Testing Activities," 2013.

[81] P. Keil and A. Jossen, "Aging of Lithium-Ion Batteries in Electric Vehicles: Impact of Regenerative Braking," 2015.

[82] "Full Size Battery Electric Vehicles," Idaho National Laboratory, [Online]. Available: http://avt.inl.gov/fsev.shtml. [Accessed 23 July 2015].

[83] "Hybrid Electric Vehicles," Idaho National Laboratory, [Online]. Available: http://avt.inl.gov/hev.shtml. [Accessed 23 July 2015].

[84] "Plug-in Hybrid Electric Vehicles/Extended Range Electric Vehicles," Idaho National Laboratory, [Online]. Available: http://avt.inl.gov/phev.shtml. [Accessed 23 July 2015].

[85] T. Gray, M. Shirk and J. Wishart, "2010 Honda CR-Z VIN 4466 Hybrid Electric Vehicle Battery Test Results," 2014.

[86] T. Gray, M. Shirk and J. Wishart, "2011 Hyundai Sonata VIN 3539 Hybrid Electric Vehicle Battery Test Results," 2014.

[87] T. Gray and M. Shirk, "2010 Toyota Prius VIN 0462 Hybrid Electric Vehicle Battery Test Results," 2013.

[88] T. Gray and M. Shirk, "2010 Ford Fusion VIN 4757 Hybrid Electric Vehicle Battery Test Results," 2013.

[89] T. Gray, "2010 Honda Insight VIN 0141 Hybrid Electric Vehicle Battery Test Results," 2013.

[90] T. Gray and M. Shirk, "2010 Toyota Prius VIN 6063 Hybrid Electric Vehicle Battery Test Results," 2013.

[91] J. Smart, "Advanced Vehicle Testing Activity Cold Weather On-road Testing of the Chevrolet Volt," 2015.

[92] Idaho National Laboratory, "Battery Technology Life Verification Test Manual," 2012.

[93] "J2288: Life Cycle Testing of Electric Vehicle Battery Modules," SAE International, [Online]. Available:

http://standards.sae.org/j2288_200806/.

[94] California Air Resources Board, "Zero-Emission Vehicle Standards for 2018 and Subsequent Model Year Passenger Cars, Light-Duty Trucks, and Medium-Duty Vehicles.," 2014.

[95] International Organization for Standardization, "ISO 12405-1: Electrically propelled road vehicles — Test specification for lithium-Ion traction battery systems — Part 1: High power applications," 2009.

[96] International Organization for Standardization, "ISO 12405-2: Electrically propelled road vehicles — Test specification for lithium-Ion traction battery systems — Part 2: High energy applications," 2010.

[97] L. Toomey, "Battery Specification for MATV, Group 31 and 34 Li-Ion Battery," U.S. Army TARDEC, Warren, MI, 2011.

[98] United States Department of Defense, "MIL-STD-810G: Department of Defense Test Method Standard for Environmental Engineering Considerations and Laboratory Tests," 2008.

[99] USABC, Idaho National Laboratory, "FreedomCAR Battery Test Manual for Power-Assist Hybrid Electric Vehicles," U.S. Department of Energy, 2003.

[100] FEV GmbH, "The New FEV Durability Test Center in Brehna near Leipzig," 2009.

[101] J.-M. Timmermans, L. Rodriguez-Martinez, N. Omar, J. V. Mierlo, I. Villarreal, M. Swierczynski, P. Rodriguez, A. Warnecke, M. Gosso, E. Marckx, G. Jutz and L. Gautier, "BATTERIES 2020 – A Joint European Effort towards European Competitive Automotive Batteries," 2015.

[102] L. Gaines, J. Sullivan, A. Burnham and I. Belharouak, "Life Cycle Analysis for Lithium-Ion Battery Production and Recycling," in *90th Annual Meeting of the Transportation Research Board*, Washington, D.C, 2011.

[103] L. Gaines and J. Sullivan, "A Review of Battery Life-Cycle Analysis: State of Knowledge and Critical Needs," October 1, 2010.

[104] J. Francfort, D. Karner, R. Harkins and J. Tardiolo, "Hybrid Electric Vehicle End-Of-Life Testing On Honda Insights, Gen I Civics And Toyota Gen I Priuses," 2006.

[105] B. Dickinson, J. Baer, O. A. Velev and D. Swan, "Performance, Management and Testing Requirements for Hybrid Electric Vehicle Batteries".

[106] B. Price, E. Dietz and J. Richardson, "Life Cycle Costs of Electric and Hybrid Electric Vehicle Batteries and End-of-Life Uses".

[107] J. Smart, J. Francfort, D. Karner, M. Kirkpatrick and S. White, "Advanced Vehicle Testing Activity: Plug-In Hybrid Electric Vehicle Testing and Demonstration Activities," 2009.

[108] T. Gray, M. Shirk and J. Wishart, "2010 Honda Civic Hybrid Ultra Battery Conversion 5577 - Hybrid Electric Vehicle Battery Test Results," 2013.

[109] T. Gray, M. Shirk and J. Wishart, "2011 Chevrolet Volt VIN 0815 Plug-In Hybrid Electric Vehicle Battery Test Results," 2013.

[110] A. Pesaran, S. Santhanagopalan and G. H. Kim, "Addressing the Impact of Temperature Extremes on Large Format Li-Ion Batteries for Vehicle Applications," 2013.

[111] C. H. Park, J. H. Yoon and J. D. Choi, "A Quantitative Study for Critical Factors of Automotive Battery Durability," SAE International, 2007.

[112] H. Horie, T. Abe, T. Kinoshita and Y. Shimoida, "A Study on an Advanced Lithium-ion Battery System for EVs," *The World Electric Vehicle Journal,* vol. 2, no. 2, pp. 25-31, 2008.

[113] L. Gaillac, "Accelerated Testing of Advanced Battery Technologies in PHEV Applications," *The World Electric Vehicle Journal,* vol. 2, no. 2, pp. 83-92, 2008.

[114] D. Skaggs, J. Smith and R. P. Hill, "The Electric Vehicle Fleet Experience at Southern California-Edison," *The World Electric Vehicle Journal,* vol. 2, no. 4, pp. 135-139, 2008.

[115] J. P. Rugh, A. Pesaran and K. Smith, "Electric Vehicle Battery Thermal Issues and Thermal Management Techniques," in *Alternative Refrigerant and System Efficiency Symposium*, Scottsdale, Arizona USA, 2011.

[116] Idaho National Laboratory, "Battery Test Manual," 2010.

[117] A. A. Pesaran, T. Markel, H. S. Tataria and D. Howell, "Battery Requirements for Plug-In Hybrid Vehicles - Analysis and Rationale".

[118] Y. Xing, Q. Miao, K.-L. Tsui and M. Pecht, "Prognostics and Health Monitoring for Lithium-ion Battery," 2011.

[119] M. Ebner, F. Marone, M. Stampanoni and V. Wood, "Visualization and Quantification of Electrochemical and Mechanical Degradation in Li Ion Batteries," *Science,* vol. 342, pp. 716-719, 2013.

[120] J. C. Forman, S. J. Moura, J. L. Stein and H. K. Fathy, "Optimal Experimental Design for Modeling Battery Degradation," in *ASME 2012 5th Annual Dynamic Systems and Control Conference*, Fort Lauderdale, FL, 2012.

[121] J. Zhang and J. Lee, "A review on prognostics and health monitoring of Li-ion battery," *Journal of Power Sciences,* vol. 196, pp. 6007-6014, 2011.

[122] C.-S. N. Shiau, N. Kaushal, C. T. Hendrickson, S. B. Peterson, J. F. Whitacre and J. J. Michalek, "Optimal Plug-In Hybrid Electric Vehicle Design and Allocation for Minimum Life Cycle Cost, Petroleum Consumption, and Greenhouse Gas Emissions," *Journal of Mechanical Design,* vol. 132, 2010.

[123] L. Kang, X. Zhao and J. Ma, "A new neural network model for the state-of-charge estimation in the battery degradation process," *Applied Energy,* vol. 121, pp. 20-27, 2014.

[124] A. Millner, "Modeling Lithium Ion Battery Degradation in Electric Vehicles," Lexington, MA.

[125] D. H. Doughty and C. C. Crafts, "FreedomCAR Electrical Energy Storage System Abuse Test Manual for Electric and Hybrid Electric Vehicle Applications," Sandia National Laboratories, 2005.

[126] Tesla Motors, Inc., "Tesla Model S Range," 2014. [Online]. Available: www.teslamotors.com.

[127] L. Knibbs, R. D. Dear and S. Atkinson, "Field study of air change and flow rate in six automobiles," *Indoor Air,* vol. 19, no. 4, pp. 303-313, 2009.

[128] Argonne National Laboratory, "Diagnostic Examination of Generation 2 Lithium-Ion Cells and Assessment of Performance Degradation Mechanisms," 2005.

[129] S. J. Harris and P. Lu, "Effects of Inhomogeneities - Nanoscale to Mesoscale - on the Durability of Li-Ion Batteries," *Journal of Physical Chemistry C,* vol. 117, pp. 6481-6492, 2013.

[130] S. J. Gerssen-Gondelach and A. Faaij, "Performance of batteries for electric vehicles on short and longer term," *Journal of Power Sources,* vol. 212, pp. 111-129, 2012.

[131] S. Han, H. Aki and S. Han, "A Practical Battery Wear Model for Electric Vehicle Charging Applications," 2013.

[132] S. Santhanagopalan, Q. Guo, P. Ramadass and R. E. White, "Review of models for predicting the cycling performance of lithium ion batteries," *Journal of Power Sources,* vol. 156, pp. 620-628, 2006.

[133] V. Marano, S. Onori, Y. Guezennec, G. Rizzoni and N. Madella, "Lithium-ion Batteries Life Estimation for Plug-in Hybrid Electric Vehicles," 2009.

[134] S. Brown, "Diagnosis of the Lifetime Performance Degradation of Lithium-Ion Batteries: ocus on Power-Assist Hybrid Electric Vehicle and Low-Earth-Orbit Satellite Applications," Universitetsservice US-AB, Stockholm, 2008.

[135] P. Spagnol, S. Onori, N. Madella, Y. Guezennec and J. Neal, "Aging and Characterization of Li-Ion Batteries in a HEV Application for Lifetime Estimation".

[136] M. B. Pinson and M. Z. Bazant, "Theory of SEI Formation in Rechargeable Batteries: Capacity Fade, Accelerated Aging and Lifetime Prediction".

[137] K. Takei, K. Kumai, Y. Kobayashi, H. Miyashiro, N. Terada, T. Iwahori and T. Tanaka, "Cycle life estimation of lithium secondary battery by extrapolation method and accelerated aging test," *Journal of Power Sources,* vol. 97, pp. 697-701, 2001.

[138] M. Dubarry, N. Vuillaume, B. Y. Liaw and T. Quinn, "Vehicle Evaluation, Battery Modeling, and Fleet-testing Experiences in Hawaii: A Roadmap to Understanding Evaluation Data and Simulation," *Journal of Asian Electric Vehicles,* vol. 5, no. 2, pp. 1033-1042, 2007.

[139] K. N. Genikomakis, C. S. Ioakimidis, A. Murillo, A. Trifonova and D. Simic, "A Life Cycle Assessment of a Li-ion urban electric vehicle battery," in *EVS27*, Barcelona, 2013.

[140] M. Zackrisson, L. Avellán and J. Orlenius, "Life cycle assessment of lithium-ion batteries for plug-in hybrid electric vehicles -- Critical issues," *Journal of Cleaner Production,* vol. 18, pp. 1519-1529, 2010.

[141] M. Contestabile, G. Offer, R. North, M. Akhurst and J. Woods, "Electric Vehicles: A Synthesis of the Current Literature with a Focus on Economic and Environmental Viability," LCAworks, 2012.

[142] M. Dubarry, "Test Plan to Assess Electric Vehicle Cell Degradation under Electric Utility Grid Operations," 2015.

[143] R. Graham, "Comparing the Benefits and Impacts of Hybrid Electric Vehicle Options," 2001.

[144] J. D. Graham, "Electromobility: Comparing Public Policies in Europe, the United States, and China".

[145] Y. S. Jung, A. S. Cavanagh, L. A. Riley, S.-H. Kang, A. C. Dillon, M. D. Groner, S. M. George and S.-H. Lee, "Ultrathin Direct Atomic Layer Deposition on Composite Electrodes for Highly Durable and Safe Li-Ion Batteries," *Advanced Materials,* vol. 22, pp. 2172-2176, 2010.

[146] O. Karabasoglu and J. Michalek, "Influence of driving patterns on life cycle cost and emissions of hybrid and plug-in electric vehicle powertrains," *Energy Policy,* 2013.

[147] D. Karner and J. Francfort, "Hybrid and plug-in hybrid electric vehicle performance testing by the US Department of Energy Advanced Vehicle Testing Activity," *Journal of Power Sources,* vol. 174, pp. 69-75, 2007.

[148] T.-H. Kim, J.-S. Park, S. K. Chang, S. Choi, J. H. Ryu and H.-K. Song, "The Current Move of Lithium Ion Batteries Towards the Next Phase," *Advanced Energy Materials,* pp. 1-13, 2012.

[149] M. T. Lawder, P. W. Northrop and V. R. Subramanian, "Model-Based SEI Layer Growth and Capacity Fade Analysis for EV and PHEV Batteries and Drive Cycles," *Journal of The Electrochemical Society,* vol. 161, no. 14, pp. A2099-A2108, 161.

[150] D. Liu, Y. Luo, Y. Peng, X. Peng and M. Pecht, "Lithium-ion Battery Remaining Useful Life Estimation Based on Nonlinear AR Model Combined with Degradation Feature," in *Annual Conference of Prognostics and Health Management Society*, 2012.

[151] S. Renganathan, G. Sikha, S. Santhanagopalan and R. E. White, "Theoretical Analysis of Stresses in a Lithium Ion Cell," *Journal of The Electrochemical Society,* vol. 157, no. 2, pp. A155-A163, 2010.

[152] S. M. Rezvanizaniani, Z. Liu, Y. Chen and J. Lee, "Review and recent advances in battery health monitoring and prognostics technologies for electric vehicle (EV) safety and mobility," *Journal of Power Sources,* vol. 256, pp. 110-124, 2014.

[153] M. Safari, M. Morcrette, A. Teyssot and C. Delacourt, "Life Prediction Methods for Lithium-Ion Batteries Derived from a Fatigue Approach," *Journal of The Electrochemical Society,* vol. 157, no. 7, pp. A892-A898, 2010.

[154] E. Samadani, "Modeling of Lithium-ion Battery Performance and Thermal Behavior in Electrified Vehicles," University of Waterloo, 2015.

[155] H. Sattler, "Prüfanforderungen an Li-Batterien für Elektrofahrzeuge: Übersicht vorhandener Normen sowie zukünftige Standards".

[156] C. Wu, C. Zhu, Y. Ge and Y. Zhao, "A Review on Fault Mechanism and Diagnosis Approach for Li-Ion Batteries," Hindawi Publishing Corporation, 2015.

[157] M. Yilmaz and P. T. Krein, "Review of Battery Charger Topologies, Charging Power Levels, and Infrastructure for Plug-In Electric and Hybrid Vehicles," *IEEE Transactions on Power Electronics,* vol. 28, no. 5, pp. 2151-2169, 2013.

[158] T. Yuksel and J. Michalek, "Development of a Simulation Model to Analyze the Effect of Thermal Management on Battery Life," SAE International, 2012.

[159] Q. Zhang and R. E. White, "Calendar life study of Li-ion pouch cells," *Journal of Power Sources,* vol. 173, pp. 990-997, 2007.

[160] SECONDARYSOURCE, A. Barré, B. Deguilhem, S. Grolleau, M. Gérard, F. Suard and D. Riu, "A review on lithium-ion battery ageing mechanisms and estimations for automotive applications," *Journal of Power Sources,* vol. 241, pp. 680-689, 2013.

[161] SECONDARYSOURCE, Q. Badey, G. Cherouvrier, Y. Reynier, J.-M. Duffault and S. Franger, "Ageing forecast of lithium-ion batteries for electric and hybrid vehicles," *Current Topics in Electrochemistry,* vol. 16, pp. 65-79, 2011.

[162] SECONDARYSOURCE, M. Kassem, J. Bernard, R. Revel, S. Pelissier, F. Duclaud and C. Delacourt, "Calendar aging of a graphite LiFePO4 cell," *Journal of Power Sources,* vol. 208, pp. 296-305, 2012.

[163] SECONDARYSOURCE, P. B. M. Broussely, F. Bonhomme, P. Blanchard, S. Herreyre, K. Nechev and R. Staniewicz, "Main aging mechanisms in Li ion batteries," *Journal of Power Sources,* vol. 146, pp. 90-96, 2005.

[164] United Nations, "38.3 Lithium metal and lithium ion batteries," in *Recommendations on the Transport of Dangerous Goods: Manual of Tests and Criteria*.

[165] USABC, Idaho National Laboratory, "FreedomCAR 42V Battery Test Manual," 2003.

[166] FEV GmbH, "FEV Dauerlaufprüfzentrum in Brehna / Leipzig," [Online]. Available: http://www.fev-dlp.de/en/fev-dauerlaufpruefzentrum-in-brehnaleipzig.html.

[167] M. Tutuianu, A. Marotta, H. Steven, E. Ericsson, T. Haniu, N. Ichikawa and H. Ishii, "Development of a World-wide Worldwide harmonized Light duty driving Test Cycle (WLTC)," 2013.

[168] N. Omar, M. Daowd, P. v. d. Bossche, O. Hegazy, J. Smekens, T. Coosemans and J. v. Mierlo, "Rechargeable Energy Storage Systems for Plug-in Hybrid Electric Vehicles - Assessment of Electrical

Characteristics," *Energies,* vol. 5, pp. 2952-2988, 2012.

[169] Y. Wu, E. Rahm and R. Holze, "Carbon anode materials for lithium ion batteries," *Journal of Power Sources,* vol. 114, pp. 228-236, 2003.

[170] L. Fu, H. Zhang, Y. Wu, H. Wu and R. Holze, "Surface Active Sites: An Important Factor Affecting the Sensitivity of Carbon Anode Materials toward Humidity," *Electrochemical and Solid-State Letter,* vol. 8, no. 9, pp. A456-A458, 2005.

[171] M. Kassem, J. Bernard, R. Revel, S. Pélissier, F. Duclaud and C. Delacourt, "Calendar aging of a Graphite/LiFePO4 cell," *Journal of Power Sources,* vol. 208, pp. 296-305, 2012.

[172] H. Popp, J. Attia, F. Delcorso and A. Trifonova, "Lifetime analysis of four different lithium ion batteries for (plug – in) electric vehicle," 2014.

[173] L. D. Vroey, R. Jahn, N. Omar and J. V. Mierlo, "Impact of smart charging on the EV battery ageing - Discussion from a 3 years real life experience," 2015.

Appendix

Vehicle OEM	Model	Battery Supplier	Drivetrain	Drivetrain Architecture	Battery Chemistry	Format	Thermal Management
Chevy (GM)	Volt	Compact Power/ LG Chem	PHEV	Series	LMO Spinel Polymer	Prismatic	Liquid
Nissan	LEAF	AESC (NEC/ Nissan)	BEV	Series	LMO	Prismatic	Air
Fisker	Karma	A123	PHEV	Series	LFP (Nanophos-phate)	Cylindrical (26650)	Liquid
Mitsubishi	"I"	GS Yuasa	BEV	Series	LMO-NMC/ Hard Carbon	Prismatic	Air
Prius (Toyota)	PHEV	PEVE	PHEV	Parallel/ Powersplit	NCA	Prismatic	Liquid
Smart (Daimler)	fortwo ED	Duetsche ACCUmotive (Daimler & Evonik)	BEV	Series	*	*	Liquid
Tesla	Model S	Panasonic Samsung	BEV	Series	LMO	Cylindrical (18650)	Liquid
Volvo	C30 EV	Enerdel/Ener1	BEV	Series	LMO-NMC/Hard Carbon	Prismatic	Air
BMW	ActiveE	S8 LI Motive (BMW, Bosch, Samsung)	BEV	Series	NMC	Prismatic	Liquid
Toyota	Rav4 EV	PEVE	BEV	Series	LMO Spinel Polymer	Cylindrical (18650)	Liquid
Scion (Toyota)	IQ-EV	PEVE	BEV	Series	LMO Spinel Polymer	Prismatic	Liquid
Ford	Focus	Compact Power/ LG Chem	BEV	Series	LMO Spinel Polymer	Prismatic	Liquid
Honda	Fit EV	GS Yuasa	BEV	Series	LMO-NMC/ Hard Carbon	Prismatic	Liquid
Coda Automotive	CODA	Lishen/LIO Energy Systems	BEV	Series	LFP	Prismatic	Liquid
Ford	C-Max Energi	Compact Power/ LG Chem	PHEV	Parallel/ Powersplit	LMO Spinel Polymer	Prismatic	Liquid
Fiat	500 EV	*	BEV	Series	*	*	*
Chevy (GM)	Spark EV	A123	BEV	Series	LFP	Prismatic	Liquid
Fisker	Nina	*	PHEV	Series	*	*	*
Honda	Accord	GS Yuasa	PHEV	Parallel	LMO-NMC/ Hard Carbon	Prismatic	Liquid
Tesla	Model X	Panasonic Samsung	EV	Series	LMO	Cylindrical (18650)	Liquid
BMW	I3	SB LI Motive (BMW, Bosch, Samsung)	(1) BEV (2) PHEV	Series	NMC	Prismatic	Liquid
BMW	I8	SB LI Motive (BMW, Bosch, Samsung)	PHEV	Series	NMC	Prismatic	Liquid
Ford	Transit Connect	Johnson Controls	BEV	Series	NCA	Cylindrical	Liquid
Azure	Balance	Johnson Controls	PHEV	Parallel	NCA	Cylindrical	Liquid

* Unknown or not available.

Note: Data current as of February 2012.

Table 20 Representative Subset of Battery Chemistries Considered by Current Automobile Manufacturers [6]

Characteristics	Units	Target
Peak Pulse Discharge Power (10 sec)	**kW**	**9**
Peak Pulse Discharge Power (1 sec)	**kW**	**11**
Peak Regen Pulse Power (5 sec)	**kW**	**11**
Available Energy for Cycling	**Wh**	**105**
Minimum Round-trip Energy Efficiency	**%**	**95**
Cold cranking power at -30 °C (three 4.5-s pulses, 10s rests between pulses at min SOC)	**kW**	**6kW for 0.5s followed by 4kW for 4s**
Accessory Load (2.5 minute duration)	**kW**	**5**
CS 48V HEV Cycle Life	**Cycles / MWh**	**75000 / 21**
Calendar Life, 30°C	**Year**	**15**
Maximum System Weight	**kg**	**≤ 8**
Maximum System Volume	**Liter**	**≤ 8**
Maximum Operating Voltage	**Vdc**	**52**
Minimum Operating Voltage	**Vdc**	**38**
Minimum Voltage during Cold Crank	**Vdc**	**26**
Maximum Self-discharge	**Wh/day**	**1**
Unassisted Operating Temp Range (Power available to allow 5s charge and 1s discharge pulse) at min. and max. operating SOC and Voltage	**°C**	**-30 to +52**
30 °C - 52 °C	**kW**	**11**
0 °C	**kW**	**5.5**
-10 °C	**kW**	**3.3**
-20 °C	**kW**	**1.7**
-30 °C	**kW**	**1.1**
Survival Temperature Range	**°C**	**-46 to +66**
Max System Production Price @ 250k units/yr	**$**	**275**

Table 21 USABC Requirements of Energy Storage Systems for 48V HEVs at EOL [11]

End of Life Characteristics at 30°C	Units	System Level	Cell Level
Peak Discharge Power Density, 30 sec pulse	W/L	1000	1500
Peak Specific Discharge Power, 30 sec pulse	W/kg	470	700
Peak Specific Regen Power, 10 sec pulse	W/kg	200	300
Useable Energy Density @ C/3 Discharge Rate	Wh/L	500	750
Useable Specific Energy @ C/3 Discharge Rate	Wh/kg	235	350
Useable Energy @ C/3 Discharge Rate	kWh	45	N/A
Calendar Life	Years	15	15
DST Cycle Life	Cycles	1000	1000
Selling Price @ 100K units	$/kWh	125	100
Operating Environment	°C	-30 to +52	-30 to +52
Normal Recharge Time	Hours	< 7 Hours, J1772	< 7 Hours, J1772
High Rate Charge	Minutes	80% ΔSOC in 15 min	80% ΔSOC in 15 min
Minimum Operating Voltage	Vdc	420	N/A
Minimum Operating Voltage	Vdc	220	N/A
Peak Current, 30 seconds	A	400	400
Unassisted Operating at Low Temperature	%	> 70% Useable Energy @ C/3 Discharge rate at -20°C	> 70% Useable Energy @ C/3 Discharge rate at -20°C
Survival Temperature Range, 24 Hr	°C	-46 to +66	-46 to +66
Maximum Self-discharge	%/month	< 1	< 1

Table 22 USABC Goals for Advanced Batteries for BEVs – CY 2020 Commercialization [13]

Characteristics	Units	PHEV-20 Mile	PHEV-40 Mile	xEV-50 Mile
Commercialization Timeframe		2018	2018	2020
AER	Miles	20	40	50
Peak Pulse Discharge Power (10 sec)	kW	37	38	100
Peak Pulse Discharge Power (2 sec)	kW	45	46	110
Peak Regen Pulse Power (10 sec)	kW	25	25	60
Available Energy for CD Mode	kWh	5.8	11.6	14.5
Available Energy for CS Mode	kWh	0.3	0.3	0.3
Minimum Round-trip Energy Efficiency	%	90	90	90
Cold cranking power at -30 °C (3 2sec pulses)	kW	7	7	7
CD Life / Discharge Throughput	Cycles/MWh	5000/29	5000/58	5000/72.5
Calendar Life, 30°C	Year	15	15	15
Maximum System Weight	kg	70	120	150
Maximum System Volume	Liter	47	80	100
Maximum Operating Voltage	Vdc	420	420	420
Minimum Operating Voltage	Vdc	220	220	220
Maximum Self-discharge	%/month	< 1	< 1	< 1
Unassisted Operating Temp Range	°C	-30 to +52	-30 to +52	-30 to +52
30 °C - 52 °C	%	100	100	100
0 °C	%	50	50	50
-10 °C	%	30	30	30
-20 °C	%	15	15	15
-30 °C	%	10	10	10
Survival Temperature Range	°C	-46 to +66	-46 to +66	-46 to +66
Max System Production Price @ 250k units/yr	$	2200	3400	4250

Table 23 USABC Goals for Advanced Batteries for PHEVs for FY 2018 to 2020 Commercialization [12]

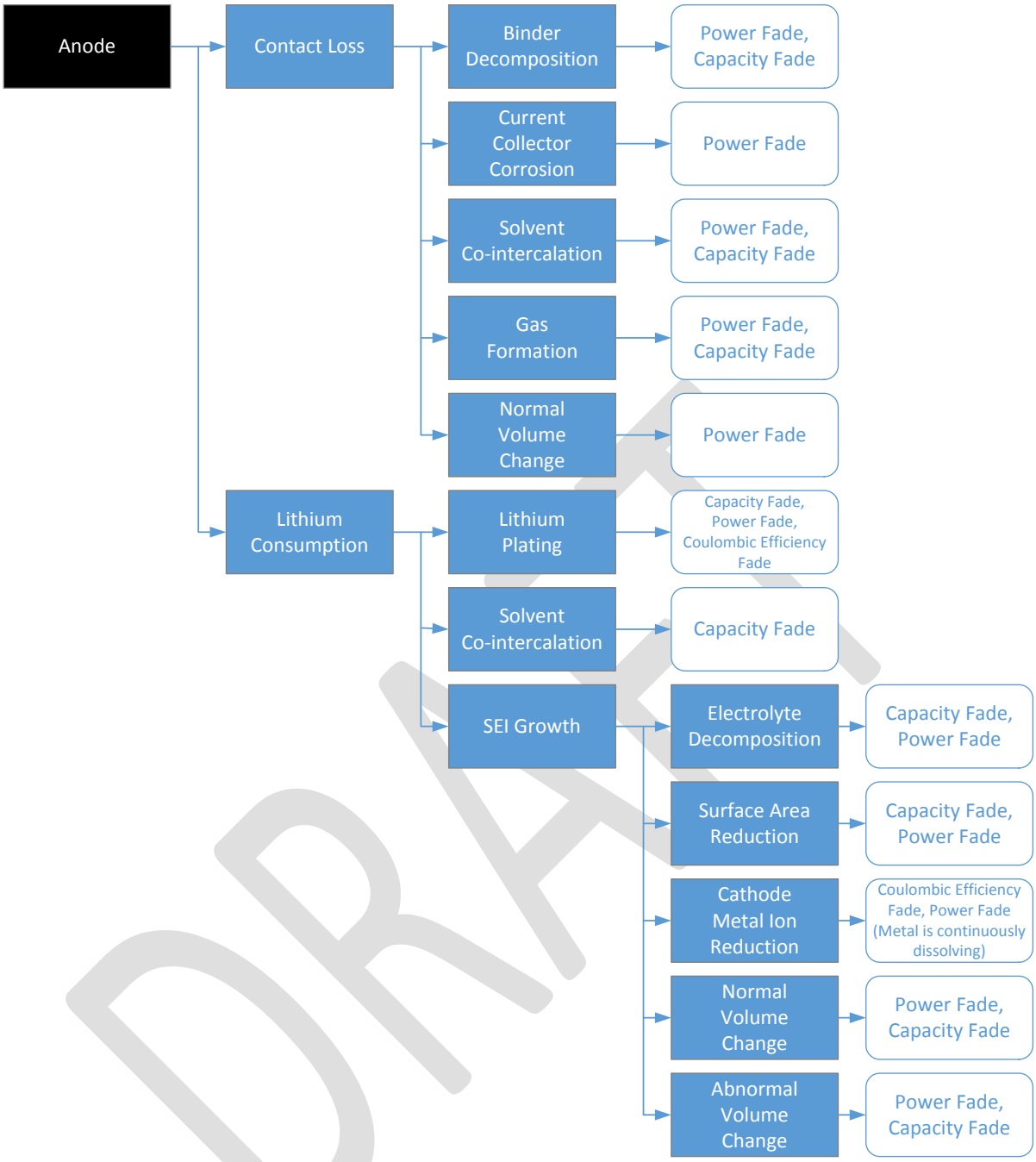

Figure 104 Degradation Mechanisms of the Anode **[41]**

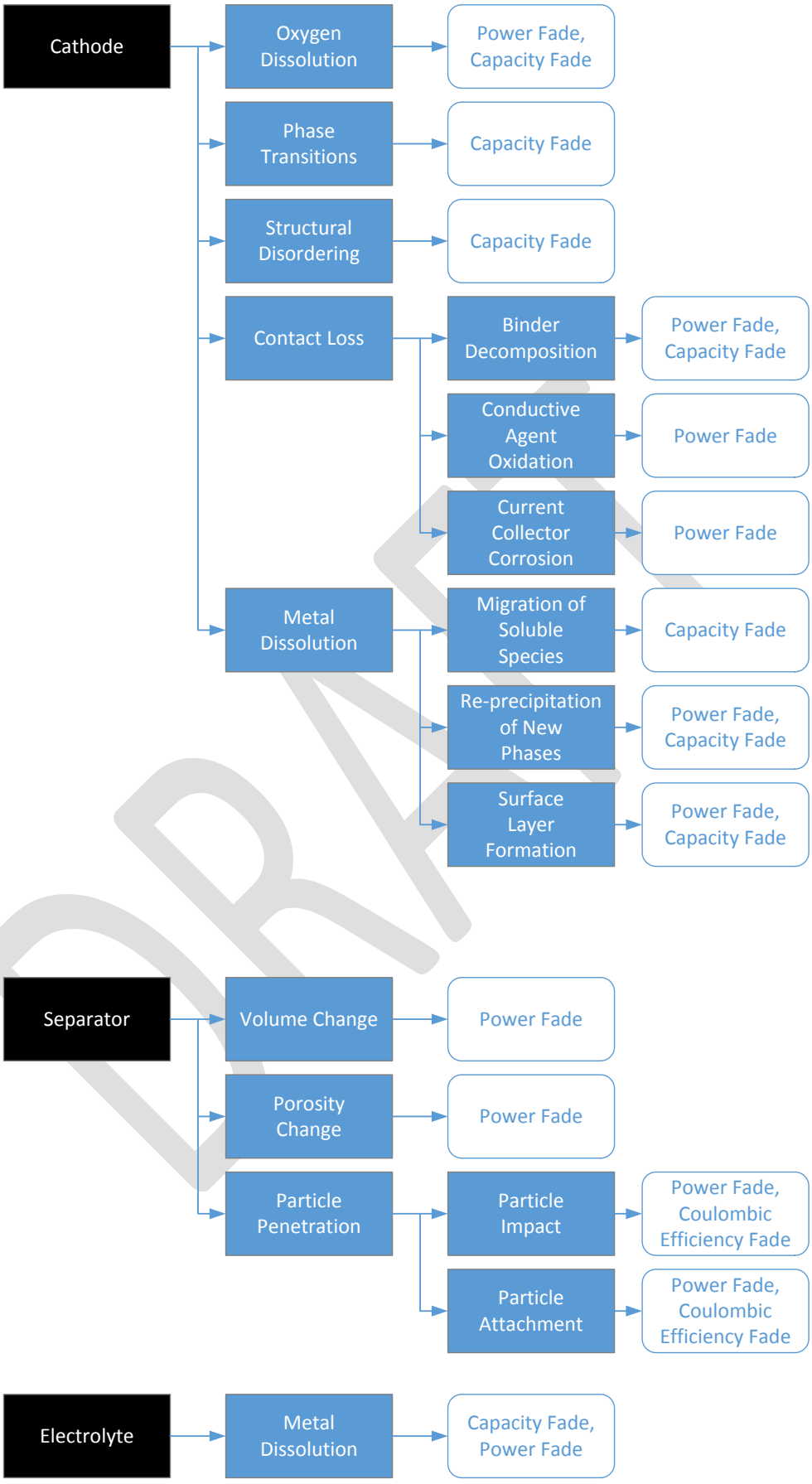

Figure 105 Degradation Mechanisms of the Cathode, Separator, and Electrolyte **[41]**